Alan G. Davenport Wind Engineering Group

WIND TUNNEL TESTING: A GENERAL OUTLINE

May 2007

The Boundary Layer Wind Tunnel Laboratory
The University of Western Ontario, Faculty of Engineering Science
London, Ontario, Canada N6A 5B9; Tel: (519) 661-3338; Fax: (519) 661-3339
Internet: www.blwtl.uwo.ca; E-mail: info@blwtl.uwo.ca

TABLE OF CONTENTS

LIST OF TABLES

LIST OF FIGURES

1 INTRODUCTION

This document provides a general outline of common wind tunnel tests performed at the Boundary Layer Wind Tunnel Laboratory (BLWTL) at the University of Western Ontario. It also details some of the techniques used to analyse the data from these tests. Since it is a general outline, it will cover some tests and analyses not performed for a particular project. Other than the wind climate modelling discussed in Section 2 and Appendices A and B, and the prediction methodology discussed in Appendices D and E, the various tests and analysis methodology are independent and the reader may skip sections that are not relevant. Also, this report does not, by any means, attempt to cover all of the types of tests and analyses performed at the Laboratory. Unusual tests are covered in separate reports for the projects employing them.

In determining the effects of wind for a particular development, there are two main ingredients to consider. The first comprises the aerodynamic characteristics of the development. These are simply the effects of the wind when it blows from various directions. This information only has limited value, however, without knowing how likely it is that the wind will blow from those directions and how strongly it is likely to blow. This climatological information, in the form of a probability distribution of wind speed and direction, is the second main ingredient needed for determining wind effects for a particular development. The aerodynamic information is characteristic of the particular development and its immediate surroundings, while the wind climate information is characteristic of the geographical location of the development. Both are necessary to determine the wind effects for a particular development and, when combined, provide statistical predictions of the wind effects which are independent of wind direction.

At the BLWTL, the aerodynamic characteristics of the development are commonly determined through model studies of the project. These studies may include measurements of various types of information of interest, such as cladding loads, structural loads and pedestrian level wind speeds, as detailed in the following sections of this report. The probability distribution of wind speed and direction, is determined from analyses of historical wind speed and direction records taken near the site of the development. Details of these analyses are included in Appendix A. Tropical cyclones, such as hurricane or typhoon winds present a special case and their associated statistical characteristics are handled separately using different analysis methods. These are detailed in Appendix B.

In all cases, tests carried out at the BLWTL are in accordance with the state-of-the-art, and meet or exceed such test requirements as documented by the ASCE Manual of Practice (1).

2 THE MODELLING OF THE SITE AND THE WIND

2.1 General

The basic tool used is the Laboratory's Boundary Layer Wind Tunnel. This wind tunnel is designed with a very long test section, which allows extended models of upwind terrain to be placed in front of the model of the development under test. The modelling is done in more detail close to the site. The wind tunnel flow then develops characteristics which are similar to the wind over the terrain approaching the actual site. This methodology has been highly developed and further details can be found in References 2, 3 and 4.

The modelling is comprised of the following components:

1. A detailed model of the development. Different types of model are used for the various types of test. These are discussed below in the sections on the individual tests.
2. A detailed proximity model of the surrounding area, built in block outline from wood and Styrofoam. Depending on the scale and size of the model, this may extend for a radius of approximately 500 to 600 metres.
3. Coarsely modelled upstream terrains, chosen to represent the general roughness upstream of the site for particular wind directions. Typically, several models are chosen, each used for a range of wind directions.

For project sites close to hilly terrain or with unusual topography, topographic study may be carried out to establish the wind characteristics at the site. This may be in the form of topographic model study at a small scale (~1:3000) or computational methods. The resulting target wind characteristics will be modelled in the larger scale used in the building or bridge tests.

2.2 Scaling

The fundamental concept is that the model of the structure and of the wind should be at approximately the same scale. The natural scaling of the flow in the wind tunnel is in the range 1:400 to 1:600; however, in some cases, instrumentation or other requirements may demand a larger model. In these cases, additional flow modification devices may be used to approximate larger scale flows.

In all cases, it is the mean wind speed profile and the turbulence characteristics over the structure that are most important to match with those expected in full scale. Guidance as to the latter is obtained through direct full scale measurements as compiled by ESDU (5, 6). Such data are also used to ensure that the test speeds near the top of the building are properly interfaced with full scale wind speeds predicted to occur at the full scale site.

3 THE CLADDING LOADS TESTS

3.1 Pressures and Suctions on Exterior Surfaces

Detailed measurements of the pressures and suctions on exterior surfaces of the building or structure are made using a rigid model that accurately represents the detailed exterior geometry of the development. The model contains numerous (typically 300 to 800) holes or "taps" which are connected via tubing to pressure transducers. The transducers convert the pressure at the point where the tap is located to an electrical signal which is then measured by the Laboratory's computerized data acquisition system. The technology employed allows all pressures on the building to be measured essentially simultaneously for a particular wind direction. Measurements are usually made at 10° intervals for the full 360° azimuth range. A detailed description of the procedures followed and the definitions used are presented in Appendix C.

These aerodynamic measurements made in the wind tunnel are subsequently combined with the statistics of the full scale wind climate at the site using the methodology outlined in Appendices D and E to provide predictions of pressures and suctions for various return periods.

3.2 Scaling

The aerodynamic pressure coefficients can be converted to full scale pressure values based on consistent length, time and velocity scaling between full scale and model scale. This applies very well for sharp-edged structures. For structures with curved surfaces, additional care has to be taken to ensure that the flow regime is consistent in model and full scale, as well as in the interpretation of the results.

For typical building tests, length scale is in the order of 1:300 to 1:500. Velocity scale is approximately 1:3 to 1:5. Time scale is in the order of 1:100. For example, 36 seconds in model scale represents about an hour in full scale and the data will be taken about 100 faster in the test than in full scale. Further details regarding scaling can be found in Appendix C.

3.3 Internal Pressures and Differential Pressures

The net load on cladding is the difference between the external and internal pressures. Using the methodology described in Appendix F, mean internal pressures are determined at all wind angles. These are then subtracted from the appropriate external pressure coefficients to form differential pressure coefficients. Finally, the coefficients are combined with the statistics of the full scale wind climate at the site, using the methodology outlined in Appendices D and E, to provide predictions of differential pressures and suctions for various return periods.

In the case of large opening due to operable windows or breach of the building envelope, large internal pressures may develop. Typically, the external pressure at the opening will be transmitted into the building interior volume. Building envelope at other locations within the building volume will experience both the external pressures at those external locations as well as the large internal pressure transmitted from the opening.

For free standing elements with both sides exposed to air, such as parapets and canopies, the net differential pressures are the instantaneous difference in pressures on the opposite sides.

4 THE DETERMINATION OF OVERALL STRUCTURAL LOADS AND RESPONSES

4.1 Introduction

The dynamic response of most tall buildings to wind is primarily the results of building motions in the fundamental sway and torsion modes of vibration with relatively small contributions from higher modes. The mechanical transfer function, relating the load function to the response, is straightforward. On the other hand, the aerodynamic transfer function, relating the gust structure to the wind induced forces is difficult to establish without wind tunnel model tests. A further complication exists if body motion effects interact with the load function (aerodynamic damping).

Multi-degree-of-freedom aeroelastic models have traditionally been used to study the action of wind on sensitive buildings and structures. While such simulations provide the most direct and reliable estimates, the required models are expensive and time consuming to design and construct. Two-degree-of-freedom aeroelastic models, which simulate the wind induced responses in the two fundamental sway modes of vibration, while less expensive, do not provide information on torsion effects, which may be significant for buildings of unusual shape and structural dynamic properties. In both of these cases, the model moves in the wind tunnel just as it would in full scale; its response in the wind tunnel can be scaled directly to full scale.

A high-frequency balance/model system can measure the load function directly, provided that aerodynamic damping effects are negligible, which is usual for most buildings at practical wind speeds and practical structural damping values. (Note that if such effects are important, they can be accounted for by using a supplemental testing technique in which the model is oscillated). The now commonly used high frequency force balance technique was originally developed at the BLWTL.

One other method for determining the load function is to integrate the point pressure measurements on an instant-by-instant basis to form time histories of the generalized forces.

4.2 The Force Balance Test

This technique involves testing a lightweight, stiff, geometrical representation of the building on an ultra-sensitive force balance. The technique allows direct measurements of good approximations to the steady and unsteady modal forces acting in the fundamental sway and torsional modes of vibration of the building. The dynamic responses including resonant amplification at the natural frequencies of the building are derived analytically for each mode using random vibration analysis methods and are subsequently used to provide estimates of the full scale responses of the building. As a result, this method is very accommodating of changes to the structural properties after testing, since the analytical procedure can be simply repeated using the same experimental results, which remain applicable so long as the aerodynamic characteristics of the building remains the same. A detailed description of this method is presented in Appendix G.

Time histories of the base shears and moments are taken during the tests. From these, the mean and rms (root-mean-square) base bending moments along orthogonal building axes, as well as mean and rms base torque are determined. The base bending moments represent a good approximation to the generalized modal forces in the fundamental modes. The spectra of the generalized modal forces are also determined from these time histories and used to determine the resonant component of the response. Measurements are usually taken at 10° intervals for the full 360° azimuth range.

Scaling is essentially the same as for pressure tests, requiring scaling of the structure to the flow model only, with the non-dimensionalized data being independent of test speed; however, in this case, the time scaling must be chosen carefully to ensure that the prototype's natural periods of interest fall within the accurate measuring range of the model/balance combination.

Once the responses have been determined, they are combined with the statistics of the full scale wind climate at the site, using the methodology outlined in Appendix D, to provide predictions of loads and responses for various return periods.

4.3 The Two-degree-of-freedom Aeroelastic Test

This technique requires scaling the dynamic properties (mass, stiffness and period) of the building in the fundamental sway modes and measuring the response to wind loads directly. The building is modelled as a rigid body, pivoted near the base, with the elasticity provided by appropriately selected springs. Implicit in this technique is the assumption that the sway modes do not include any coupling and can be approximated as linear, and that torsion is unimportant. These prove to be reasonable assumptions for a large range of buildings. A full discussion of this technique is contained in Appendix H.

The advantage of this technique is that the measurements will include effects of aerodynamic damping that are not included when using the force balance technique. It is also a simpler, less expensive technique than a multi-degree-of-freedom aeroelastic test. The disadvantages of the technique are that it is limited by the assumptions noted above and it is more complicated and expensive than the force balance technique while being less accommodating of changes to the dynamic properties of the building after the test. Furthermore, its advantage over the force balance technique, namely the inclusion of aerodynamic damping effects, rarely proves to be necessary since the aerodynamic damping is usually small and positive (i.e. it reinforces the inherent structural damping), but can be negative if vortex shedding plays an important role in the dynamic response. For most buildings, vortex shedding occurs at speeds well above the range of speeds that the structure will be subjected to. Nevertheless, it is useful for confirming force balance results and confirming that aerodynamic damping effects are indeed negligible.

As with other types of tests, once the aerodynamic data has been measured for a full range of wind directions, it is combined with the statistics of the full scale wind climate at the site, using the methodology outlined in Appendix D, to provide predictions of loads and responses for various return periods.

4.4 The Multi-degree-of-freedom Aeroelastic Test

This technique requires scaling the dynamic properties (mass, stiffness, periods and mode shapes) of the building in the fundamental sway modes and the fundamental torsion mode, including any coupling within modes. Some higher modes of vibration are also modelled. The responses to wind loads are then measured directly. Typically, a building is modelled as a series of lumped masses joined by appropriately sized columns; for towers, other approaches to produce the elastic model can also be used. A full discussion of this technique is contained in Appendix I.

The advantage of this technique is that the measurements will include effects of aerodynamic damping, vortex shedding, coupling within modes and some higher modes that are not fully dealt with when using the force balance technique. For most buildings, however, it can be argued that the aerodynamic damping effects are likely to be small, higher modes can be neglected and that the force balance adequately handles coupled modes analytically. Nevertheless, for more complicated structures, the additional reassurance of an aeroelastic test may be justified.

The disadvantages of the technique are that the model is time consuming and expensive to build. The model is also designed for a single set of building dynamic properties and approximations must be made if these change. The force balance technique on the other hand, yields results equally applicable to any set of building dynamic properties.

As with other types of tests, once the aerodynamic data has been measured for a full range of wind directions, it is combined with the statistics of the full scale wind climate at the site, using the methodology outlined in Appendix D, to provide predictions of loads and responses for various return periods.

4.5 Overall Loads from Local Pressure Measurements

The development of solid state pressure scanners, which permit the simultaneous measurement of pressures at many points on the surface of a building, allows the determination of instantaneous overall wind forces from the local pressure measurements. The technique allows direct computation of the steady and unsteady modal forces acting in any number of modes of vibration of the building. In similar fashion to the force balance approach, the resonant amplification due to the building's structural dynamics is derived analytically for each mode using random vibration analysis methods and results are subsequently used to provide estimates of the full scale response of the building. A detailed description of this method is presented in Appendix J. (Note that integration can also yield true time histories of loads on building subcomponents of interest, such as canopies, large panels, or roofs).

The advantages of this technique are that a single model used in a single testing session can produce both overall structural loads and cladding loads. The testing parameters would be extended to ensure that the local pressure data taken is also sufficient for the analysis of structural loads. The analysis required to determine structural loads from the local pressure information is nominally the same as that from the force balance tests. This technique also has the advantage of properly determining the generalized forces for three-dimensional non-linear mode shapes. Although these are also properly handled in multi-degree-of-freedom aeroelastic tests through the proper design of the aeroelastic model, such tests are expensive and time-consuming. The force balance technique can handle three-dimensional mode shapes but need to have corrections for non-linear modes. The pressure integration technique can also be used to examine higher modes with non-monotonic mode shapes.

A disadvantage of this technique is that the cladding pressure test model typically includes more instrumentation and takes longer to construct than a force balance test model. Also, as in the force balance technique, it does not include any effects of the building's motion through the air, such as aerodynamic damping; however, neglecting these effects is usually slightly conservative. Proper integration of local pressures to obtain overall wind forces requires that all buildings surfaces are properly represented in the model instrumentation and subsequent calculations. This may not be possible for buildings or structures with complex geometry or small components.

Once the responses have been determined, they are combined with the statistics of the full scale wind climate at the site, using the methodology outlined in Appendix D, to provide predictions of loads and responses for various return periods.

4.6 Effective Static Force Distribution

Representative effective static force distributions reflecting the combined static and dynamic response of the building are evaluated for the x, y and torque directions. The details of the procedure are included as Appendix K.

In principle, for any azimuth, effective static force distributions can be determined which reproduce the measured dynamic peak base bending moment. The particular vertical distribution chosen must reflect the actual static and dynamic loading of the building.

The loading is reasonably considered to be made up of the mean loading, the dynamic loading due to background or quasi-steady excitation and the dynamic inertial loading due to resonant oscillations. The mean loading distribution is determined from the integration of mean external local pressures from the cladding loads test or from an assumed distribution chosen to reflect the mean wind speed distribution. The inertial dynamic loading distribution is determined from the known vibration properties of the building. The measurement of the relative contribution of the unsteady and steady components at the base from one of the above structural loads tests is used to combine the mean and dynamic distributions into one total distribution. An overall effective loading diagram, independent of wind direction, is then constructed by averaging the effective force distributions, weighted by the relative importance of each wind direction.

It should be appreciated that these effective static loading distributions are representative of the most likely severe wind loading conditions expected, but the detailed loading may change somewhat for

different wind directions, since both the details of the mean pressure distribution and the mix between mean and resonant response will alter from angle to angle. Nevertheless, they provide useful distributions of loading for the design of the structural members in the overall wind resisting system.

4.7 Load Combination Factors

The determination of the wind-induced loads as described above treats the load directions independently. It should be recognized that wind loads in all three principal directions will occur simultaneously although the peak loads in each respective directions will not all occur at the same time. Load combination factors are used to specify the required simultaneous application of loads in the three directions such that the major load effects are reproduced for design purposes. These can be in the form of general load reduction factors applied to all three load directions or companion load factors where the full application of the load in the main load direction is accompanied by reduced loads in the other load directions.

Appendix K describes the companion load method used at the BLWTL. This method is based on the assumed critical load effects using generic influence factors due to base moments. While this is applicable to buildings or other like-line structures, other spatial structures such as canopies or load building frames may have different critical load effects and require other analytical procedures such as the LRC (Load-Response-Correlation) method to determine the effective load shapes and load combination factors.

5 THE PEDESTRIAN LEVEL WIND SPEED TEST

This test is usually performed using the same model that was used for the cladding loads test, and may include some landscaping details. The model is instrumented with omni-directional wind speed sensors at various locations around the development where measurements of the mean and fluctuating wind speed are made for a full range of wind angles, usually at 10° intervals.

The scaling involved is the same as that of the modelled wind flow. Thus, the ratio of a wind speed near the ground to a reference wind speed near the top of the building is assumed to be the same in model and full scale, and to be invariant with both test speed and prototype speed. Since the thermal effects in the full scale wind are neglected, strictly speaking, the results are only applicable to neutrally-stable flows which are usually associated with stronger wind speeds. However, near tall buildings, local acceleration effects due to the local geometry are usually dominant over thermal effects, and are also the most important for design considerations.

The measured aerodynamic data is combined with the statistics of the full scale wind climate at the site, using the methodology outlined in Appendix D, to provide predictions of wind speeds at the site. Two types of predictions are typically provided:

1. Wind speeds exceeded for various percentages of the time on an annual basis. Wind speeds exceeded 5% of the time can be compared to comfort criteria for various levels of activity. Very roughly, this is equivalent to a storm event of several hours duration occurring about once per week.
2. Predictions of wind speeds exceeded during events or storms with different frequencies of occurrence. Wind speeds exceeded once per year can be compared to criteria for pedestrian safety.

A more detailed description of this type of test is presented in Appendix L.

Other, non-quantitative techniques are also available to determine levels of windiness over a project site. One of these techniques is a scour technique in which a granular material is spread uniformly over the area of interest. The wind speed is then slowly increased in increments. The areas where the granular material is scoured away first are the windiest areas, while areas that are scoured later as the wind speed increases represent progressively less windy areas. Photographs of the scour patterns at increasing wind speeds can be superimposed using image processing technology to develop contour diagrams of windiness. This information can be used to determine locations for quantitative measurements, or simply to identify problem areas where remedial measures are necessary. Testing several configurations can provide comparative information for use in evaluating the effects of various architectural or landscaping details. The advantage of the scour technique is that it can provide continuous information on windiness over a broad area, as opposed to the quantitative techniques which provide wind speeds at discrete points.

An even more qualitative technique is to introduce smoke to visualize flow paths and accelerations at arbitrary places. This can be a useful exploratory technique by which to understand the flow mechanisms and how best to alter them.

6 THE TESTING OF LONG SPAN BRIDGES

The definition of wind effects on long span bridges should include not only the identification of any aerodynamic instability, but also the loading under turbulent flow conditions representative of full scale conditions. Recognition of the importance of lift and torsional loading in addition to drag loading is also essential. Thus the study of wind effects on a bridge includes some or all of the following:

1. Selection of a bridge deck system with favourable aerodynamic characteristics. There is a reasonably broad range of bridge cross-sections which have been tested, the results of which can be used as guidance in the design of new bridges.

2. Measurement and definition of the response and aerodynamic characteristics of the bridge deck. This is accomplished by testing the selected bridge cross-section using an elastically mounted section model and/or a "taut strip" model. These tests indicate any tendency to instability and the speeds at which this may occur. As well, the aerodynamic loads measured can be combined with statistics of the full scale wind climate at the site using the methodology outlined in appendix D to provide predictions of responses for various return periods. A full description of the determination of dynamic wind forces using equivalent static loads is given in Appendix M.

3. Confirmation of bridge behaviour using a multi-degree-of-freedom aeroelastic model of the entire bridge. This would be recommended in cases of innovative design and bridges of exceptional size and importance or unusual siting. The methodology for this test is similar to that for tall buildings, as described in Appendix I. Aeroelastic bridge models can also be used to determine general design load information for the bridge, and is especially useful for multi-span bridges whose spans are slightly different in dynamic properties.

4. Special Aspects. These may include the definition of loads during construction, cable movements, tower loads, fatigue and the role of damping.

7 OTHER TESTS

As mentioned in the introduction, this report is intended to give some background information on common tests performed at the BLWTL. There are many other, less common tests performed and new techniques are constantly being developed. Some of the techniques and tests available at the BLWTL are:

- dispersion of gaseous and particulate pollutants
- drifting and deposition of ice and snow
- monitoring of wind effects on full-scale structures
- influence of wind on heating, ventilation and air conditioning
- wind/wave effects on offshore structures
- wind induced iceberg drift
- influence of large-scale topography on wind patterns
- dynamics of inflated structures and tents
- evaluation of natural ventilation
- fatigue analysis
- galloping of cables and transmission lines
- interaction of multiple structures, both structurally independent and linked
- dynamics of foundations
- seismic loading
- design of additional dampers for buildings, chimneys and cables
- cooling and evaporative effects of wind
- performance of wind generators and their siting
- cross-winds on ground vehicles
- influence of wind breaks on forestry and agriculture
- soil erosion
- drift and deposition of sprays
- wind effects on ponds, used for such purposes as aquiculture or protecting mine tailings from erosion

The activities of the Laboratory are by no means limited to the items above; research is under way in many areas related to wind, waves, dynamics and earthquakes. New challenges are always welcome.

REFERENCES

(1) American Society of Civil Engineers (ASCE). “Manual of Practice for Wind Tunnel Testing of Buildings and Structures”. 1999.

(2) Davenport, A.G. and Isyumov, N. "The Application of the Boundary Layer Wind Tunnel to the Prediction of Wind Loading", International Research Seminar on Wind Effects on Buildings and Structures, Ottawa, Canada, September 1967, University of Toronto Press, 1968.

(3) Surry, D. and Isyumov, N. "Model Studies of Wind Effects - A Perspective on the Problems of Experimental Technique and Instrumentation", Int. Congress on Instrumentation in Aerospace Simulation Facilities, 1975 Record, pp. 76-90.

(4) Whitbread, R.E., "Model Simulation of Wind Effects on Structures", NPL International Conference on Wind Effects on Buildings and Structures, Teddington, England, 1963.

(5) Engineering Sciences Data Unit (ESDU). “Strong Winds In The Atmospheric Boundary Layer. Part 1: Mean-Hourly Wind Speeds”, ESDU 82026, 1982.

(6) Engineering Sciences Data Unit (ESDU). “Strong Winds In The Atmospheric Boundary Layer. Part 2: Discrete Gust Speeds”, ESDU 83045, 1983.

APPENDIX A

THE DEFINITION OF WIND CLIMATE

A.1 Introduction

The wind tunnel testing provides information regarding the dependence of particular response parameters on wind speed and direction. In order to make the most rational use of this aerodynamic information, it is necessary to synthesize it with the actual wind climate characteristics at the site. The characteristics necessary to define are those governing wind speed and direction at a suitable height above ground level at the site. The joint probability distribution of wind speed and direction then defines the wind climate, whereas all of the aerodynamic information, which includes sensitivities to building orientation and to its surroundings, is contained in the wind tunnel data.

A.2 Natural Wind

Air flowing over the earth's surface is slowed down and made turbulent by the roughness of the surface. As the distance from the surface increases, these friction effects are felt less and less until a height is reached where the influence of the surface roughness is negligible. This height is referred to as the gradient height, and the layer of air below this, where the wind is turbulent and its speed slowly increases with height, is referred to as the boundary layer. During periods of neutral atmospheric stability, typical of strong wind conditions, the gradient height or depth of the earth's boundary layer is determined largely by the terrain roughness and typically varies from 270m over open country to about 500m over built-up urban areas (A-1, A-2).

In more technical terms, for slowly-moving pressure systems, the motion of air at heights above the influence of the earth's surface is essentially parallel to the isobars and is governed by the pressure gradient, the Coriolis acceleration and the centrifugal acceleration due to isobar curvature (A-3). If conditions are such that these three effects are in balance, it is referred to as gradient wind, and as the geostrophic wind if there is no isobar curvature. The height at which this balance is first approximately achieved, that is, the height where frictional effects due to the earth's surface cease to be significant, is termed gradient height. As used here, the term gradient wind refers to the measured wind at approximately 500m. This usage is not in exact agreement with the above definition but does provide a convenient terminology.

Within the atmospheric boundary layer the flow becomes increasingly more dependent on shear stresses of mechanical and buoyant origin. The mean wind speed within the atmospheric boundary layer increases markedly with height above ground and the orientation of the mean wind speed vector rotates somewhat with respect to its direction near the surface. This horizontal rotation or veering with height is clockwise in the northern hemisphere. Based on theoretical arguments, the resulting relationship between the surface and gradient mean wind speed and direction during neutrally-stable atmospheric conditions depends on the Rossby number which relates shear forces to forces from the Coriolis acceleration (A-1). However, Davenport (A-2) and others (A-4) have shown that the ratio of the surface-to-gradient wind speed is relatively insensitive to both the latitude and the gradient wind speed and depends primarily on the upstream terrain roughness. Furthermore, estimates of the angular shift between surface and gradient height for open terrain, typical of most anemometer locations, is generally of the order of the angular resolution of the measured wind direction, making it unnecessary to correct for this rotation for most wind engineering applications. Consequently, natural wind over a particular terrain can be simulated by a turbulent boundary layer flow developed in a wind tunnel over a long fetch of appropriate model terrain roughness. Details of this approach, which leads to a representative simulation of the mean flow structure and the turbulent flow characteristics are given elsewhere (A-5).

Two models are commonly used to describe the wind characteristics within the boundary layer. The power law profile gives the variation of the mean speed with height:

$$V(z) = V_g \left(\frac{z}{z_g} \right)^m \tag{A.1}$$

where $V(z)$ is the mean wind speed at height z; V_g is the gradient wind speed for the same azimuth; and z_g and m are the gradient height and the power law exponent respectively. In general both z_g and m depend on the wind direction. This model is convenient and is used in most building codes.

The other model is based on the Harris and Deaves model described in the ESDU documents (A-6, A-7) which include the mean wind speed and turbulence characteristics.

Examining the power spectrum of all wind speed variations (the power spectrum indicates the distribution of energy with frequency), a distinct gap is found to exist at periods of about one hour (A-1, A-8, A-9). This spectral gap conveniently separates atmospheric motion into two distinct categories:

1. turbulent, with locally-stationary statistical properties

2. quasi-steady mean speeds associated with slowly-varying synoptic or climatological time scales.

For wind tunnel simulations, the first is modelled by the wind tunnel flow itself, which reproduces the turbulence characteristics of the natural wind. The second is taken into account by the wind climate model developed for the site, based on historical climatological records.

A.3 Availability of Wind Records

Wind records, in the form of relative frequency of occurrence of various wind speeds from different directions, are available for most cities in North America. For many cities such records are available for both surface winds and for upper-level winds measured at various heights above the ground. Measurements of the surface wind speed and direction are normally available from mast-mounted anemometers and directional vanes operating at synoptic and climatological stations and in some cases at pollution control or monitoring stations. The standard height for such measurements is 10 meters above the ground. Upper-level data are available only from meteorological stations equipped for tracking weather balloons either visually as for pilot balloons (pibals) or automatically as for radiosonde (rawinsonde) ascents. In the latter case, an instrument package equipped with a radio transmitter is carried aloft by a balloon and tracked automatically by a ground-based antenna. Upper-level data are provided both for standard heights above ground and for standard pressure levels. In regions where the ground elevation is near that of the mean sea level, the 500m height above ground corresponds approximately to the 950 mb (95 kPa) level. Whereas surface measurements are typically made once an hour, radiosonde ascents are made either twice or four times a day, depending on the station.

Surface data are sensitive to variations of topography, vegetation, the presence of buildings etc., and consequently are often biased by their immediate surroundings. In view of these difficulties, upper-level data provide better estimates of the local wind climate. Unfortunately, gradient wind records are not available for all stations, so that surface anemometer data, with appropriate corrections, must at times be relied upon to provide descriptions of the local wind climate. In wind tunnel simulations, the wind speed corresponding approximately to the gradient wind is the free stream speed above the simulated atmospheric boundary layer, which is usually recorded as the experimental reference speed.

For some stations, summaries of yearly extreme winds are also available for fairly long periods, say in the order of 60 years. Such data can provide checks on the results of the analysis of the detailed wind speed and direction information discussed above.

A.4 Probability Distribution of Mean Wind Speed and Direction

The relative frequency data of wind speed and wind direction at a particular surface or upper level station can be used to arrive at a description of the probability distribution of wind speed and direction. Such probability distributions can be obtained on a monthly, seasonal or annual basis. The derivation of these distributions is described below.

The probability of the wind speed, V, exceeding some value, V_1, within an azimuth of $\alpha_1 \pm \frac{\Delta\alpha}{2}$ can be written as follows:

$$P\left(V > V_1, \alpha_1 - \frac{\Delta\alpha}{2} < \alpha < \alpha_1 + \frac{\Delta\alpha}{2}\right) = P\left(\alpha_1 - \frac{\Delta\alpha}{2} < \alpha < \alpha_1 + \frac{\Delta\alpha}{2}\right) \times P\left(V > V_1 \,\middle|\, \alpha_1 - \frac{\Delta\alpha}{2} < \alpha < \alpha_1 + \frac{\Delta\alpha}{2}\right) \tag{A.2}$$

The first term on the right-hand side is the marginal probability of the wind direction being within the azimuth sector $\alpha_1 \pm \frac{\Delta\alpha}{2}$ regardless of the wind speed; the second term is the probability of exceeding a wind speed V_1, conditional upon the wind direction being within that sector.

It is convenient to fit the joint probability of wind speed and direction given in equation A.2 by a mathematical model. The conditional probability above (i.e. the second term on the right-hand side) can be fitted by a Weibull distribution of the following form:

$$P\left(V > V_1 \,\middle|\, \alpha_1 \pm \frac{\Delta\alpha}{2}\right) = e^{-\{V_1 / C(\alpha_1)\}^{K(\alpha_1)}} \tag{A.3}$$

where $K(\alpha_1)$ and $C(\alpha_1)$ are the Weibull coefficients pertaining to the sector defined by $\alpha_1 \pm \frac{\Delta\alpha}{2}$. Although other mathematical models have been used to describe the probability distribution of wind speed and direction (A-2, A-10, A-11), the simplicity of the Weibull distribution offers practical advantages. The applicability of the Weibull model has been confirmed for a large number of upper-level and surface stations. Wind records are usually divided into sixteen compass directions and consequently $\Delta\alpha = 22.5^{o}$.

The marginal probability of the wind direction being within a particular sector (i.e. the first term on the right-hand side of equation A.2) is the relative frequency of occurrence of all wind speeds within that sector. Denoting this relative frequency of occurrence by $A(\alpha)$, the probability of exceeding a wind speed V, from wind directions within an azimuth of $\alpha_1 \pm \frac{\Delta\alpha}{2}$, can now be written as:

$$P(>V, \alpha) = A(\alpha)\, e^{-\{V_1 / C(\alpha_1)\}^{K(\alpha_1)}} \tag{A.4}$$

From the definition of $A(\alpha)$ it follows that $\sum_{all\ sectors} A(\alpha) = 1$. The parameters $A(\alpha), C(\alpha)$ and $K(\alpha)$ can be evaluated from the relative frequency records of surface or upper-level wind speeds for the standard sixteen compass directions. They can then be linearly interpolated to provide coefficients for intermediate wind directions.

The marginal probability of exceeding a particular wind speed, namely the probability of exceeding that wind speed from any wind direction, is obtained from equation A.4 as follows:

$$P(>V) = \sum_{\text{all sectors}} A(\alpha) e^{-\{V_1 / C(\alpha_1)\}^{K(\alpha_1)}} \tag{A.5}$$

This can be repeated for various wind speeds to obtain the probability distribution of wind speed regardless of wind direction. Alternatively, this distribution can be obtained by directly fitting the marginal histogram of wind speed (arrived at by summing the histograms for all compass directions) with a Weibull distribution. The *K* parameter of this distribution is generally of the order of 2, suggesting that the marginal distribution of wind speed is similar to a Rayleigh distribution.

The above model can be used to obtain surface or upper-level descriptions of the wind climate. In the absence of actual upper-level data, the probability distribution of gradient wind speed and direction can be estimated from the Weibull model derived from the surface anemometer records. Based on equation A.1, this can be done by directly adjusting the Weibull parameter *C*,

$$C_g(\alpha) = b(\alpha) C_s(\alpha) \tag{A.6}$$

where C_g and C_s are the respective Weibull parameters for gradient and surface wind speeds. For an anemometer located in approximately homogeneous terrain, b can be assumed to be independent of wind direction and is given by:

$$b = \left(\frac{z_g}{z_s} \right)^m$$

where z_s is the height at which the surface measurements were made.

A.5 Applicability of the Wind Climate Model

The reliability of the wind model obtained as outlined above depends largely on the length of data record available and the type of storms that frequent a given region. Typically, wind records range from 10 to 20 years. This is generally found sufficient to provide good estimates of extreme events for wind climates dominated by the effects of extratropical cyclones, i.e., the low pressure systems commonly seen on weather charts (A-12), because these generally affect very extensive areas and occur quite frequently.

In regions where physically smaller and less frequent storms contribute significantly to the wind climate, available wind records may not be sufficient. Such regions would include, for example, those frequented by tornadoes or by tropical cyclones. The severest of the latter are commonly termed hurricanes. Along the U. S. Gulf Coast and Florida Peninsula in the U.S., severe tropical cyclones dominate the climate of strong winds. Along the New England Coast such storms contribute to the wind climate but to a lesser extent than along the Gulf Coast. Because of the rarity of these storms and their relatively small size, a typical twenty-year record is not sufficient to obtain a reliable statistical estimate. Furthermore, there is the difficulty that instruments often fail in hurricane force winds. Similar comments can be made regarding the contribution to the wind climate by tornado-generating thunderstorms in the mid-western U.S. region.

A different approach, based on computer simulations of events such as tropical cyclones, can lead to more reliable statistical predictions of building response. Such an approach has been used by the Boundary Layer Wind Tunnel Laboratory on many occasions and is described in detail in References A-13 and A-14, and in Appendix B of this report.

The reliability of the wind model can also be affected by severe topography in two ways. Large hills or mountains can severely distort surface wind measurements, and can essentially increase the height at which gradient conditions are first approximated. Furthermore, severe winds can originate in regions near mountain ranges due to thermal instabilities in the atmosphere. These downslope winds are referred to by several names such as Santa Ana winds, chinooks, etc. and are particularly prevalent in West coast

areas and areas just east of the Rocky Mountains. Their detailed structure is not well understood, particularly in regions close to the mountains where significant vertical flows can occur, leading to severe spatial inhomogeneities near the ground. Away from the close proximity of the mountains, the flow appears to take on the characteristics of "normal" storm winds, although little information exists on the boundary layer structure away from the surface. In areas affected by such winds, conservative modelling of the approaching flows is the current state-of-the-art.

References

(A-1) Davenport, A.G., "The Relationship of Wind Structure to Wind Loading", Symposium on Wind Effects on Buildings and Structures, Teddington, 1973.

(A-2) Davenport, A.G., "The Dependence of Wind loads on Meteorological Parameters", Proc. International Seminar on Wind Effects on Buildings and Structures, Ottawa, 1967.

(A-3) Sutton, O.G., "Micrometeorology", McGraw-Hill Book Co., 1953.

(A-4) McNamara, K.F. "Characteristics of the Mean Wind Flow in the Planetary Boundary Layer and Its Effects on Tall Towers", Ph.D. Thesis, University of Western Ontario, 1975.

(A-5) Davenport, A.G. and Isyumov, N. "The Application of the Boundary Layer Wind Tunnel to the Prediction of Wind Loading", Proc. International Seminar on Wind Effects on Buildings and Structures, Ottawa, 1967.

(A-6) Engineering Sciences Data Unit (ESDU). “Strong Winds In The Atmospheric Boundary Layer. Part 1: Mean-Hourly Wind Speeds”, ESDU 82026, 1982.

(A-7) Engineering Sciences Data Unit (ESDU). “Strong Winds In The Atmospheric Boundary Layer. Part 2: Discrete Gust Speeds”, ESDU 83045, 1983.

(A-8) Van Der Hoven, I., "Power Spectrum of Horizontal Wind Speed in the Frequency Range From 0.007 to 900 Cycles Per Hour", Journal of Meteorology, Vol. 14, 1957.

(A-9) Lumley, J.L. and Panofsky, H.A., "The Structure of Atmospheric Turbulence", Interscience Publishers, John Wiley & Sons, 1964.

(A-10) Davenport, A.G., Isyumov, N. and Jandali, T. "A Study of Wind Effects for the Sears Project", University of Western Ontario, Engineering Science Research Report, BLWT-5-71, 1971.

(A-11) Baynes, C.J., "The Statistics of Strong Winds for Engineering Applications", Ph.D. Thesis, University of Western Ontario, Engineering Science Research Report, BLWT-4-74, 1974.

(A-12) Gomes, L. and Vickery, B.J., "On the Prediction of Extreme Wind Speeds From the Parent Distribution", Research Report No. R241, University of Sydney, March 1974.

(A-13) Tryggvason, B.V., Surry, D. and Davenport, A.G. "Predicting Wind-Induced Response in Hurricane Zones", Journal of the Structural Division, ASCE, Vol. 102, No. ST12, Proc. Paper 12630, December 1976, pp 2333-2350.

(A-14) Georgiou, P.N., Davenport, A.G. and Vickery, B.J., "Design Wind Speeds in Regions Dominated by Tropical Cyclones", Journal of Wind Engineering and Industrial Aerodynamics, Vol. 13, No. 1, December 1983 (presented at 6th International Conference of Wind Engineering, Brisbane, Australia, March 1983.

APPENDIX B

THE DEFINITION OF A HURRICANE WIND CLIMATE

B.1 Introduction

The wind tunnel testing provides information regarding the dependence of particular response parameters on wind speed and direction. In order to make the most rational use of this aerodynamic information, it is necessary to synthesize it with the actual wind climate characteristics at the site. The characteristics necessary to define are those governing wind speed and direction at a suitable height above ground level at the site. The joint probability distribution of wind speed and direction then defines the wind climate, whereas all of the aerodynamic information, which includes sensitivities to building orientation and to its surroundings, is contained in the wind tunnel data.

The definition of this joint probability function for some locations is complicated by the fact that they are in areas that sometimes experience winds due to hurricanes or typhoons. Since these storms, known generically as tropical cyclones, arise from different meteorological phenomena than do "normal" extratropical winds and hence have different speed and directional characteristics, it is safest to separate the two and examine building loads and responses under each independently. The terminology covering tropical cyclones is shown in the table below, and follows the classification system established by the National Hurricane Center, Miami, Florida.

Classification of Meteorological Systems	
Name	**Description**
Tropical Cyclone	A non-frontal low pressure synoptic-scale system developing over tropical or subtropical waters having definite organized circulation
Subdivided in Terms of Intensity Into:	
Tropical Depression	$V_{ms} \leq 33$ *knots*
Tropical Storm	33 *knots* $< V_{ms} <$ 64 *knots*
Hurricane	$V_{ms} \geq 64$ *knots*

Note: V_{ms} = maximum sustained (1-minute), surface (10 metre) wind speed.

B.2 The Approach Used

Tropical cyclones are considered meteorologically to be relatively "small" and their infrequent occurrence rate makes adequate sampling difficult. This problem is aggravated in the case of surface records by the vulnerability of surface anemometers to damage. Frequently the crucial observations of wind speed during hurricanes are lost. Furthermore, the routine relocation of anemometers and changes to the urban environment affect the uniformity of the exposure and continuity of the records. This has prompted the search for alternative approaches to surface observations for defining the wind climate arising from tropical cyclones.

The approach developed by the Boundary Layer Wind Tunnel Laboratory at The University of Western Ontario to predicting design wind speeds in areas which are dominated by tropical cyclones involves a simulation method similar to that suggested in Reference B-1. It has been employed in case

studies detailed in References B-2, B-3 and B-4 for North American locations; References B-5, B-6 and B-7 for Australian locations and Reference B-8 for the Hong Kong region.

In essence, this so-called "Monte Carlo" method creates, by computer simulation, a large number of time histories of tropical cyclone passages past a given locality. These are then used to provide estimates of extreme wind speeds, directional characteristics, etc. over what are effectively long periods of time. Statistics of key meteorological parameters of the simulated storms, such as the probability distribution of their central pressure differences, match similar statistics of actual storms affecting the site. Thus, the occurrence characteristics of tropical cyclones in the immediate vicinity of the site must be established in both the time-wise and geographical sense, and the windfield associated with them defined. In the case of the North Atlantic, for example, this approach makes use of historical records compiled by the National Oceanic and Atmospheric Administration (NOAA) documenting the tracks and intensities of all known tropical cyclones dating from 1886. One of the distinguishing features of the simulation model used is the inclusion of all tropical cyclones in the analysis, not just those reaching hurricane intensity. This extension increases the data base and, consequently, the reliability of the analysis concerning the definition of the statistical distributions required by the simulation.

The windfield model used in the simulation was developed in collaboration with the staff of the National Hurricane Center and has undergone considerable refinement by other researchers (B-9,B-10,B-11,B-12). In addition to defining the windfield at gradient height, where surface friction effects are negligible, the model predicts surface wind speeds at the 10-metre level and accounts for varying roughness of the underlying terrain. The model keeps track of the weakening experienced by tropical cyclones when they make landfall and undergo the process known as "filling", during which a significant reduction in wind speeds is observed as the tropical cyclone loses the oceanic heat source from which its energy is derived.

A general description of this simulation procedure and its application to deriving extreme wind speed estimates is found in reference B-13, along with further discussion of the applicability of the approach. Current model with refinement from the earlier model can be found in References B-9, B-10, B-11 and B-12.

B.3 Verifying the Approach

The windfield model has been checked by obtaining actual wind traces from tropical cyclone events and comparing them to the wind speeds predicted by the model. One such example is shown in Figure B.1 comparing model speeds with those obtained from the Waglan Island anemometer station during the passage of typhoon Ellen through the Hong Kong area in September 1983. It can be seen that the match of model speeds with actual recorded speeds is particularly good at the time that the maximum winds occurred.

In a study following the passage of Hurricane Alicia through Texas in August 1983, the simulation windfield model was used to recreate the time history of winds experienced in downtown Houston utilizing actual meteorological data obtained during the passage of the storm (central pressure, storm speed, etc.). In a unique set of circumstances, an accelerometer record was obtained during the most intense part of the storm for a 300 metre high-rise tower which had undergone detailed wind tunnel testing at this Laboratory. The model time history of Alicia's winds were combined with the wind tunnel test results, and the resulting predicted accelerations were compared to the actual recorded ones, as shown in Figure B.2. The agreement is seen to be excellent and adds considerable confidence to the continuing calibration that the windfield model has undergone.

B.4 The Wind Climate for a Particular Site

For most locations, a 500 kilometre simulation circle around the site is used. Historical data of hurricanes within this circle are examined to determine probability distributions of the relevant parameters for the simulation. A summary of the parameters required by the simulation is given in the table below. A time period of several thousand years is typically used for the simulation.

Statistical Simulation Parameters	
Parameter	Distribution
Annual Occurrence Rate	Poisson
Central Pressure Difference (mbars)	Weibull
Radius to Maximum Winds (km)	Log-Normal
Translation Velocity (m/s)	Log-Normal
Minimum Approach Distance (km)	Polynomial
Approach Angle (degrees)	Von Mises

As a simulation proceeds, a separate record is kept of all wind speeds and their respective directions (the "parent" distribution) as well as the individual peak wind speeds recorded for each tropical cyclone generated (the "extreme" distribution). These distributions are fitted independently using standard maximum likelihood estimating techniques. The results are a probability distribution of wind speed and direction and a graph of extreme wind speed versus return period.

References

(B-1) Russell, L.R. and Schueller, G.F., "Probabilistic Models for Texas Gulf Coast Hurricane Occurrences", J. Pet. Tech., March 1974.

(B-2) Tryggvason, B.V., Surry, D. and Davenport, A.G. "Predicting Wind-Induced Response in Hurricane Zones", Journal of the Structural Division, ASCE, Vol. 102, No. ST12, Proc. Paper 12630, December 1976, pp 2333-2350.

(B-3) Batts, M.E., Cordes, M.R., Russell, L.R., Shaver, J.R. and Simiu, E., "Hurricane Wind Speeds in the U.S.A.", NBS Building Series 124, Nat. Bur. of Standards, Washington, D.C., 1980.

(B-4) Georgiou, P.N., Davenport, A.G. and Vickery, B.J., "Design Wind Speeds in Regions Dominated by Tropical Cyclones", Journal of Wind Engineering and Industrial Aerodynamics, Vol. 13, No. 1, December 1983 (presented at 6th International Conference of Wind Engineering, Brisbane, Australia, March 1983).

(B-5) Martin, G.S., "Probability Distributions for Hurricane Wind Gust Speeds on the Australian Coast", Proc. I. E. Aust. Conf. on Appl. Probability Theory to Structural Design, Melbourne, 1974.

(B-6) Gomes, L. and Vickery, B.J., "On the Prediction of Tropical Cyclone Gust Speeds Along the Northern Australian Coast", Inst. Eng. Aust. C.E. Trans., CE 18, Vol. 2, pp. 40-49, 1976.

(B-7) Tryggvason, B.V., "Computer Simulation of Tropical Cyclone Wind Effects for Australia", Wind Engineering Report 2/79, Department of Civil and Systems Engineering, James Cook University, Townsville, Australia, 1979.

(B-8) Georgiou, P., Mikitiuk, M.J., Surry, D. and Davenport, A.G., "The Wind Climate for Hong Kong", The University of Western Ontario, Engineering Science Research Report, BLWT-SS2-1984.

(B-9) Vickery, P.J. and Twisdale, L.A. (1995), “Prediction of Hurricane Wind Speeds in the United States”, *Journal of Structural Engineering*, Vol. 121, No. 11, pp. 1691-1699.

(B-10) Vickery, P.J., Skerlj, P.F. and L.A. Twisdale (2000a), “Simulation of Hurricane Risk in the U.S. Using and Empirical Track Model, *Journal of Structural Division*, ASCE, October.

(B-11) Vickery, P.J., Skerlj, P.F. Steckley, A.C. and L.A. Twisdale (2000b) “A Hurricane Wind Field Model for Use in Hurricane Wind Speed Simulations”, *Journal of the Structural Division*, ASCE, October.

(B-12) Twisdale, L.A. and P.J. Vickery (1993), “Uncertainties in the Prediction of Hurricane Windspeeds”, Proceedings of *Hurricanes* of 1992, ASCE, pp. 706-715, December.

(B-13) Georgiou, P. "Design Wind Speeds in Tropical Cyclone-Prone Regions", Ph.D. Thesis, Faculty of Engineering Science, University of Western Ontario, 1985.

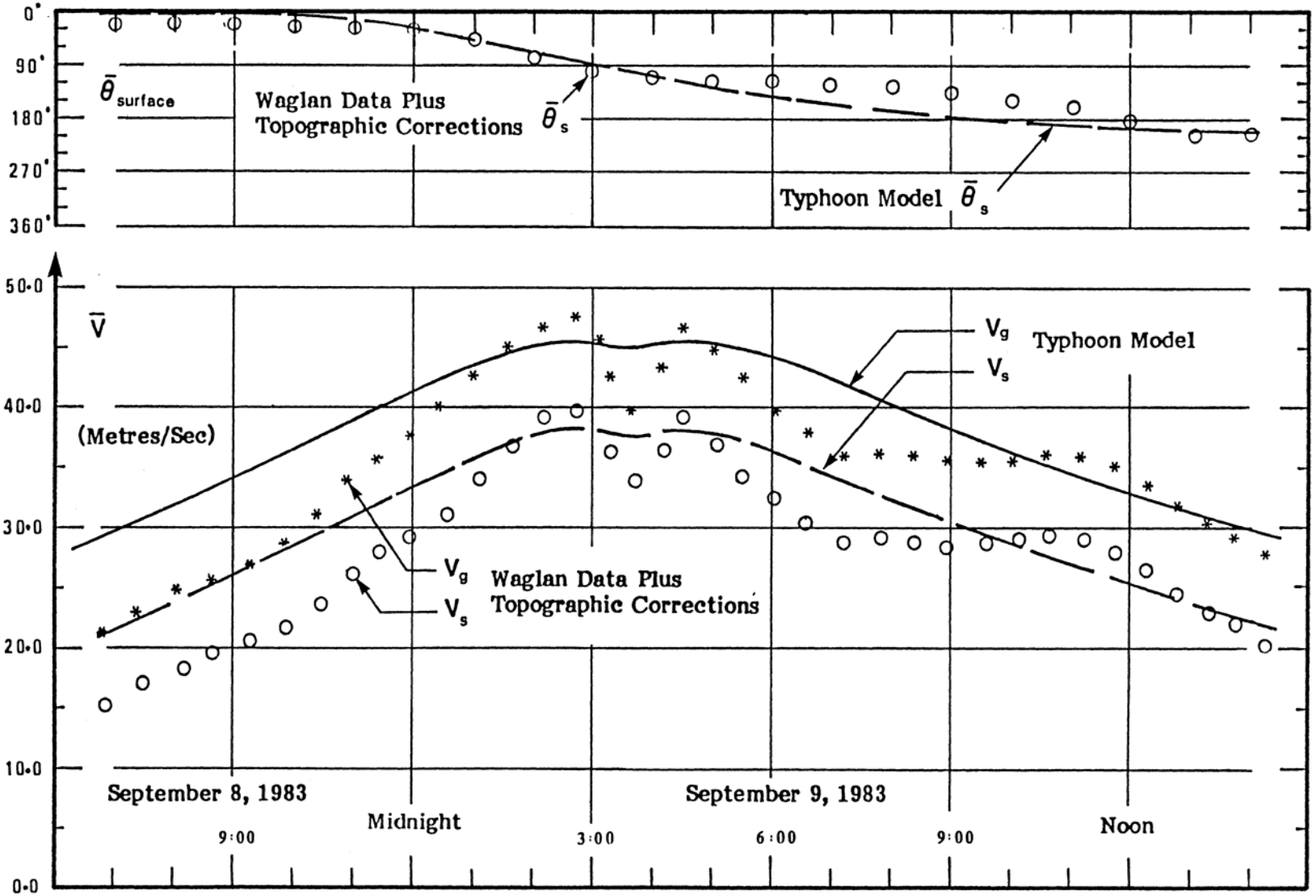

FIGURE B.1 COMPARISON OF TYPHOON WIND SPEEDS AT WAGLAN ISLAND TO MEASURED DATA CORRECTED FOR TOPOGRAPHIC EFFECTS

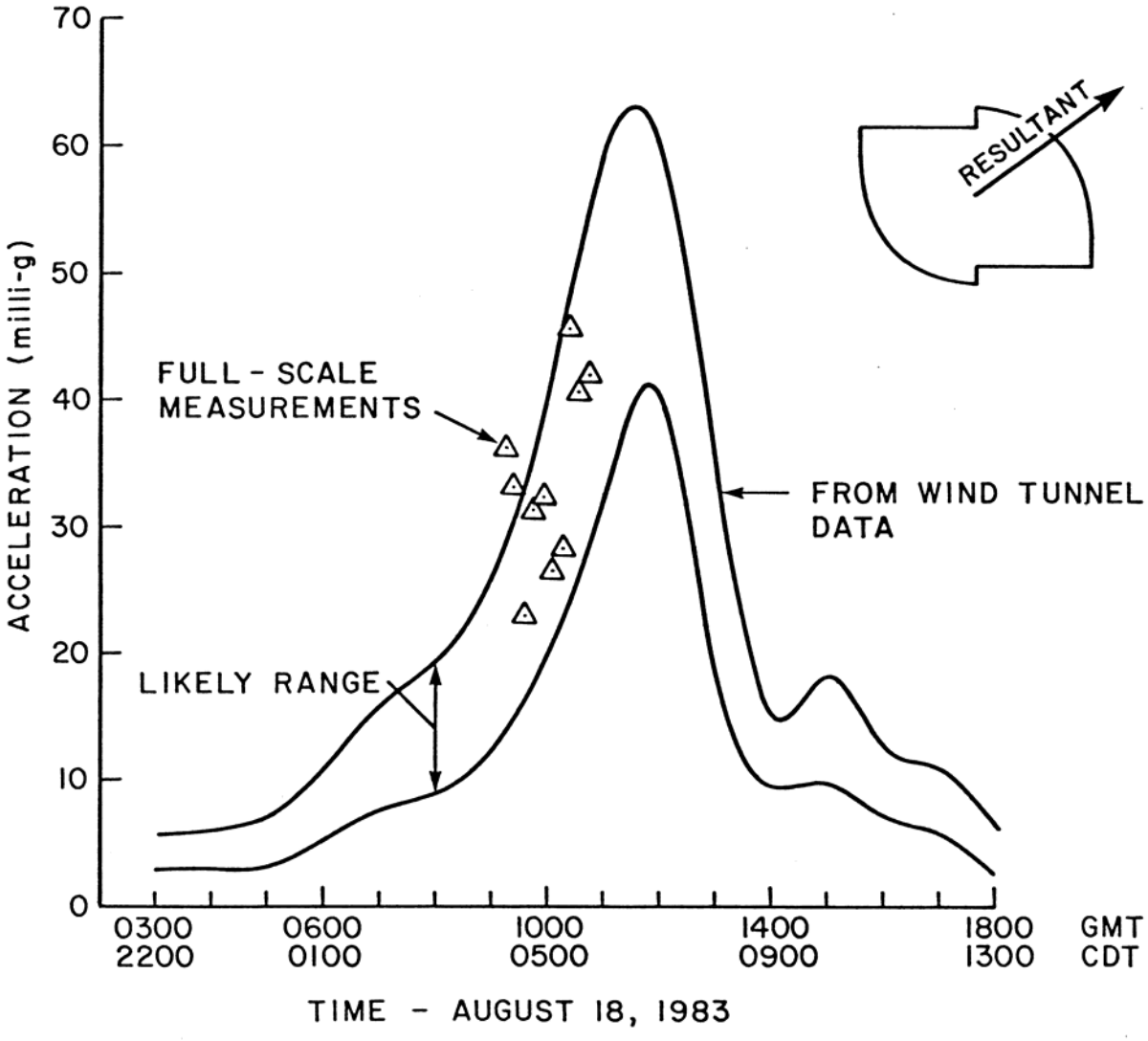

FIGURE B.2 PREDICTED PEAK ACCELERATIONS FOR THE ALLIED BANK DURING HURRICANE ALICIA

APPENDIX C

THE MEASUREMENT AND PREDICTION OF SURFACE PRESSURE

C.1 Experimental Technique

Measurements of wind-induced surface pressure at a point are accomplished by allowing the surface pressure to act on a transducer which provides an electrical analogue of the pressure. The electrical signal is digitized and then stored in its entirety for later processing.

In practice, the transmission of the surface pressure to the transducer is complicated in two ways. First, there are usually a large number of measuring positions, requiring the use of a large number of transducers. Secondly, the model is generally too small to allow the transducers to be very close to the measuring locations. The resulting use of relatively long lengths of pneumatic tubing leads to a modification of the pressure at the transducer compared to that at the model surface.

These problems are dealt with as follows: pressure taps on the model are connected pneumatically to electronic pressure scanning modules, each capable of handling 16 different taps. The modules use internal multiplexers which are sequentially scanned at a selectable fixed scan rate. The maximum rate that a particular input can be scanned is inversely proportional to the number of inputs on each module; 16 inputs were considered optimal for wind engineering applications at the BLWTL. The sampling rate is typically 400 or 500 samples per second per input. All modules are synchronized and the 16 outputs from each module are time-shifted analytically so that the signals from all taps can be considered simultaneous.

The pneumatic connection between model and scanning module is typically 1/16”ID plastic tubing containing a restricting insert of small bore at a specific point along its length. The function of the restrictor is to add damping to the resonant system made up of the pressure tube and the connecting volume adjacent to the pressure transducer. The resulting pressure system with about two-foot long tubes responds with negligible attenuation or distortion of surface pressure fluctuations with frequencies up to about 200 Hz. Although some response is obtained for signals of several hundred Hertz, these higher frequencies suffer increasing attenuation.

The data acquisition system records the digitized signals from the scanning modules at the set scanning rate (typically 400 Hz). Typically, sampling is continued for a period of up to about a minute in real time (see Section C.3). The reference dynamic pressure, usually measured in the free stream above the boundary layer, is recorded similarly. All of this data is stored for later analysis, which includes the determination of maximum, minimum, mean and rms pressures for each tap.

C.2 Experimental Time Scale

Scaling relationships for wind tunnel studies are based on established similarity requirements. Wind-induced pressures are normally measured using an instrumented rigid model which is subjected to simulated atmospheric flow conditions representative of the natural wind at the project site.

The length scale of wind tunnel models is dictated by the characteristics of the flow generated in the wind tunnel. Consequently, in The University of Western Ontario's boundary layer wind tunnels, model length scales are typically in the range of 1:400 to 1:500. However, there is some flexibility in the selection of the velocity scale and consequently the time scale $\lambda_T = \lambda_L / \lambda_V$. Pressure tests are carried out at intermediate speeds which are high enough not to unduly reduce full scale frequencies that can be detected. The velocity and time scales are then based on the ratio of this speed to the full scale wind speed relevant to design (typically the 50 or 100 year wind speed). Thus for a length scale of 1:500, a

wind tunnel speed of 50 fps (15 m/s), and a design speed of 45 m/s, the velocity and time scales are about 1:3 and 1:150 respectively. Consequently, the experimental sampling rate of 400 Hz corresponds to about 2.5 samples per second in full scale, and pressure fluctuations with frequencies up to about 1.3 Hz in full scale can be detected without distortion or attenuation.

C.3 Choice of Sampling Period

The choice of sampling period is determined essentially by two considerations. First, the period must be sufficiently long to provide statistically stable estimates of the mean and rms pressures. Secondly, measured maximum and minimum pressures must provide representative estimates of peaks encountered during a full scale interval of approximately one hour, because these are used in combination with the statistics of hourly mean wind speeds to predict full scale peak pressures. Sampling periods used to satisfy these requirements typically range between 30 and 60 seconds. In order to improve the reliability of the extreme peaks in the record, the Leiblein fitting method (C-1) is typically applied. It uses ten segmental peaks obtained from the data to obtain fitted parameters of an extreme value distribution. These are then used to predict a best estimate of the overall record peak.

C.4 Definition of the Pressure Coefficients

Pressures are usually measured with respect to the mean static pressure in the wind tunnel test section corresponding to the mean static pressure in the full scale wind flow. Pressure coefficients are obtained by normalizing the measured pressures by the mean dynamic pressure measured at a convenient reference height, usually selected to be in the free stream above the boundary layer or at the roof height of the building being tested. The pressure coefficients are thus defined as follows:

Mean Pressure Coefficient:
$$C_{\bar{p}} = \frac{\frac{1}{T}\int_0^T p(t)\,dt}{q} \tag{1}$$

Rms Pressure Coefficient:
$$\sigma_{C_p} = \frac{\sqrt{\frac{1}{T}\int_0^T (p(t)-\bar{p})^2\,dt}}{q} \tag{2}$$

Maximum Pressure Coefficient:
$$C_{\hat{p}} = \frac{p_{max}}{q} \tag{3}$$

Minimum Pressure Coefficient:
$$C_{\check{p}} = \frac{p_{min}}{q} \tag{4}$$

where:

$p(t)$	is the instantaneous surface pressure measured with respect to the mean static reference pressure;
σ_{C_p}	is the rms value of $p(t)$ for the sampling period T
p_{max}	is the maximum value of *p(t)* for the sampling period T ;
p_{min}	is the minimum value of *p(t)* for the sampling period T ;
t	is time;
T	is the sampling period;

$q = \frac{1}{2}\rho \bar{V}^2$ is the reference mean dynamic pressure;

ρ is the air density;

$\bar{V}$ is the reference mean wind speed, normally measured in the free stream above the boundary layer in which case it corresponds to the hourly mean gradient wind speed in full scale. However, in all cases, the matching of full scale design speeds and wind tunnel test speeds is essentially carried out at building height.

Note that the instantaneous pressure, $p(t)$, can be either positive or negative. Thus $C_{\bar{p}}, C_{\hat{p}}$ and $C_{\check{p}}$ are signed quantities. The sign convention is such that a negative pressure coefficient corresponds to a suction acting on the surface.

For design purposes, predictions of peak positive pressures and peak negative pressures (suctions) for various return periods are required. Contribution to predicted peak positive pressures arise only from wind directions for which $C_{\hat{p}}$ is positive. Similarly, only wind directions for which $C_{\check{p}}$ is negative contribute to predictions of peak suctions.

C.5 General Characteristics of the Pressure Response

The unsteady (i.e. time-varying) pressures or suctions are due to the natural gustiness of the wind and the unsteady character of the flow within the wake formed by the structure. Typically, peak suctions or pressures, over the period of an hour, can be several times the value of the average pressure for that hour.

As seen from plots of the pressure coefficients versus azimuth for numerous previous tests, measurements at 10° intervals are adequate to describe the azimuthal variation of the facade pressures. More detailed measurements are not found to substantially alter the predicted pressures and suctions. This might be expected since turbulent fluctuations of the flow cause momentary changes in wind direction in excess of 10°, a phenomenon which is reproduced in the model simulation.

C.6 Predictions of Peak Pressures and Suctions

Predictions of expected local pressures relevant to the design of cladding elements are determined by the integration of the gradient wind statistics with the experimental aerodynamic pressure as described in detail in Appendix D.

It is not completely determined within the current state-of-the-art what local pressure is most meaningful for cladding design, when the complexities of the total interaction are considered. Nevertheless, there are two reasonable alternatives available. The first utilizes the concept of the peak factor, *g*, defined such that the *design peak* = |*mean*| + *g(rms)* where *g* can be chosen simply as representative of conservative experimental values [Reference C-2] or to allow for material resistance properties as discussed in Reference C-3. The latter approach often suggests considerably lower values of *g* than the former. The second alternative is to use the actually-measured peak values themselves when available, although these are subject to considerably more statistical scatter than rms or average *g* values. However, for the methodology considered here, the associated integration over all azimuths effectively reduces this scatter. Hence this approach appears well suited to provide a conservative estimate for local cladding loads, independent of cladding response considerations, and is generally adopted for design studies of buildings.

C.7 Limitations on the Predicted Peak Pressures and Suctions

Values of predicted pressures and suctions do not constitute wind-induced pressures for a particular wind direction but reflect pressures which may arise from many combinations of wind speed and wind

direction. Furthermore, it should be noted that all data are wind-induced pressures on the exterior surfaces of the building taken with respect to the mean ambient static pressure in the undisturbed wind flow. In the use of these data for the design of individual cladding components an allowance should thus be made for interior pressures over and above this ambient value (see Appendix E). The local peak pressures do not occur simultaneously over the entire exterior of the building and are thus not intended to be used to provide estimates of overall unsteady wind loads.

Also note that frequency limitations of the experimental system (see section C.2) and other factors imply that the peak pressures reflect peaks that are sustained for at least one second, but may last for considerably longer periods of time (typically in the order of 3 to 4 seconds). Furthermore, the estimated pressures include no allowance for possible resonance or other material response characteristics.

References

(C-1) Lieblein, J. “Efficient Methods of Extreme-Value Methodology”, Technical Report NBSIR 74-602, National Bureau of Standards, Washington, D.C., October 1974.

(C-2) Davenport, A. G., Isyumov, N. and Jandali, T., "A Study of Wind Effects for the Sears Project", University of Western Ontario, Engineering Science Research Report, BLWT-5-1971.

(C-3) Davenport, A. G., Discussion of paper, "Wind Pressures on Buildings - Probability Densities", by Peterka, J. A. and Cermak, J. E., Proc. Paper 11373, Journal of the Structural Division, ASCE., Vol. 101, No. ST6, June 1975. Discussion in Journal of the Structural Division, ASCE, Vol. 102, No. ST11, November 1976.

APPENDIX D

PREDICTING PEAK RESPONSES FOR VARIOUS RETURN PERIODS

D.1 Introduction

The wind tunnel testing provides information on the dependence of particular response parameters on wind speed and direction. In order to make the most rational use of the aerodynamic information from the wind tunnel test, it is necessary to synthesize it with the actual wind climate characteristics at the site to produce predictions of responses for various return periods. The wind climate characteristics necessary to define are those governing wind speed and direction at a suitable height above ground level at the site. The joint probability distribution of wind speed and direction thus defines the wind climate, whereas all of the aerodynamic information, which includes sensitivities to a project's orientation and to its surroundings, is contained in the wind tunnel data. The derivation of such probability distributions is discussed in Appendices A and B.

A number of prediction methods may be used to derive design values from the aerodynamic data and the wind climate information. They are summarized in Reference D-1. This appendix discusses the upcrossing method used at the Boundary Layer Wind Tunnel Laboratory, which deals with the synthesis of the wind tunnel data with wind climate model to produce predictions for various return periods.

D.2 The Prediction Process

To illustrate the prediction process, the example of predicting a peak local pressure at a point on a building is used. Essentially, the same process is used for predicting any response. The process is illustrated in Figure D.1, and is explained below.

Figure D.1a illustrates a wind tunnel test in which turbulent wind, blowing from a particular azimuth, α, impacts a building, giving rise to some time-varying pressure distribution over the building's surfaces. The pressure fluctuations measured at the particular point shown in the illustration is denoted $p(t)$. The variation of this pressure with time is shown in Figure D.1b. The average pressure over the sampling time period is shown as $\bar{p}$ and the largest, or peak, pressure in this time period is shown as $\breve{p}$. These pressures can be normalized by the reference dynamic pressure, $\frac{1}{2}\rho V^2$ to form mean and peak pressure coefficients for this azimuth, α, as shown. This process can be repeated for a full range of azimuths to obtain mean and peak pressure coefficients at all azimuths. A plot of such coefficients is shown in polar form in Figure D.1c. These constitute the aerodynamic data from the wind tunnel test.

The next step in the prediction process is to choose a full-scale peak pressure level, say 1 kPa. The full-scale velocity required to produce this pressure level at a particular azimuth can be determined from the peak pressure coefficient measured at that angle, by simply rearranging the definition of the pressure coefficient (as shown below Figure D.1c). This can be repeated at all azimuths to yield a velocity contour for that pressure level. Similar contours can be developed for other pressure levels; Figure D.1f shows some of these contours. Each of these velocity contours can be combined with the probability distribution of wind speed and direction (shown in Figure D.1d) to determine the probability of exceeding the particular pressure level. This is accomplished for a particular pressure level by summing over all azimuths the probability of exceeding the velocities on the velocity contour for that pressure level. This is shown in Figure D.1e. The result is the parent probability distribution of pressure, given in Figure D.1g, which describes the total fraction of the time that the particular pressure level is exceeded. It does not, however, indicate how often this happens; whether for a single long period or many short periods. To

determine the return period associated with a particular pressure level, the rate of outward crossing of its velocity contour is needed. The formula for this value is shown in Figure D.1h and is derived below.

D.3 The Rate of Up-crossing of Peak (Maximum or Minimum) Response Values

The expected number of excursions beyond a level x per unit time, or the rate of crossing with positive slope, according to Rice's theory (D-2), is given by:

$$N_x(x) = \int_0^\infty \dot{x}\, p(x, \dot{x})\, dx \tag{D.1}$$

where $\dot{x}$ is the rate of change of x and $p(x, \dot{x})$ is the joint probability density function of x and $\dot{x}$. For a stationary random process, x and $\dot{x}$ are statistically independent, thus

$$p(x, \dot{x}) = p(x)\, p(\dot{x}) \tag{D.2}$$

For a Gaussian process,

$$\int_0^\infty \dot{x}\, p(\dot{x})\, d\dot{x} = \frac{\sigma_{\dot{x}}}{\sqrt{2\pi}} \tag{D.3}$$

where $\sigma_{\dot{x}}$ is the standard deviation of $\dot{x}(t)$. Thus, the crossing rate now becomes

$$N_x(x) = \frac{\sigma_{\dot{x}}}{\sqrt{2\pi}}\, p(x) \tag{D.4}$$

The statistical frequency or the cycling rate of process $x(t)$ is defined as

$$\nu = \frac{1}{2\pi}\ \frac{\sigma_{\dot{x}}}{\sigma_x} \tag{D.5}$$

Substituting this in equation D.4 yields

$$N_x(x) = \sqrt{2\pi}\ \nu\, \sigma_x\, p(x) \tag{D.6}$$

Extending Rice's theory, Davenport (D-3) has shown that for a two-dimensional variable, $x = x(V, \alpha)$, the crossing rate of a particular boundary $x = x_1$ becomes:

$$N_x(x) = \sqrt{2\pi}\ \nu\, \sigma \int_0^{2\pi} \sqrt{1 + \left(\frac{d V_1}{V_1\, d\alpha}\right)^2}\ p_V(V_1, \alpha)\, d\alpha \tag{D.7}$$

where $x_1 = x(V_1, \alpha)$ and $p_V(V, \alpha)$ is the joint probability density function of V and α.

Approximating the probability distribution of the wind speed V and the direction α by a generalized Weibull distribution,

$$p_V(>V, \alpha) = A(\alpha)\, e^{|V/C(\alpha)|^{K(\alpha)}} \tag{D.8}$$

the probability density function of V and α becomes

$$p_V(V,\alpha) = A(\alpha)\frac{K(\alpha)}{C(\alpha)}\left(\frac{V}{C(\alpha)}\right)^{|K(\alpha)-1|} e^{-|V/C(\alpha)|^{K(\alpha)}}\, d\alpha \tag{D.9}$$

Hence the crossing rate of a particular boundary $x_1 = x_1(V_1, \alpha)$ from Equation D.7 becomes:

$$N_x(x_1) = \sqrt{2\pi}\ \nu\ \alpha \int_0^{2\pi}\left\{1 + \frac{d\,V_1}{V_1\, d\alpha}\right\}^{\frac{1}{2}} A(\alpha)\frac{K(\alpha)}{C(\alpha)}\left(\frac{V}{C(\alpha)}\right)^{|K(\alpha)-1|} e^{-|V/C(\alpha)|^{K(\alpha)}} d\alpha \tag{D.10}$$

The cycling rate, ν, and the standard deviation, σ, in Equation D.10 are taken as those of the wind speed, V, regardless of direction; namely they are based on the marginal statistical properties of V and $\dot{V}$. With ν expressed in terms of occurrences per annum, $N_x(x_1)$ gives the yearly crossing rate.

The return period, or the average interval of time between events during which the response equals or exceeds the response boundary $x = x_1$, is the inverse of the crossing rate of that boundary. Consequently, from Equation D.10 the return period for the response level $x = x_1$ in years is taken as

$$R_x(x_1) = \frac{1}{N_x(x_1)} \tag{D.11}$$

The risk of exceeding the response level associated with the return period $R_x(x_1)$ in a time period L is:

$$r(x_1) = 1 - \left(1 - \frac{1}{R_x(x_1)}\right)^L \tag{D.12}$$

From the above equation, the risk of exceeding x_1 within a time interval of $L = R_x(x_1)$ is approximately 63 percent.

References

(D-1) Irwin, P, Garber, J and Ho, E., “Integration of Wind Tunnel Data with Full Scale Wind Climate”, 10th Americas Conference on Wind Engineering, Baton Rouge, Louisiana, U.S.A., May 2005.

(D-2) Rice, S.O., "Mathematical Analysis of Random Noise", Bell Tech. Journal Vol. 18 and 19, 1945.

(D-3) Davenport, A.G., "The Prediction of Risk Under Wind Loading", 2nd International Conf. on Structural Safety and Reliability (ICOSSAR), Sept. 1977, Munich Germany.

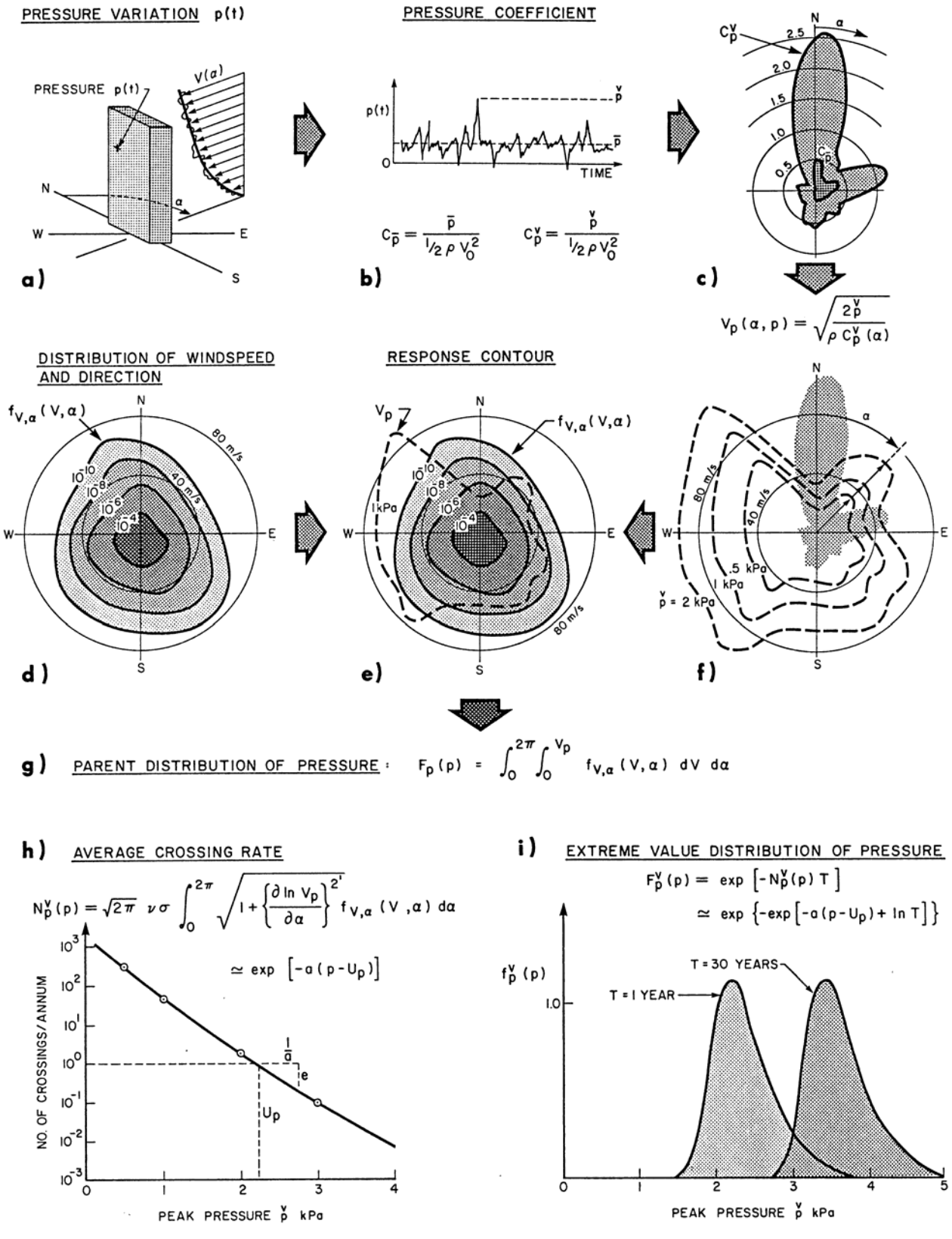

FIGURE D.1 ILLUSTRATION OF THE PREDICTION PROCESS

APPENDIX E

STORM PASSAGE PREDICTIONS OF WIND LOADS AND RESPONSES

E.1 Overview

Predictions of wind loads and load effects for full-scale buildings and structures are made by combining the azimuthal variation of wind loads and load effects from wind tunnel tests with statistical information on winds in the project area. For regions where extra-tropical winds dominate, historical records of wind speed and direction are used to develop statistical models of the wind climate. At the Boundary Layer Wind Tunnel Laboratory (BLWTL), available records of hourly wind speed and direction are used to arrive at a parent probability distribution of hourly mean wind speeds and directions. Extreme wind loads and load effects are then predicted using the crossing-rate theory developed by Rice (E-1) and adopted to wind engineering applications by Davenport (E-2, E-3). This method is presented in more detail in another appendix.

A similar statistical approach can also be used for regions where high winds are due to tropical storms. However, rather than relying on historical records of wind speed and direction at specific locations, regional statistical properties of tropical storms are assembled and then used in Monte Carlo computer simulations to generate and track the passage of such storms over many thousands of years.

Signatures of tropical storms show that near-maximum wind speeds can be experienced at a particular location within the same storm for substantially different wind directions. This is illustrated in Figure E.1 which shows the observed wind speed and wind direction at two weather stations in Hong Kong during Typhoon York. At Waglan Island and Cheung Chau, the highest wind speeds were observed some 6 hours apart with wind directions changing from north to south. Depending on the directional characteristics of a particular structural response, this provides more opportunities for the wind storm to effect extreme load effects.

The approach for tracking wind-induced loads and responses of buildings and structures during the passage of individual storms and the subsequent prediction of extreme values using the theory of Poisson arrivals is described by Isyumov et al (E-4). The following description uses excerpts from that paper.

E.2 Extreme-value Predictions from Time-domain Analysis

The wind-induced responses of a building or structure, including deflections, moments, accelerations and local pressure can be assembled at every time step k during a typhoon j. For any particular response, this can be written as,

$$x_{j,k} = \phi_{x_1}\left(V_{j,k}, \alpha_{j,k}\right) \tag{E.1}$$

where ϕ, is a response function predetermined from the wind tunnel study; and $V_{j,k}$ and $\alpha_{j,k}$ are the mean wind speed and wind direction at every time step k during storm j.

Tracking each storm, the maximum value of the response during each storm is determined. This maximum is denoted as $\hat{x}_j$ for storm j. Denoting the average occurrence rate of typhoons or hurricanes as λ storms/year, the number of storms during n years becomes $N = \lambda n$. Typically n = 10,000 years; λ = 2 storms/year.

The Poisson Distribution is commonly used to predict the occurrence of rare events such as earthquakes, extreme floods, traffic accidents, etc. It is also a good mathematical model for predicting the consequences of typhoons or hurricanes. The approach taken is as follows:

The cumulative distribution of the storm maximum responses, $\hat{x}_{j=1,N}$ is determined and denoted as $F(\hat{x})$. As defined earlier $N = \lambda n$ where n is the number of years in the simulation. The expectation of not exceeding a response level of $\hat{x}_j = \hat{x}_1$ during any storm becomes $F(\hat{x}_1)$.

The corresponding expectation of exceeding $\hat{x}_1$ during any year becomes

$$\nu_{\hat{x}_1} = (1 - F(\hat{x}_1))\lambda \tag{E.2}$$

where λ is the average number of storms per year.

If there are no exceedances or "crossings" of $\hat{x}_1$ during any year, it can be concluded that $\hat{x}_1$ is the maximum value with an annual probability determined from the Poisson distribution to be

$$P_{\hat{x}}(\hat{x} \le \hat{x}_1) = \frac{(\nu_{\hat{x}_1})^0 e^{-\nu_{\hat{x}_1}}}{0!} = e^{-\nu_{\hat{x}_1}} \tag{E.3}$$

The corresponding annual probability of exceedance is

$$P_{\hat{x}}(\hat{x} > \hat{x}_1) = 1 - e^{-\nu_{\hat{x}_1}} \tag{E.4}$$

The return period associated with $\hat{x}_1$ becomes

$$R_{\hat{x}_1} = \frac{1}{1 - e^{-(1-F(\hat{x}_1))\lambda}} \tag{E.5}$$

Extremes determined from Poisson arrivals have a firm analytical basis and provide good estimates of extremes for return periods of interest.

E.3 Examples of Predictions of Wind Loads and Effects

Investigation at the BLWTL indicates that a time-domain analysis, which tracks the impact of particular typhoons or hurricanes, can result in predicted wind loads and effects which are larger than obtained with a conventional analysis. The principal reason for this appears to be the greater importance of changes in wind direction experienced during tropical storms. A particular building can be subjected to near storm maximum wind speeds over a band of wind direction, typically ranging up to 180°. Depending on the directional characteristics of the response, this can result in an extreme response that is greater than the response that occurs at the time of the maximum wind speed.

The influence of the directional characteristics of the response on predicted extremes has been studied for two tall buildings, assumed to be located in Hong Kong and in Shanghai. Also examined are generic response signatures, with a dependence on wind speed and a broad range of directional dependence. These generic responses were assumed to be of the form,

$$x_i(V, \alpha) = a_i(\alpha) V^{b_i(\alpha)} \tag{E.6}$$

where $a_i(\alpha)$ is a relative shape function of response quantity i and $b_i(\alpha)$ expresses its velocity dependence. The velocity exponent $b_i(\alpha)$ was not varied with wind direction, namely it was taken as

$b_i(\alpha) = b_i$ using values of 2, 2.5 and 3.0 for local pressures, base moments and torque and accelerations respectively. The shape function was taken to be of the form

$$a_i(\alpha) = a_{1_i} + a_{2_i} e^{-(\alpha / B_i)^2} \qquad \text{(E.7)}$$

where a_{1_i} is a constant varied to represent the average or base response, a_{2_i} is the amplitude of a local peak response with half maximum amplitude bandwidth of B_i.

Typical generic response shapes are shown in Figure E.2. Typical peak local suctions were assumed to have either singular or double peaks of different bandwidth B. Peak local pressures were assumed to have relatively broad single peaks. Peak moments and accelerations were taken to have single or double peaks at 180° apart. The base torque tends to have the greatest directional variation and typical response shapes were taken as double peaks at 180° apart or four peaks spaced at 90o. In all cases the maximum value of $a_i(\alpha)$ was normalized to unity. The position of the peak in each response shape, denoted as α_m, was varied in 40° increments over the entire compass. In all cases response predictions were made using the conventional method and by tracking the effects of each simulated storm. The time step in this analysis was taken as 1 hour. All extreme value predictions from the time domain analysis are based on Poisson arrivals described above.

Figure E.3 summarizes the results of this analysis using generic wind load and wind effect signatures. Frequency distributions of r, the ratio of each predicted quantity obtained from storm passages relative to the standard or conventional prediction, are given for 10-year return period corner accelerations, 50-year overturning moments and the 50-year torque. Average values of r are seen to be systematically greater than 1, with a highest mean value of $\mu = 1.24$ for base moments in Shanghai. Figure E.4 shows similar comparisons for buildings A and B with specific response properties, located either in Hong Kong and in Shanghai. All results have been normalized by predictions made with the conventional BLWTL methodology. The trends are similar to those observed for the generic responses in Figure E.3. Finally, Figure E.5 shows similar comparisons of predicted peak local pressures and suctions. Data are shown for Building A using actually measured pressure coefficients, and for generic peak pressures and suctions shapes. Again the time domain predictions tend to be higher than those made with standard or conventional procedures.

E.4 Wind Directionality

The results of the above analyses show that the time-domain approach, which actually tracks the impact of particular storms, tends to result in larger predictions for responses which have a pronounced directional variation. In other words, tropical storms which have a greater directional swing during their passage are more effective in finding critical directions. The normally assumed benefits of wind directionality are therefore reduced in regions where tropical storms are dominant.

This trend of a reduced benefit of directionality is illustrated in Figure E.6 which shows directionality factors for generic accelerations, overturning moments, base torque and local pressures. The directional factor for response quantity i is defined as the ratio of the actually predicted response for a return period of 50 years to the response calculated using the 50-year velocity pressure and the maximum value of the aerodynamic coefficient for response quantity i. A systematic increase in K_D is obtained using the storm passage analysis method. The value of $K_D = 0.85$, suggested in ASCE 7-05 for the main wind force resisting system of buildings and its components and claddings is shown for comparison. While relatively conservative for extra-tropical wind climates for which the conventional extreme value analysis was developed, the value of $K_D = 0.85$ still nearly envelops directional benefits in hurricane or typhoon regions.

All time-domain response predictions presented above have been based on a 1-hour time step. The BLWTL storm passage tracking procedure has since been improved to use a smaller time step of 20

minutes which better captures the variability of the storm impact on buildings and structures and provides a more complete detailed description of the response with time. This permits improved predictions of non-linear structural actions and the accumulation of stress reversal and fatigue damage.

In some climatic regions, extreme wind-induced loads and effects occur due to the combined influence of tropical and extra-tropical winds. In such wind climates, it is necessary to recognize that both tropical and extra-tropical winds contribute to the probability of exceeding particular wind loads and effects. The approach followed in such combined climate situations is as follows:

$$P_{Total}(< x_1) = P_t(< x_1)\, P_{nt}(< x_1) \tag{E.8}$$

where $P_{Total}(< x_1)$ is the total annual probability of not exceeding a wind load or wind-induced effect of $x = x_1$ due to the action of all winds; and where $P_t(< x_1)$ and $P_{nt}(< x_1)$ are the annual probabilities of not exceeding x_1 during tropical and extra-tropical winds respectively.

REFERENCES

(E-1) S. Rice, Mathematical analysis of random noise, Bell System Tech. J., 23 (1944) 282-332 and 24 (1945) 46-156.

(E-2) A.G. Davenport, The dependence of wind loads on meteorological parameters, Proc. Int. Res. Sem. On Wind Effects on Buildings and Structures, Univ. of Toronto Press, Ottawa, 1967, Vol. 1, pp. 19-82.

(E-3) A.G. Davenport, The prediction of risk under wind loading, Proc. 2nd Int. Conf. on Structural Safety and Reliability. Munich, 1977, pp. 511-538.

(E-4) N. Isyumov, M.J. Mikitiuk, P.C. Case, G.R. Lythe and A. Welburn. Prediction of wind loads and responses from simulated tropical storm passages. Proc. 11th Int. Conf. on Wind Engineering, Lubbock, May 2002. CD-ROM.

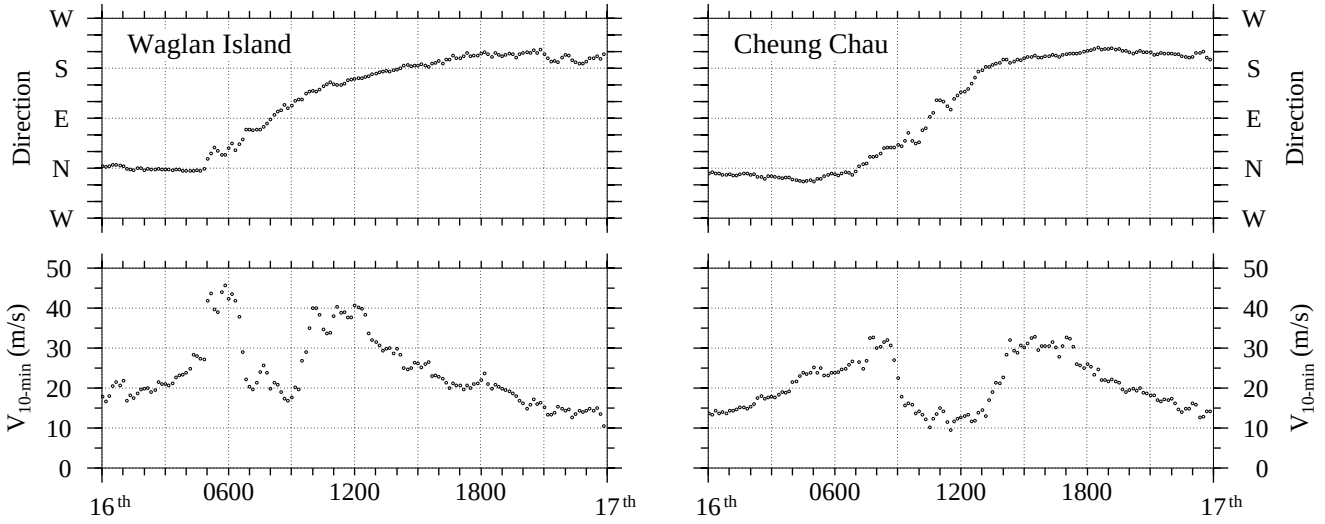

FIGURE E.1 OBSERVED 10-MINUTE AVERAGE SURFACE WIND SPEED AND WIND DIRECTION AT HONG KONG DURING TYPHOON YORK (SEPTEMBER 16, 1999).

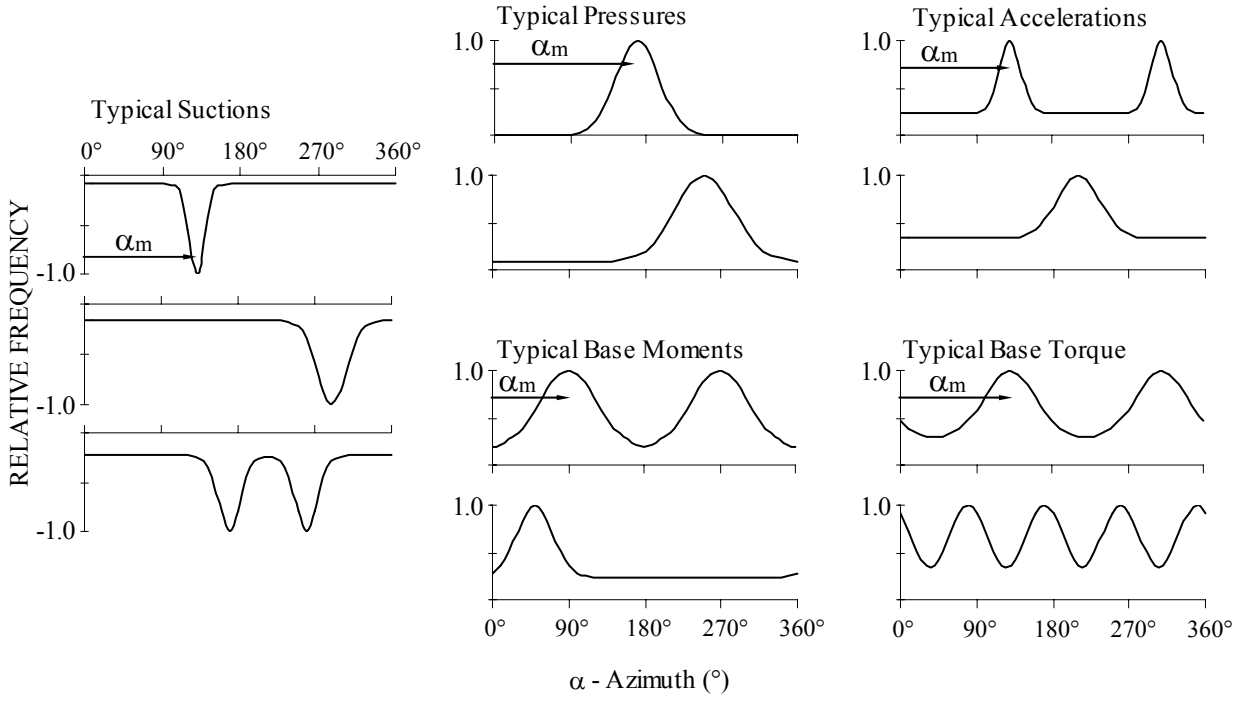

FIGURE E.2 TYPICAL WIND INDUCED RESPONSE SHAPES

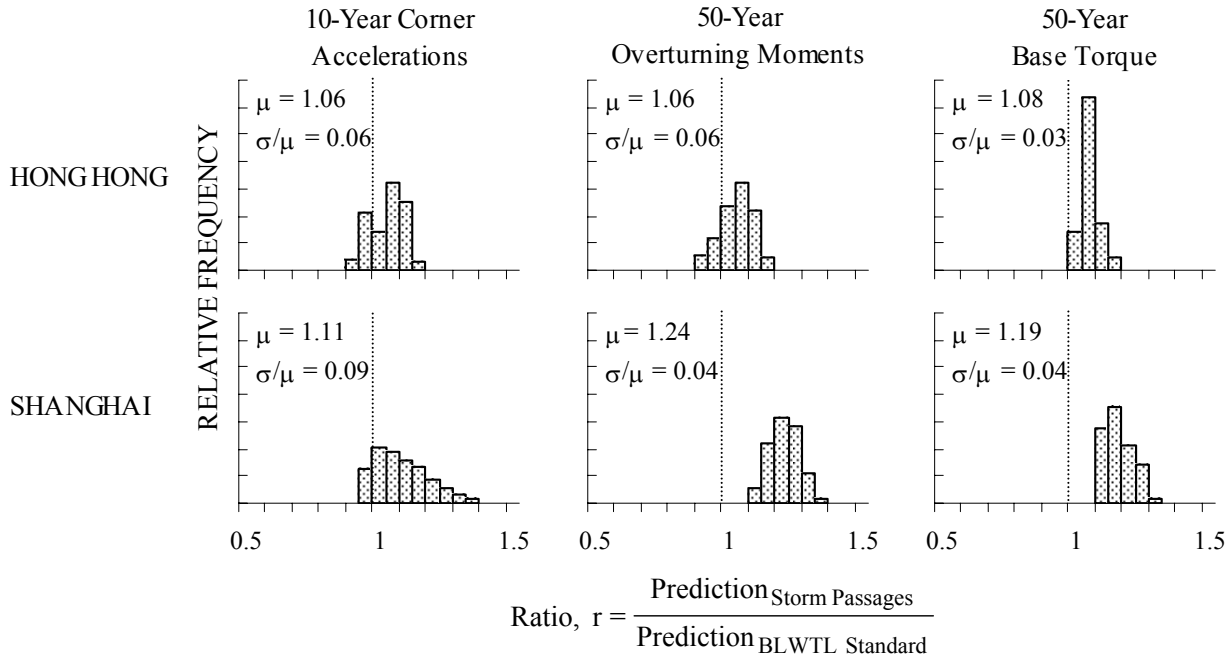

FIGURE E.3 COMPARISON OF GENERIC WIND LOADS AND EFFECTS PREDICTED FOR DIFFERENT WIND DIRECTIONS USING CONVENTIONAL STATISTICAL METHODS AND TRACKING THE EFFECTS OF INDIVIDUAL STORMS

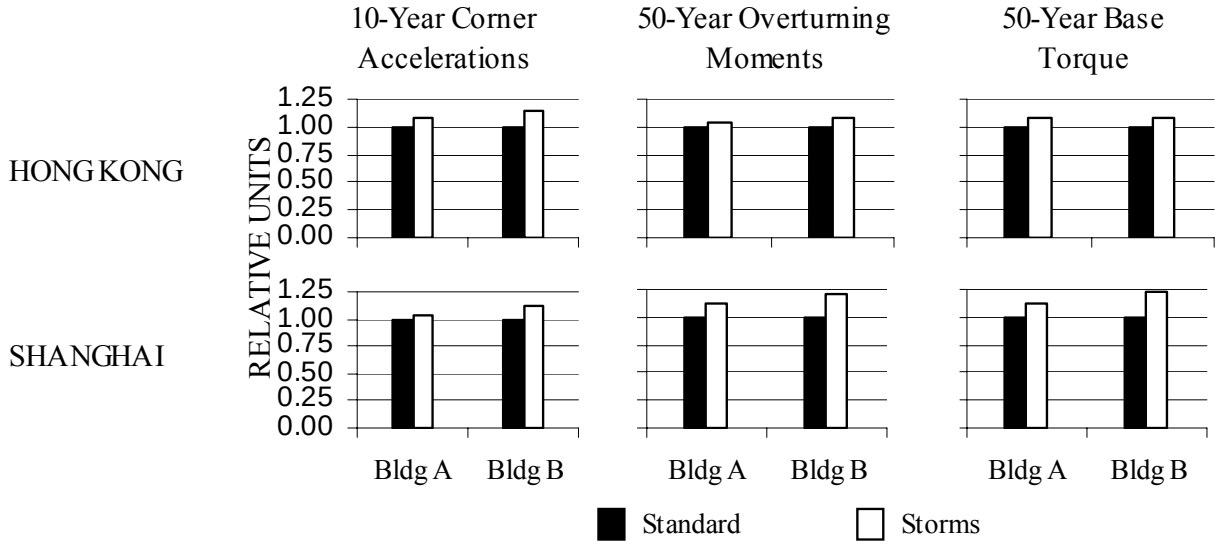

FIGURE E.4 COMPARISON OF PEAK STRUCTURAL WIND LOAD EFFECTS FOR BUILDINGS A AND B HYPOTHETICALLY LOCATED IN DIFFERENT WIND REGIONS PREDICTED BY CONVENTIONAL STATISTICAL METHODS AND BY TRACKING THE EFFECTS OF INDIVIDUAL STORMS

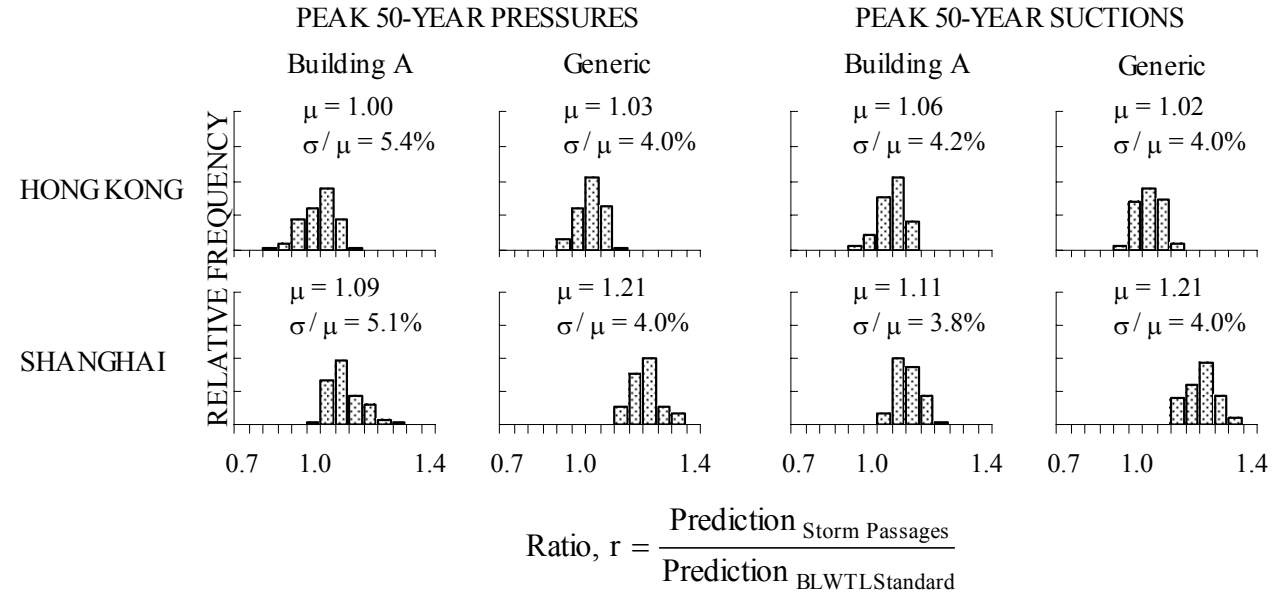

FIGURE E.5 COMPARISONS OF PREDICTED LOCAL PEAK PRESSURES AND SUCTIONS FOR A SPECIFIC BUILDING AND FOR A GENERIC PRESSURE COEFFICIENT DATA SET IN DIFFERENT WIND REGIONS USING CONVENTIONAL STATISTICAL METHODS AND BY TRACKING THE EFFECTS OF INDIVIDUAL STORMS

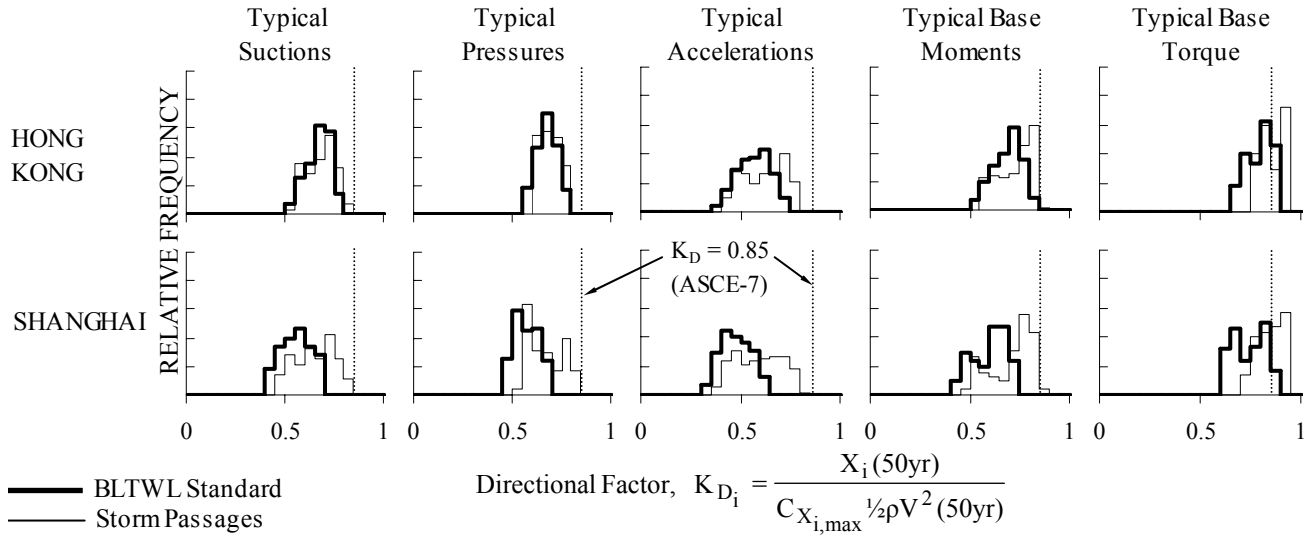

FIGURE E.6 DIRECTIONALITY FACTORS FOR GENERIC PEAK STRUCTURAL LOADS AND RESPONSES USING CONVENTIONAL PREDICTIVE METHODS AND STORM PASSAGE TRACKING

APPENDIX F

DETERMINATION OF INTERNAL PRESSURE COEFFICIENTS AND THE FORMATION OF DIFFERENTIAL PRESSURE COEFFICIENTS

F.1 Summary

This appendix describes an approach to the determination of internal pressure coefficients from the measured external pressure coefficients. Also described is the formation of differential pressure coefficients from these calculated internal pressure coefficients and the measured external pressure coefficients. The methodology used here is based on Reference F-1 and this appendix is largely excerpted from there.

F.2 Introduction

Estimates of internal pressures are needed in determining net wind loads for the design of the cladding and glazing of buildings. Although estimates of internal pressures may be obtained from building code specifications, the extensive coverage of external pressure measurements from wind tunnel studies allowing much better estimates of internal pressures for use with the measured external pressures. Their accurate determination is also important with respect to energy conservation since the leakage of air through the building skin will be proportional to the difference between the external and internal pressures.

Although the importance of determining internal pressures is clear, it is not a quantity which can be determined exactly. In fact, internal pressures are influenced by many factors which are uncertain in themselves, such as the character of the leakage paths or whether windows or other exterior openings will be left open or will be broken during wind storms. The complex distribution of exterior pressures and the influence of the dynamic exterior pressures on the internal pressures must also be taken into account.

In spite of these difficulties, reasonable estimates of the internal pressure can be determined which take them into account. This requires that the uncertainties be expressed in statistical terms. In the following sections, mean internal pressures are examined both for buildings with uniformly distributed leakage and for buildings with large openings. Fluctuating internal pressures are also briefly examined.

F.3 Mean Internal Pressures: Distributed Leakage

It has been determined experimentally (see Reference F-1) that the following relationship holds

$$Q = c\, A\, (\Delta p)^n \tag{F.1}$$

where Q is the air leakage rate through the exterior wall; c is a flow coefficient; A is the area of the exterior wall; p is the pressure difference across the exterior wall; and n is a flow exponent. Although the flow exponent can vary over the range of 0.5 to 1.0, buildings with HVAC systems appear to converge on a value of 0.65.

This equation can be used to estimate the internal pressure by noting that the net volume flow over all the building surfaces must be zero. With the statistical distribution of the external pressure coefficients (C_p's) given by $f\, C_p\, (C_p)$, and using equation F.1, then the net volume flow is,

$$Q(m) = A\,c \int_{-\infty}^{\infty} (C_p - C_{pi})^{1-m} f_{C_p}(C_p)\, d\, C_p \tag{F.2}$$

where C_{pi} the internal pressure coefficient, m is a variable equal to $1-n$, and the integration is over the entire range of external pressure coefficients. The first term of a Taylor expansion on m is,

$$Q(0) = A\,c \int_{-\infty}^{\infty} (C_p - C_{pi})\, f_{C_p}(C_p)\, d\, C_p = 0 \tag{F.3}$$

or

$$C_{pi} \approx \int_{-\infty}^{\infty} C_p\, f_{C_p}(C_p)\, d\, C_p$$
$$\approx E(C_p)$$

This expected value of C_p, which is simply the spatial average of the exterior mean pressure, is a first approximation to C_{pi}.

The next term of the Taylor expansion provides a further correction which can be easily shown to be:

$$C_{pi} = E(C_p) - m\,\sigma_{C_p} \int_{-\infty}^{\infty} \theta\, ln\,|\theta|\, f_\theta(\theta)\, d\theta \tag{F.4}$$

in which the reduced pressure term is represented by

$$\theta = \frac{|C_p - E(C_p)|}{\sigma_{C_p}}$$

where σ_{C_p} is the standard deviation of the C_p distribution.

The standard deviation of the distribution of the mean external pressures also provides us with a first approximation to the variability or uncertainty of the mean internal pressure coefficient; specifically, for the situation in which one window, selected at random, is left open in an otherwise sealed building. Because of background leakage and other practical considerations, this is a severe assumption even in a building in which windows can be opened. A proposition of N independent leakage paths thus reducing the standard deviation by $1/\sqrt{N}$, is probably closer to the mark. If $N = 4$, the standard deviation is halved; for $N = 25$, the standard deviation is reduced to 20%.

For buildings in which the windows do not open, the variability depends only on the variability in the leakage distributions. The standard deviation of C_{pi} would, under most practical circumstances, appear to be much smaller, even negligible.

F.4 Mean Internal Pressures: Large Openings

If a building has a single large opening of area a_1 under a local mean pressure coefficient C_{p_1}, with no other leakage, then the mean internal pressure must be equal to C_{p_1}. However, in practice, this case is unlikely to occur since there will also be distributed leakage through the rest of the skin of the building. The resulting internal pressure, C_{p_i} for this case is given approximately by

$$a_{equiv}\sqrt{C_{p_{i_0}} - C_{p_i}} = a_1\sqrt{C_{p_1} - C_{p_i}} \tag{F.5}$$

where $C_{p_{i_0}}$ is the mean internal pressure without the large opening and a_{equiv} is the area equivalent to the distributed leakage paths. The equivalent area for tall buildings is given by the following relationship (see Reference F-1):

$$a_{quiv} \approx 0.0006\, A_w$$

where A_w is the area of the wall or walls through which leakage is occurring.

Since C_{p_i} must lie between $C_{p_{i_0}}$ and C_{p_1}, the sign of one of the terms is negative and we can easily show that,

$$C_{p_i} = \frac{a_1^2\, C_{p_1} + a_{eq}^2\, C_{p_{i_0}}}{a_1^2 + a_{eq}^2} \tag{F.6}$$

If the location of the large opening is unknown, as in the case of accidental window breakage, the above relationship can still be used to determine the range of internal pressure, both with and without the background leakage.

Without the background leakage, the expected value of the mean internal pressure coefficient is $E(C_p)$, that is the mean value of the external pressure coefficient. The standard deviation is σC_p, i.e. that of the mean external pressure coefficients. With the distributed leakage, the expected internal pressure is again $E(C_p)$ but the standard deviation of the mean internal pressure coefficient is $\sigma C_p\, a_1^2 \,/\, (a_1^2 + a_{eq}^2)$. Clearly, if the position of the opening is known and it can be linked systematically with the wind direction, this range in the pressure coefficient can be cut down.

F.5 Fluctuating Internal Pressures

Due to the fluctuating nature of the external pressures some of these fluctuations will be transmitted to the internal pressure. The exact nature of the transmission will depend on the leakage path and size of openings (see Reference F-1).

In the case of distributed leakage, experimental data have shown that the amplitude of the internal fluctuating pressure is much smaller than that of the external pressure. This means that, when the internal pressure is subtracted from the external pressure, the amplitude of the fluctuating pressure difference will differ little from the external fluctuating pressure, since the internal and external fluctuating pressures add more or less as the square root of sums of squares. This is the situation expected for a tall building, even if some openings are present, as long as the area considered is well away from the openings. Thus peak differential pressures can be formed by subtracting mean internal pressures from the peak external pressures.

If large openings are present on the facade of a tall building, say due to storm damage, local internal pressure fluctuations will be similar to the local external pressure fluctuations but attenuated at high frequencies. This may lead to local differential pressures higher than expected in other local areas of the building and hence may cause a secondary failure; however, it is fairly clear that the secondary failure, if induced by this mechanism, then stops any further cascade - i.e. the internal pressure stabilizes near the expected values. Such local problems are beyond the scope of the current calculations.

F.6 Forming Differential Pressure Coefficients at BLWTL

In designing the cladding and glazing of a building, it is the difference between the external and internal pressure that is of interest. This difference is the net load that the element will be subjected to.

The external pressures are measured directly in the wind tunnel. The internal pressures are determined from these external pressures using the methodology described in the previous sections. The internal pressures may then be subtracted from the external pressures to form differential pressures. Details of this procedure are described below.

For the uniform leakage case, the mean internal pressure coefficient is determined from equation F.4, which includes the second order correction (equation F.6 is used when there are predetermined large openings). The standard deviation of the mean internal pressure coefficient, σC_{pi} , is simply derived from the standard deviation of the mean external pressure coefficients (except when there are large openings - see section F.3 above), by dividing it by the square root of the number of leakage paths. Using these mean and standard deviation mean internal pressure coefficients, upper and lower bound mean internal pressure coefficients can be calculated as follows:

$$\left(C_{pi}\right)_{lower} = C_{pi} - 3.5\ \sigma C_{pi}$$
$$\left(C_{pi}\right)_{upper} = C_{pi} + 3.5\ \sigma C_{pi} \qquad \text{(F.7)}$$

These coefficients represent the likely bounding values associated with inhomogeneities of the leakage paths. Clearly, if the building skin is uniformly porous, the number of leakage paths is infinite. A more conservative number of 25 is more typical, and allows for some residual time variation of the internal pressures which is not directly computable.

These coefficients are then subtracted from the external pressure coefficients as follows:

$$\left(\hat{C}_p\right)_{diff} = \left(\hat{C}_p\right) - \left(C_{pi}\right)_{lower}$$
$$\left(\breve{C}_p\right)_{diff} = \left(\breve{C}_p\right) - \left(C_{pi}\right)_{upper}$$

Finally, these differential pressure coefficients are integrated with the meteorological data to provide predictions of differential pressures for various return periods, using the methodology described in Appendix D.

In consideration or larger openings either due to operable windows being left open or due to breach of the building envelope, the single opening case is considered critical for design. The typical size of an opening such as operable windows or doors can usually be classified as large openings relative to the interior volume; as discussed above. The external pressure at the opening is assumed to transmit into the interior volume without dynamic amplification. A conservative assumption is made that there is also no attenuation to the dynamic pressure transmitted. The net differential pressures may be calculated by differencing the external pressure for any location in the building and the pressure at the assumed large opening location. The critical pairs of locations are often on wall surfaces on adjacent walls forming a corner unit.

A simple but conservative estimate may be made by taking 100% of the predicted pressure at the design location and add 80% of the predicted suction at the large opening, and vice versa. This takes into account the unlikely simultaneously occurrence of the peak pressure and peak suction at different building locations, and particularly on different building faces.

F.7 Limitations of Predicted Differential Pressures

The internal pressures calculated here are strictly those induced by wind and do not include stack effects or the direct effect of mechanical systems. This latter effect is likely to be small. Nor do the internal pressures calculated here include any effects of interior partitions and other restrictions of interior air flows, which could lead to considerably higher loads in special cases. For example a corner office which lost a light in a cornering wind would immediately be subjected to an interior pressure equivalent to the exterior pressure existing at the broken light. This could be of opposite sign to the exterior pressures on other lights in the office (around the corner). If the office were reasonably sealed, then the pressure alleviation associated with the total volume and the normal leakages of the entire building might not come into play. This might then lead to a secondary failure; however, at that point one would expect the "domino" process to stop. Other general limitations are the same as those listed for external pressures in Appendix C.

References

(F-1) Davenport, A.G. and Surry, D., "The Estimation of Internal Pressures Due to Wind With Application to Cladding Pressures and Infiltration", Presented at the ASCE Structural Engineering Conference, Houston, Texas October 1983.

APPENDIX G

DETERMINATION OF TOTAL DYNAMIC LOADS USING A RIGID MODEL/FORCE BALANCE TECHNIQUE

G.1 Summary

This Appendix describes an approach to the prediction of the dynamic response of structures to wind loads using rigid foam models mounted on a sensitive, high-frequency balance. The force balance, models, and instrumentation are described and applications are illustrated. This Appendix is largely excerpted from Reference G-1.

G.2 Introduction

Steady progress has been made in the description of the response of taller buildings to wind (see references G-2 and G-3). The main components of the response come from each of the fundamental modes, excited by their respective modal forces. The mechanical transfer function, relating the load function to the response, is straightforward. On the other hand, the aerodynamic transfer function, relating the gust structure to the wind induced forces is difficult to establish without wind tunnel model tests. A further complication exists if body motion effects interact with the load function (aerodynamic damping).

Multi-degree-of-freedom aeroelastic models have traditionally been used to study the action of wind on sensitive buildings and structures. While such simulations provide the most direct and reliable estimates, the required models are expensive and time consuming. Two-degree-of-freedom aeroelastic models, which simulate the wind induced responses in the two fundamental sway modes of vibration, while less expensive, do not provide information on torsional effects, which may be significant for buildings of unusual shape and structural properties.

If aerodynamic damping effects are negligible, which is usual for most buildings at practical wind speeds and practical structural damping values, then a high-frequency balance/model system can measure the load function directly. Such a sensitive high frequency balance has been developed at the Boundary Layer Wind Tunnel Laboratory of The University of Western Ontario (BLWT). Simple foam models, cut only to the correct size, without involving other scaling factors, provide an economical and rapid description of the modal forces.

The response predictions for actual structures is analogous to the gust factor approach (see reference G-2, for example). Typical force spectra measured with the BLWT balance have been presented previously (G-4). More emphasis is given here to reviewing the technique.

G.3 Concepts of the Force Method

The response of a tall building to wind loads essentially consists of a mean response plus unsteady responses in each of its fundamental modes. Computation of the modal responses is complicated because of the need to include factors such as the mode shape, correlation and size of the gusts, and aerodynamic effects. Prediction of the mean response is fairly straightforward.

The generalized force - its mean value $\overline{F}$, its root-mean-square σ_F^2, and its spectrum $S_F(f)$ - is defined from the pressure by

$$\overline{F} = \frac{1}{T}\int_0^T \int_A p(z,t)\,\mu(z)\,dA\,dt$$

$$\sigma_F^2 = \int_A \int_A p(z,t)\,p(z',t)\,\mu(z)\,\mu(z')\,dA\,dA' - \overline{F}^2 \qquad \text{(G.1)}$$

$$S_F(f) = \int_A \int_A S_p(z,z',f)\,\mu(z)\,\mu(z')\,dA\,dA'$$

In these, $p(z,t)$ and $\mu(z)$ are the instantaneous pressures and the mode shapes at point z, respectively; $S_p(z,z',f)$ is the cross-spectrum of pressures at points z and z' at frequency f; and, dA and dA' are elementary areas at positions z and z' of the projected area A.

Tall buildings have fundamental mode shapes which more or less vary linearly with height. The generalized forces in the fundamental sway modes in such cases are proportional to the overturning moments which can then be measured directly. These measurements can be adjusted to correct for differences in mode shape. Torsional forces and aerodynamic damping effects need special consideration and will be described at greater length below.

G.4 Concept of the Balance

The difficulties in the experimental determination of the dynamic forces lie primarily in the demanding frequency response of the measuring system. The requirements of a force balance are to have high sensitivity, high rigidity, stability and uncoupled measurement of the orthogonal force components. The first two of these requirements are opposing in nature, but the BLWT balance provides an excellent compromise. The measurement problem is illustrated in Figure G.1 which indicates that the balance/model system natural frequency must be well above the range of frequencies of interest for the actual building response (i.e. the frequencies to which an aeroelastic model would be designed). If this can be accomplished, electronic filtering can remove the mechanical response introduced by the system's natural frequency and still leave the wind force spectrum intact over the primary range of interest.

The design chosen is believed to represent the best compromise for the load ranges to be used. The balance system is basically a statically-determinate frame with force links and miniature load cells equipped with semiconductor strain gauges forming a full Wheatstone bridge. The detailing and machining requires extreme care. Instrumentation of the balance makes use of high quality strain gauging, integrated chip amplifiers and appropriate filters. Space requirements do not permit further discussion, however, a complete description is available in reference G-5.

G.5 Linear Elastic Response Calculations with the BLWT Balance

The linear time-varying response of an elastic system can be expressed in the general form:

$$R(t) = \overline{R} + g(r)\,\sigma_R \qquad \text{(G.2)}$$

where $\overline{R}$ is the mean response, σ_R the rms response and $g(t)$ is a dimensionless time varying factor.

A particular response of interest is the peak response $\hat{R}$, in which case the corresponding value of g is roughly 3 to 4. The rms response, σ_E, can be broken down into two components; a quasi-static component σ_B; and a resonant component, σ_{Re}, so that the equation for the peak response becomes

$$\hat{R} = \overline{R} + g\left(\sigma_B^2 + \sigma_{Re}^2\right)^{1/2} \tag{G.3}$$

where:

$$\sigma_B = \frac{\sigma_F}{K} \tag{G.4}$$

$$\sigma_{Re} = \sqrt{\frac{\pi}{4}\ \frac{1}{\xi_s + \xi_a}\ \frac{f_0\ S_F(f_0)}{K^2}} \tag{G.5}$$

In these σ_F is the rms generalized force, K the generalized stiffness (which can be determined from the natural frequency and the generalized mass), ξ_s and ξ_a the structural and aerodynamic damping and $S_F(f_0)$ the power spectrum of the generalized force at the natural frequency f_0.

Equation G.5 is the well known result for the response of a lowly damped system (the structure), with a mechanical admittance function similar to that given in Figure G.1 for the balance, to a random force whose spectrum is fairly smooth such as is the case for the aerodynamic forces, also shown in Figure G.1. Using mean square addition of the components above gives:

$$\sigma_R = \frac{\sigma_F}{K}\sqrt{1 + \frac{\pi}{4}\ \frac{1}{\xi_s + \xi_a}\ \frac{f_0\ S_F(f_0)}{\sigma_F^2}} \tag{G.6}$$

This representation has been given in various references (G-2, for example) and is the basis of gust factor approaches. The difficult problem in evaluating equation (G.6) has always been the determination of the rms generalized force, σ_F and its normalized spectrum $f_0\ S_F(f_0) / \sigma_F^2$. The balance results give these data directly. Then equation G.3 can give the peak response using a suitable value of g, which is straightforward to estimate (G-2).

The acceleration response can be estimated in a straightforward manner from the above by noting that *acceleration* $= \omega^2$ *deflection*. This frequency-squared weighting takes advantage of the fact that the resonant response usually dominates the total root-mean-square acceleration, which can then be written $\omega^2\ \sigma_{Re}$.

The aerodynamic damping is body-motion dependent, and cannot be measured with the force balance method. It can be measured with conventional aeroelastic models, or using a technique developed at the BLWTL in which the simple force balance model is oscillated during the test. Nevertheless, there are indications (G-4) that the value of the aerodynamic damping is small and positive for typical buildings in the drag direction, and positive too in the lift direction up to the velocity where vortex shedding has a major contribution to the response. This velocity is usually higher than typical design wind speeds, and is indicated in the force spectra by a narrow-band peak. The result is that equation G.6 gives slightly conservative values, except for lift forces at high velocities.

A comparison of response predictions using the force balance method and from an aeroelastic test under identical conditions, was carried out by Tschanz (G-5). It showed that the force balance method somewhat overestimates the response in all cases, even at high velocities in the lift direction, indicating that the aerodynamic damping may be positive for all tested wind speeds. Thus, the force balance method approach serves as an economic and valid method to predict the response of structures to wind loads.

Response predictions can also be made for modes of vibration with coupled degrees of freedom. Also, the fundamental mode shapes of tall buildings tend to depart from a linear variation with height and are more commonly of the form:

$$\mu_z = \left(\frac{z}{H} \right)^{\beta} \qquad \text{(G.7)}$$

where $1 \le \beta \le 1.5$

Corrections can be applied to the measured base moments to obtain improved estimates of the generalized forces in situations when $\beta > 1$ (G-7). Such corrections are particularly important in estimates of the building accelerations.

G.6 Torsional Response

Torsional movement can be particularly disturbing to occupants. Of the buildings causing problems, full scale or wind tunnel measurements often show that aerodynamic torsional loading is the culprit. It is hence important to assess the torsional response, especially if there are eccentricities in mass or stiffness. Simple pivoting (two-degree-of-freedom) models only give information on the fundamental translational response, so expensive multi-degree-of-freedom models have been previously required for assessment of the torsional response.

The BLWT force balance/model combination gives an approximation to the torsional response, having in effect a constant magnitude mode shape in equation G.1, instead of a mode shape varying with height, with a maximum value at the top of the structure. This invariably results in an overestimate of the generalized torque. A mode shape adjustment factor of 0.7 is commonly applied to the measured base torque in order to improve estimates of dynamic building torque. Torsional generalized forces may be more accurately determined by the pressure integration technique, as discussed in Appendix J.

References

(G-1) Tschanz, T. "Measurement of Total Dynamic Loads Using Elastic Models With High Natural Frequencies", Proc. of Int. Workshop on Wind Tunnel Modelling Criteria and Techniques, National Bureau of Standards, Gaithersburg, Maryland, April 14-16,1982.

(G-2) Davenport, A.G. "The Treatment of Wind Loading on Tall Buildings", Symposium on Tall Buildings at University of Southampton, 13-15, April 1966, Pergamon Press, pp. 3-44.

(G-3) Davenport, A.G., Mackey, S. and Melbourne, W.H., Council on Tall Buildings, Committee 9, 1980, "Wind Loading and Wind Effects", Chapter CL-3, Vol. CL of Monograph on Planning and Design of Tall Buildings, ASCE, New York.

(G-4) Davenport, A.G. and Tschanz, T. "The Response of Tall Buildings to Wind: Effects of Wind Direction and the Direct Measurement of Force", Proceedings Fourth U. S. National Conference on Wind Engineering Research, July 27-29, 1981, Seattle, WA.

(G-5) Tschanz, T., "The Base Balance Measurement Technique and Application to Dynamic Wind Loading of Structures", Ph.D. Thesis, The University of Western Ontario, Faculty of Engineering Science, London, Ontario, September, 1982.

(G-6) Rosati, P.A., "The Response of a Square Prism to Wind Load", Research Report BLWT-II-1968, M.E. Sc. Thesis Supervised by A.G. Davenport.

(G-7) Vickery, P.J., Steckley, A., Isyumov, N. and Vickery, B.J., " The Effect of Mode Shape on the Wind-Induced Response of Tall Buildings", 5th U.S. National Conference on Wind Engineering, Texas Tech University, November 6-8, Lubbock, Texas.

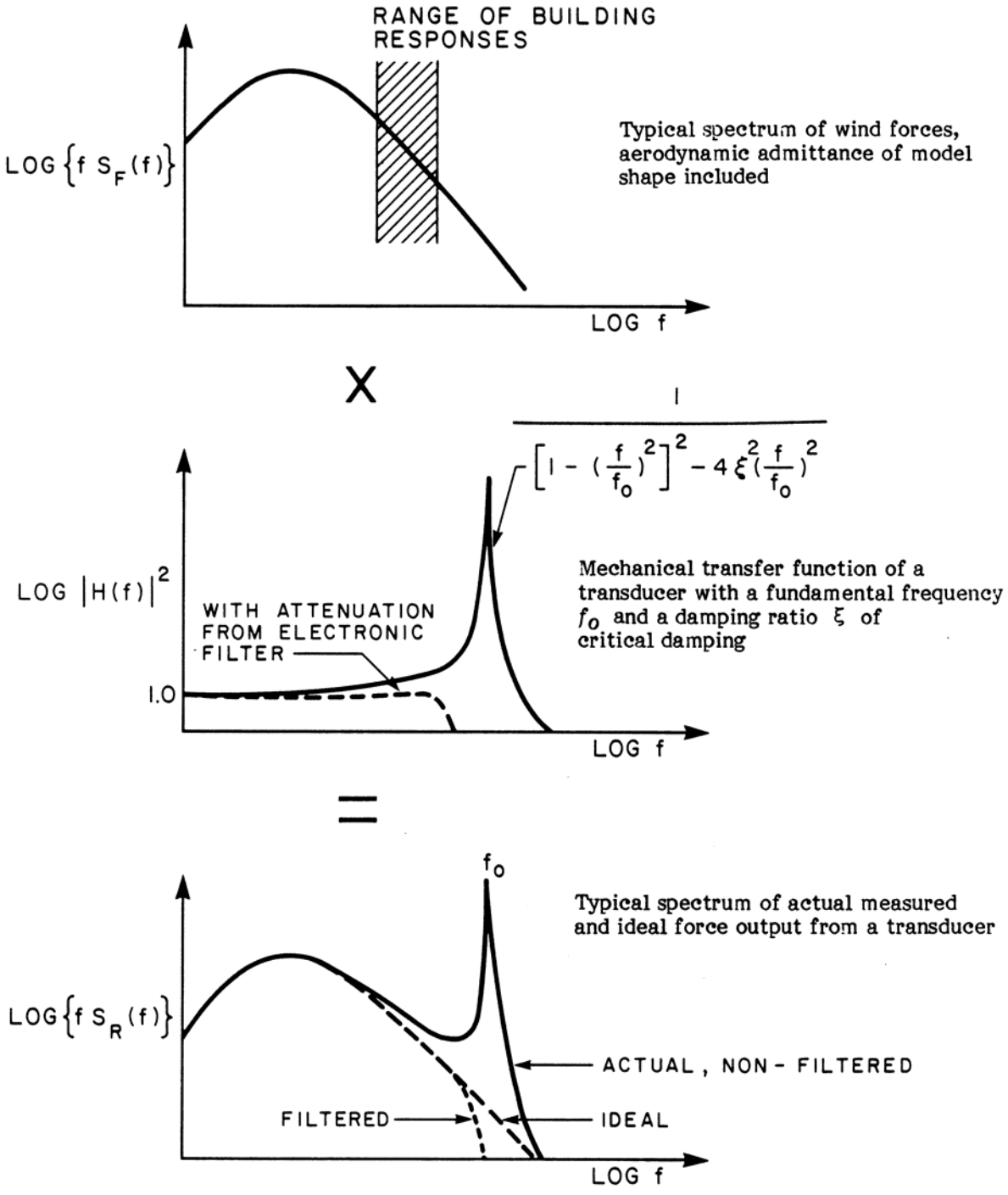

FIGURE G.1 DYNAMIC RESPONSE OF THE BALANCE-MODEL COMBINATION

APPENDIX H

AEROELASTIC SIMULATIONS OF BUILDINGS USING TWO-DEGREE-OF-FREEDOM MODELS

H.1 Introduction

Aeroelastic wind tunnel simulations of tall buildings provide direct information on overall mean and dynamic wind induced loads and responses of the main structural system. These dynamic responses represent the action of the unsteady aerodynamic forces on the entire building envelope seen through the mechanical admittance of the building. The objectives of this Appendix are to provide background information on aeroelastic modelling methods, with emphasis on two-degree of freedom models which simulate the dynamic properties of a building in its two fundamental sway modes of vibration.

H.2 Aeroelastic Modelling

The choice of the aeroelastic modelling approach for a tall building depends largely on the complexity of the structural system and the exterior geometry. For many tall buildings the structural system and geometry are such that the response is primarily in the fundamental sway modes of vibration, with relatively minor contributions from higher sway modes and from torsional modes of vibration. Thus, only the two sway modes need to be modelled. Furthermore, the mode shapes of the fundamental sway modes of tall buildings tend to be approximately linear. These conditions allow a simple aeroelastic simulation technique to be used consisting of modelling the building as a rigid body pivoted near the base, with the elasticity provided by appropriately selected springs (see Figure H.1). This type of model is known as a two-degree-of-freedom or "stick" model. Results of a number of aeroelastic studies of tall buildings carried out at the Boundary Layer Wind Tunnel Laboratory indicate that this modelling technique adequately defines the most significant components of the wind induced dynamic response. An important practical advantage of this approach is the freedom of readily varying the building mass, the sway frequencies and their ratio, and the structural damping (see Section H.3 below).

The scaling requirements for aeroelastic modelling are based on established similarity theory. Detailed discussions of aeroelastic modelling requirements to simulate wind induced effects on structures are discussed elsewhere (H-1, H-2 and H-3). Providing that the salient properties of natural wind are modelled in the wind tunnel (including the mean velocity profile, the turbulence intensities and the scale of turbulence), similarity of the aeroelastic behaviour of a sharp edged building is achieved by modelling the geometry of the building to a length scale consistent with the length scales of the modelled wind and maintaining equality of the following non-dimensional quantities in model and full scale:

$$\rho_s / \rho - \textit{density ratio}$$

$$E / \left(\rho V^2\right), G / \left(\rho V^2\right) - \textit{similarity of elastic force}$$

$$\xi - \textit{critical damping ratio}$$

where $\rho_s, \rho, E, G, V,$ and ξ are respectively the bulk density of the building, the air density, Young's modulus, the torsional modulus, a reference wind speed and the structural damping.

The above similarity requirement for elastic forces can be replaced by the reduced frequency, $f D / V$, which is maintained constant in model and full scale for the particular modes of vibration included in the simulation. For exact scaling it would also be necessary to maintain equality of the

Reynolds number, $V D / \nu$. This is, however, generally not practical as full scale Reynolds numbers are typically three orders of magnitude greater than those achieved in low speed wind tunnels. Although equality of Reynolds number is important for rounded shapes where the location of flow separation from the curved surface is dependant on Reynolds number, it is less significant for sharp edged bodies where flow separation tends to occur at the building corners. As a result, the influence of Reynolds number on the overall flow around such buildings is generally not found to be significant, particularly in turbulent boundary layer flows. A possible exception to this is the influence of Reynolds numbers on the growth of local boundary layers on the building surfaces. The commonly followed approach to minimize this effect, is to exaggerate the surface roughness of the model building faces. The argument for this approach is that the growth of the local surface boundary layer is more dependent on the Reynolds number of the surface roughness rather than that of the main flow.

The length scaling, λ_L, which is the ratio of all corresponding model and full scale lengths, is primarily determined by the ratio of the model to full scale turbulence length scales which are conveniently defined by the peak wavelength of the spectrum of the velocity fluctuations. Full scale measurements indicate that the wavelength of turbulence in the longitudinal direction is in the order of 5,000 feet. The comparable turbulence wavelength in The University of Western Ontario's Boundary Layer Wind Tunnel is approximately 10-12 feet. As a result, the length scale commonly used for aeroelastic studies ranges between 1:400 and 1:500. Since the air density is the same in both model and full scale, equality of the density ratio, ρ_s / ρ, implies that the bulk building density of the model must be the same as that of the prototype. The model time scale, and consequently the ratio of the model to full scale periods of vibration of the building, is determined from the reduced frequency scaling once the velocity scale has been selected.

H.3 Details of the Aeroelastic Model

A schematic drawing of a particular two-degree of freedom aeroelastic model is given in Figure H.1 for illustration. The dynamic properties of the tower in the two fundamental sway modes of vibration are modelled by representing the tower as a rigid body rotating on a set of gimbals about a selected pivot point. The two full-scale mode shapes are seen to be approximated by a linear mode shape with an effective point of rotation at the pivot point. Below this point the building is modelled as a rigid body attached to the wind tunnel turntable. A rigid aluminium rod is attached to the bottom of the model through the gimbals and extends downward below the turntable. This rod is restrained by appropriately selected springs to provide the required stiffness in the x and y directions. The springs are attached to the rod through small force transducers instrumented with electrical resistance strain gauges. Damping is provided by an eddy current damping device. The structural damping of the model can be readily changed by varying the current through the electromagnet.

The design of such aeroelastic models is based on the dynamic properties of the full scale building. Since the mode shapes of this type of aeroelastic model are linear, the modelling of the building mass reduces to modelling an effective mass moment of inertia about the pivot point. This full scale effective mass moment of inertia can be shown to be the average generalized mass in the x and y directions times the square of the distance from the assumed rotation to the top of the building.

H.4 Experimental Procedure and Preliminaries

The aeroelastic model is calibrated to relate the output of the strain gauged force transducers at the x and y supporting springs to the applied bending moments about the point of rotation associated with x and y forces. The calibration procedure also relates the output from the force transducers to the sway deflections and the sway accelerations in the x and y directions. Throughout this discussion, x and y base bending moments are defined as moments due to forces in the x and y directions respectively, about the pivot point.

Measurements of the aeroelastic model response for a particular wind angle comprise measurements of mean, root-mean-square (rms), maximum and minimum values of the x and y base bending moments,

as well as other selected wind-induced responses such as sway accelerations and/or sway displacements. All measurements are made with the on-line digital computer-based data acquisition system of the Laboratory, over a period of time corresponding to approximately 1 hour in full scale. Such measurements are taken for the full range of azimuth, typically at intervals of 10°, and for selected full scale gradient wind speeds and structural damping ratios. The actual damping of the aeroelastic model in the x and y directions is determined from the decay of free vibrations of the model in each of these directions. This procedure is also used to check the natural frequencies of vibration of the model.

H.5 Predictions of Peak Wind-Induced Response

The aeroelastic response data are combined with the annual design probability distribution of gradient wind speed to provide predictions of peak base bending moments (about the pivot point) and peak sway acceleration near the top of the building. The procedure used for obtaining predictions of peak levels of the wind loads and responses are described in Appendix D. In some situations, directly measured maximum and minimum values of the response are used in such predictions. An alternative method, which leads to statistically more stable predictions, is to use peak values formed from the measured mean and rms values of the response:

Maximum Value: $$\hat{M}_x\left(\overline{V}_g, \alpha\right) = \overline{M}_x\left(\overline{V}_g, \alpha\right) + g_x\, \tilde{M}_x\left(\overline{V}_g, \alpha\right)$$

Minimum Value: $$\check{M}_x\left(\overline{V}_g, \alpha\right) = \overline{M}_x\left(\overline{V}_g, \alpha\right) - g_x\, \tilde{M}_x\left(\overline{V}_g, \alpha\right)$$

where $\overline{M}_x\left(\overline{V}_g, \alpha\right)$ and $\tilde{M}_x\left(\overline{V}_g, \alpha\right)$ are the mean and rms x-direction bending moments for a mean gradient wind speed $\overline{V}_g$ and direction α, and where g_x is the average value of the x-moment peak factor. This average peak factor is determined from a statistical analysis of maximum and minimum values of the x-moment for various wind speeds and directions. Similar estimates of maximum and minimum values are made for all response parameters studied.

References

(H-1) Whitbread, R.E., "Model Simulation of Wind Effects on Structures", NPL International Conference on Wind Effects on Buildings and Structures, Teddington, England, 1963.

(H-2) Isyumov, N., "Wind Tunnel Methods for Evaluating Wind Effects on Buildings and Structures", Proceedings International Symposium on Experimental Mechanics, University of Waterloo, June 1972.

(H-3) Isyumov, N., "The Aeroelastic Modelling of Tall Buildings", Wind Tunnel Modelling for Civil Engineering Applications, Cambridge University Press, 1982.

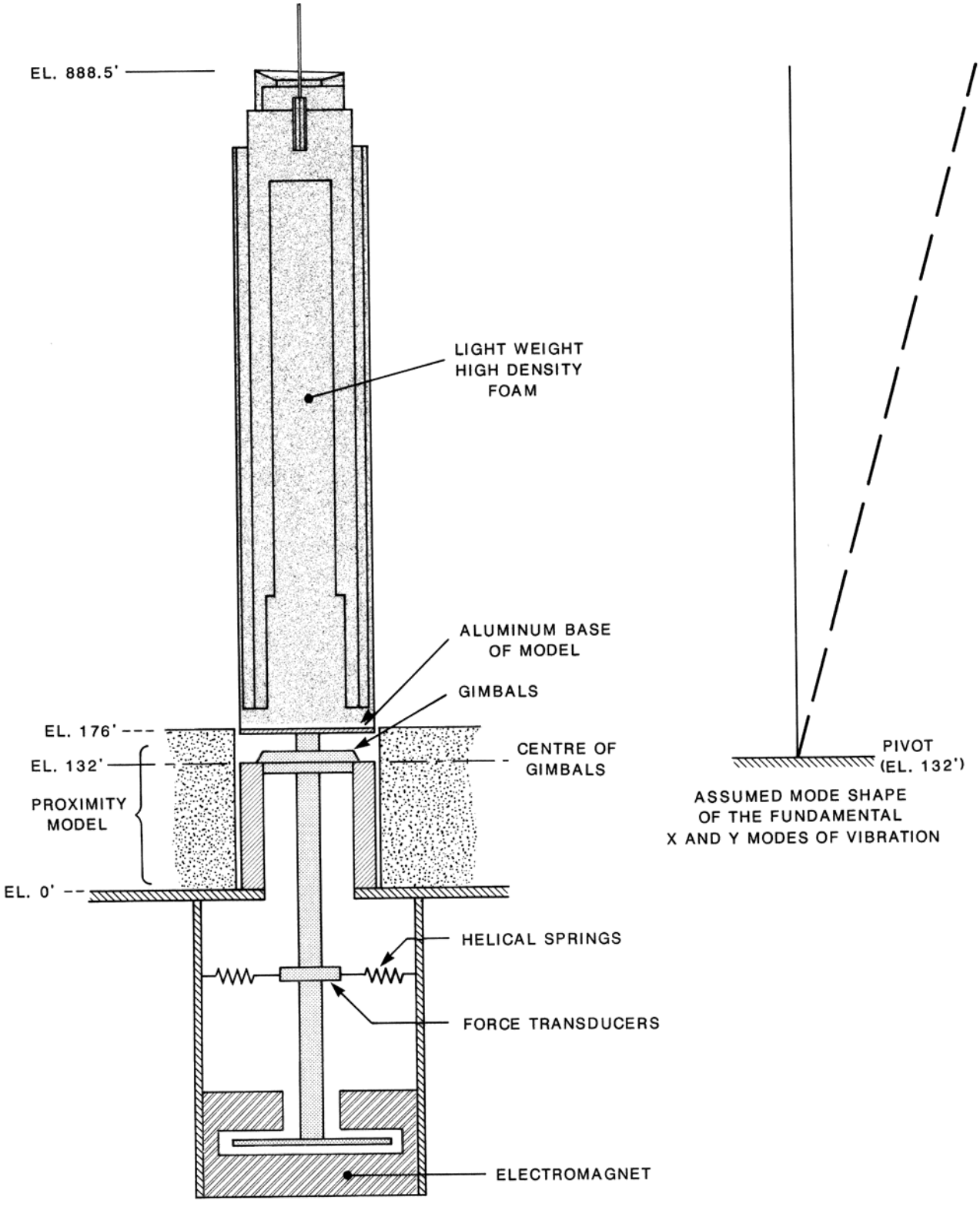

FIGURE H.1 SCHEMATIC OF THE AEROELASTIC MODEL

APPENDIX I

AEROELASTIC SIMULATIONS OF BUILDINGS USING MULTI-DEGREE-OF-FREEDOM MODELS

I.1 Introduction

Aeroelastic wind tunnel simulations of tall buildings provide direct information on overall mean and dynamic wind induced loads and responses of the main structural system. These dynamic responses represent the action of the unsteady aerodynamic forces on the entire building envelope seen through the mechanical admittance of the building. The objective of this Appendix is to provide background information on aeroelastic modelling methods, with emphasis on multi-degree-of-freedom models which simulate the dynamic properties of a building in its two fundamental sway modes of vibration and in its fundamental torsion mode.

I.2 Aeroelastic Modelling

The choice of the aeroelastic modelling approach for a tall building depends largely on the complexity of the structural system and the exterior geometry. For many tall buildings the structural system and geometry are such that the response is primarily in the fundamental sway modes of vibration, with relatively minor contributions from higher sway modes and from torsional modes of vibration. However, for some buildings the contribution of the fundamental torsional mode becomes significant. As well, for some structural systems or geometries there is strong coupling between directions within modes such that the modes are 3-dimensional in character. This latter detail in particular makes it necessary to design an aeroelastic model which simulates these complicated modes while maintaining consistent scaling parameters in both sway and torsion directions. Such a model is known as a multi-degree-of-freedom aeroelastic model.

The scaling requirements for aeroelastic modelling are based on established similarity theory. Detailed discussions of aeroelastic modelling requirements to simulate wind induced effects on structures are discussed elsewhere (I-1, I-2 and I-3). Providing that the salient properties of natural wind are modelled in the wind tunnel (including the mean velocity profile, the turbulence intensities and the scale of turbulence), similarity of the aeroelastic behaviour of a sharp edged building is achieved by modelling the geometry of the building to a length scale consistent with the length scales of the modelled wind and maintaining equality of the following non-dimensional quantities in model and full scale:

$$\rho_s \,/\, \rho - \textit{density ratio}$$

$$E \,/\, \left(\rho V^2\right), G \,/\, \left(\rho V^2\right) - \textit{similarity of elastic force}$$

$$\xi - \textit{critical damping ratio}$$

where $\rho_s, \rho, E, G, V,$ and ξ are respectively the bulk density of the building, the air density, Young's modulus, the torsional modulus, a reference wind speed and the structural damping.

The above similarity requirement for elastic forces can be replaced by the reduced frequency, $f\,D\,/\,V$, which is maintained constant in model and full scale for the particular modes of vibration included in the simulation. For exact scaling it would also be necessary to maintain equality of the Reynolds number, $V\,D\,/\,\nu$. This is, however, generally not practical as full scale Reynolds numbers are typically three orders of magnitude greater than those achieved in low speed wind tunnels. Although

equality of Reynolds number is important for rounded shapes where the location of flow separation from the curved surface is dependant on Reynolds number, it is less significant for sharp edged bodies where flow separation tends to occur at the building corners. As a result, the influence of Reynolds number on the overall flow around such buildings is generally not found to be significant, particularly in turbulent boundary layer flows. A possible exception to this is the influence of Reynolds numbers on the growth of local boundary layers on the building surfaces. The commonly followed approach to minimize this effect, is to exaggerate the surface roughness of the model building faces. The argument for this approach is that the growth of the local surface boundary layer is more dependent on the Reynolds number of the surface roughness rather than that of the main flow.

The length scaling, λ_L, which is the ratio of all corresponding model and full scale lengths, is primarily determined by the ratio of the model to full scale turbulence length scales which are conveniently defined by the peak wavelength of the spectrum of the velocity fluctuations. Full scale measurements indicate that the wavelength of turbulence in the longitudinal direction is in the order of 5,000 feet. The comparable turbulence wavelength in The University of Western Ontario's Boundary Layer Wind Tunnel is approximately 10-12 feet. As a result, the length scale commonly used for aeroelastic studies ranges between 1:400 and 1:500. Since the air density is the same in both model and full scale, equality of the density ratio, ρ_s / ρ, implies that the bulk building density of the model must be the same as that of the prototype. The model time scale, and consequently the ratio of the model to full scale periods of vibration of the building, is determined from the reduced frequency scaling once the velocity scale has been selected.

I.3 Details of the Aeroelastic Model

In addition to reproducing the exterior geometry, an aeroelastic model of a tall building simulates its dynamic properties in the lower modes of vibration which are likely to be excited by wind action. In a typical study, the building is represented by a lumped mass system in which each mass has two sway and one torsional degree of freedom. For illustration, Figure I.1 shows a schematic representation of a multi-degree-of-freedom model for a particular building. In the model, each mass is consists of a stiff plate or "floor" made of either aluminium or magnesium. The floors are connected by clamped aluminium columns which provide the required stiffness in sway and in torsion. The required structural damping is achieved by adding strips of foam tape connecting the floors. These strips add negligible stiffness while dissipating vibrational energy. The geometric modelling is completed with sections of balsa wood skins which are attached to each floor so as not to make contact with each other.

The completed model is attached to a strain-gauged balance at its base. The balance measures overall base bending moments and torsion. Three accelerometers are normally located at the top mass to provide measures of the translational accelerations and the rotational accelerations at that height. One accelerometer is mounted to measure accelerations in one direction, say the x direction, while the other two are mounted to measure accelerations in the orthogonal direction. These two accelerometers are mounted symmetrically about the axis of twist so that their difference yields values of the torsional acceleration.

I.4 Experimental Procedure and Preliminaries

The aeroelastic model is calibrated to relate the output of the strain-gauged base balance to the applied bending moments. Both static and dynamic calibrations are performed. The dynamic calibration is used to determine the frequencies of vibration of the model and to provide verification of the required mode shapes. Throughout this discussion, x and y base bending moments are defined as moments due to forces in the x and y directions respectively.

The model, mounted on the strain-gauged base balance and positioned at the centre of the detailed city model on the wind tunnel turntable, is typically tested for a full range of wind directions at azimuth intervals of 10° and for a representative range of wind speeds. All measurements are made using the on-line digital data acquisition system of the Laboratory which allows real time transformations of the accelerometer data into accelerations in the two translational directions and torsion. For each

combination of wind speed and wind direction, measurements of the maximum, minimum, mean and rms aeroelastic response are carried out for a sampling period corresponding to one hour in full scale. Measurements of the frequencies of vibration and the structural damping are made at the beginning of a test and at regular intervals in order to assure the performance of the model.

I.5 Predictions of Peak Wind-induced Response

The aeroelastic response data are combined with the annual design probability distribution of gradient wind speed to provide predictions of peak base bending moments and torsion as well as accelerations near the top of the building. The procedure used for obtaining predictions of peak levels of the wind loads and responses are described in Appendix D. In some situations, directly measured maximum and minimum values of the response are used in such predictions. An alternative method, which leads to statistically more stable predictions, is to use peak values formed from the measured mean and rms values of the response:

Maximum Value: $$\hat{M}_x\left(\overline{V}_g, \alpha\right) = \overline{M}_x\left(\overline{V}_g, \alpha\right) + g_x\, \tilde{M}_x\left(\overline{V}_g, \alpha\right)$$

Minimum Value: $$\check{M}_x\left(\overline{V}_g, \alpha\right) = \overline{M}_x\left(\overline{V}_g, \alpha\right) - g_x\, \tilde{M}_x\left(\overline{V}_g, \alpha\right)$$

where $\overline{M}_x\left(\overline{V}_g, \alpha\right)$ and $\tilde{M}_x\left(\overline{V}_g, \alpha\right)$ are the mean and rms x-direction bending moments for a mean gradient wind speed $\overline{V}_g$ and direction α, and where g_x is the average value of the x-moment peak factor. This average peak factor is determined from a statistical analysis of maximum and minimum values of the x-moment for various wind speeds and directions. Similar estimates of maximum and minimum values are made for all response parameters studied.

References

(I-1) Whitbread, R.E., "Model Simulation of Wind Effects on Structures", NPL International Conference on Wind Effects on Buildings and Structures, Teddington, England, 1963.

(I-2) Isyumov, N., "Wind Tunnel Methods for Evaluating Wind Effects on Buildings and Structures", Proceedings International Symposium on Experimental Mechanics, University of Waterloo, June 1972.

(I-3) Isyumov, N., "The Aeroelastic Modelling of Tall Buildings", Wind Tunnel Modelling for Civil Engineering Applications, Cambridge University Press, 1982.

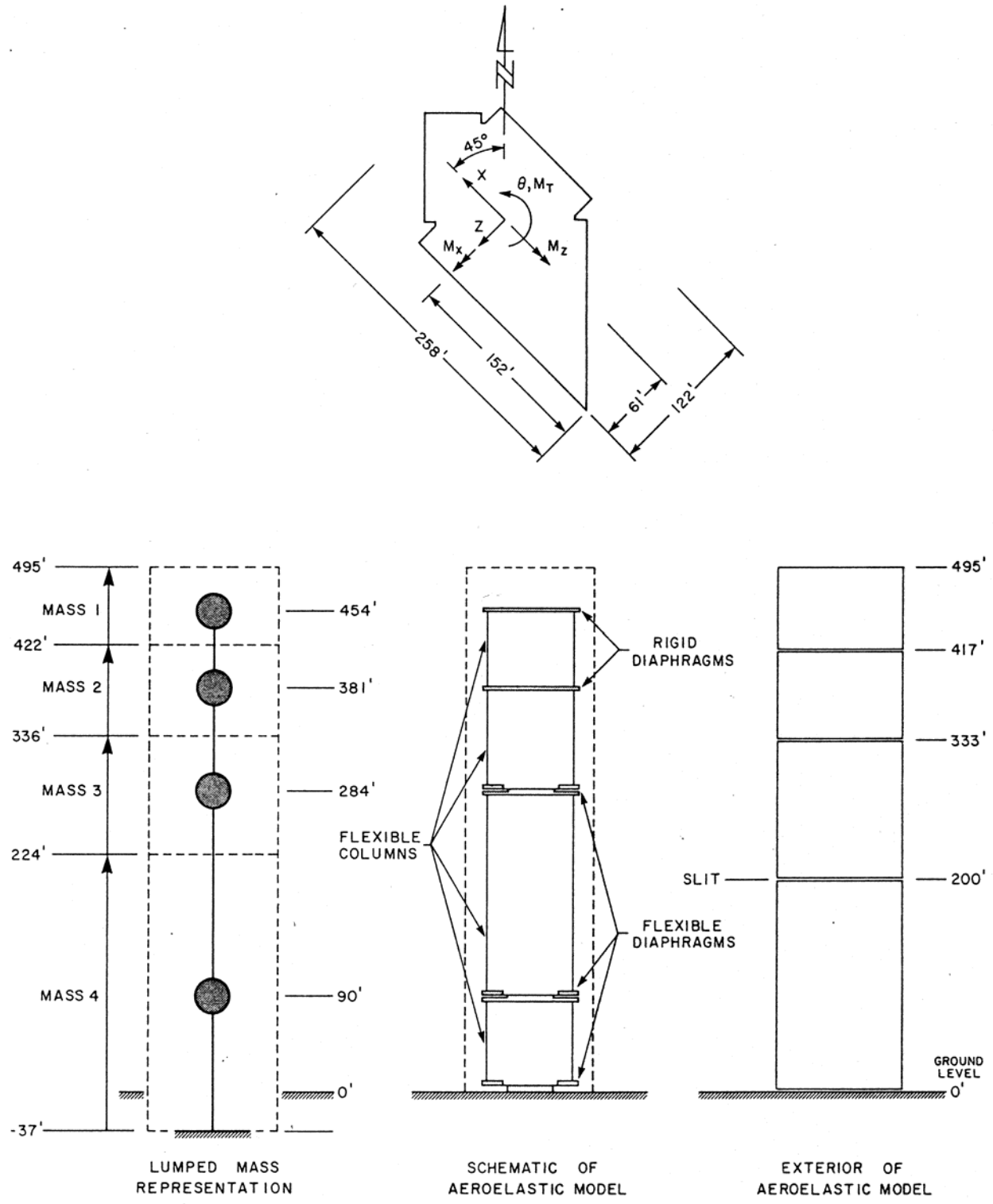

FIGURE I.1 SCHEMATIC OF THE AEROELASTIC MODEL

APPENDIX J

DETERMINATION OF TOTAL DYNAMIC LOADS FROM THE INTEGRATION OF SIMULTANEOUSLY MEASURED PRESSURES

J.1 Summary

This appendix describes an approach to the determination of total dynamic loads from the simultaneously measured external point pressures. The instantaneous generalized forces are determined from the pressure measurements and are then used in a standard random vibration analysis to provide estimates of the total dynamic loads and responses of the structure. These loads and responses are then combined with the statistics of the full scale wind climate at the site, using the methodology described in Appendix D, to provide predictions of loads and responses for various return periods. This approach is described in detail in References J-1 and J-2.

J.2 The Integration Procedure

For each wind azimuth, the experimental mean pressures at particular points are multiplied by their corresponding tributary areas to yield tributary forces:

$$\begin{aligned} F_{xi}(t) &= p_i(t)\, a_{xi} \\ F_{yi}(t) &= p_i(t)\, a_{yi} \\ F_{\theta i}(t) &= F_{xi}(t)\, arm_{xi} + F_{yi}\, arm_{yi} \end{aligned} \tag{J.1}$$

where $F_{xi}(t), F_{yi}(t)$ and $F_{\theta i}(t)$ are the x, y and torsional tributary force at location i and time t, $p_i(t)$ is the pressure at location i and time t, a_{xi} and a_{yi} are the tributary areas at location i projected perpendicular to the x and y axes and arm_{xi} and arm_{yi} are the torque arms associated with x and y loads at location i.

These tributary forces are multiplied by the mode shape at that location and summed over the entire building to yield generalized forces:

$$F_j^*(t) = \sum_i \left(F_{xi}(t)\, \phi_{xji} + F_{yi}(t)\, \phi_{yji} + F_{\theta i}(t)\, \phi_{\theta ji} \right) \tag{J.2}$$

where F_j^* is the generalized force for mode j and ϕ_{xji}, ϕ_{yji} and $\phi_{\theta ji}$ are the x, y and torsional components of mode j at location i.

The time-varying generalized force from equation J.2 can be analysed to determine the mean, standard deviation (or rms) and the power spectrum of the generalized force.

J.3 Response Calculations

The linear time-varying response of an elastic system can be expressed in the general form:

$$R(t) = \overline{R} + g(t)\, \sigma_R \tag{J.3}$$

where $\dot{R}$ is the mean response, σ_R the rms response and $g(t)$ is a dimensionless time varying factor.

A particular response of interest is the peak response $\hat{R}$, in which case the corresponding value of g is roughly 3 to 4. The rms response, σ_R, can be broken down into two components; a quasi-static component σ_B; and a resonant component, σ_{Re}, so that the equation for the peak response becomes

$$\hat{R} = \overline{R} + g\left(\sigma_B^2 + \sigma_{Re}^2\right)^{1/2} \tag{J.4}$$

where:

$$\sigma_B = \frac{\sigma_F}{K} \tag{J.5}$$

$$\sigma_{Re} = \sqrt{\frac{\pi}{4}\ \frac{1}{\xi_s + \xi_a}\ \frac{f_0\ S_F(f_0)}{K^2}} \tag{J.6}$$

In these σ_F is the rms generalized force, K the generalized stiffness (which can be determined from the natural frequency and the generalized mass), ξ_s and ξ_a the structural and aerodynamic damping and $S_F(f_0)$ the power spectrum of the generalized force at the natural frequency f_0.

Equation J.6 is the well established expression for the response of a lightly damped system (the structure) to a random force whose spectrum is fairly smooth such as is the case for the aerodynamic forces. Using mean square addition of the components above gives:

$$\sigma_R = \frac{\sigma_F}{K}\sqrt{1 + \frac{\pi}{4}\ \frac{1}{\xi_s + \xi_a}\ \frac{f_0\ S_F(f_0)}{\sigma_F^2}} \tag{J.7}$$

This representation has been given in various references and is the basis of gust factor approaches. The difficult problem in evaluating equation (7) has always been the determination of the rms generalized force, σ_F and its normalized spectrum $f_0\ S_F(f_0) / \sigma_F^2$. The instantaneous integrated pressure results give these data directly. Then equation J.4 can give the peak response using a suitable value of g, which is straightforward to estimate (J-3).

The acceleration response can be estimated in a straightforward manner from the above by noting that $\textit{acceleration} = \omega^2\ \textit{deflection}$. This frequency-squared weighting implies that the background response contributes almost nothing to the root-mean-square acceleration, which can then be reduced to $\omega^2\ \sigma_{Re}$. Peak accelerations are estimated as for peak deflections.

The aerodynamic damping is body-motion dependent, and cannot be measured with the integrated pressure method. It can be measured with conventional aeroelastic models, or using a technique developed at the BLWTL in which the simple force balance model is oscillated during the test. Nevertheless, there are indications (J-4) that the value of the aerodynamic damping is small and positive for typical buildings in the drag direction, and positive too in the lift direction up to the velocity where vortex shedding has a major contribution to the response. This velocity is usually higher than typical design wind speeds, and is indicated in the force spectra by a narrow-band peak. The result is that equation J.7 gives slightly conservative values, except for lift forces at high velocities.

References

(J-1) Ho, T.C.E. "The Determination of Overall Structural Loads and Responses With High-Speed Scanned Wind Tunnel Pressure Data", Proc. of Eighth U.S. National Conference on Wind Engineering, Baltimore, Maryland, USA. June 5-7, 1997.

(J-2) Ho, T.C.E, Lythe, G.R. and Isyumov, N. “The Prediction of Structural Loads and Responses From the Integration of Simultaneously Measured Pressures”, Proc. of Tenth Int. Conf. on Wind Engineering”, Copenhagen, Denmark, June 21-24, 1999.

(J-3) Davenport, A.G. "The Treatment of Wind Loading on Tall Buildings", Symposium on Tall Buildings at University of Southampton, 13-15, April 1966, Pergamon Press, pp. 3-44.

(J-4) Davenport, A.G. and Tschanz, T. "The Response of Tall Buildings to Wind: Effects of Wind Direction and the Direct Measurement of Force", Proceedings Fourth U. S. National Conference on Wind Engineering Research, July 27-29, 1981, Seattle, WA.

APPENDIX K

THE EVALUATION AND USE OF EFFECTIVE STATIC FORCE DISTRIBUTIONS

K.1 Effective Static Force Distributions

Effective static force distributions are intended to provide a simplified static loading for design of the structure. As such, they are representative of the combined load due to static (mean) and dynamic forces; and, in the interest of overall simplicity, they are averaged over all azimuths with weighting factors to reflect the most important wind directions.

In principle, for any azimuth, effective static force distributions can be determined which reproduce the measured dynamic peak base bending moment. The particular vertical distribution chosen must reflect the actual static and dynamic loading of the building.

The actual loading is made up of:

1. the mean loading;
2. the dynamic loading due to background or quasi-steady excitation; and,
3. the dynamic inertial loading due to resonant oscillations.

The distribution of this loading can be reconstructed form the mean force distribution results of the pressure test (component 1), the known vibration properties of the building (component 3), and the determination from the load time histories of the relative contribution of the unsteady and steady components at the base. The distribution of the background dynamic loading (component 2) is assumed to follow the distribution of the mean loading. In the absence of measured distributed load data, the quasi-steady dynamic loads (component 1 and 2) are estimated using trapezoidal load shape).

For component 3, the resonant load distribution is determined from the mass and mode shapes of the building as follows (the x-direction is carried as an example):

$$\tilde{A}_x(z) = \frac{\textit{resonant rms force per unit height}}{\textit{resonant rms base bending moment}} = \frac{m(z)\,\phi_x(z)}{\int_0^H z\, m(z)\,\phi_x(z)\,dz} \qquad \text{(K.1)}$$

where $m(z)$ = mass per unit height at height z above plaza level

$\phi_x(z)$ = x component of mode shape for the dominant x mode at height z above plaza level

H = total height of the building

For each wind, the quasi-steady peak dynamic loading (component 1 and 2) is combined with the resonant distribution as follows:

$$\textit{Combined distribution} = C_1 \times \textit{mean distribution} + C_2 \times \textit{resonant distribution}$$

where

$$\frac{C_1}{C_2} = \frac{\textit{measured quasi} - \textit{steady dynamic moment}}{\textit{measured resonant dynamic moment}}$$

These proportions of mean and resonant components will vary with the dynamic properties of the building, notably the damping. For instance, the proportion of the resonant component in the total will increase with increasing wind speed and will decrease with increasing damping. For this reason, a conservative speed is taken to evaluate the combination; usually the 50 or 100-year return period speed.

An overall effective loading shape, independent of wind direction, is then constructed by averaging the effective force distributions found for the most important wind directions.

The effective load shapes, which are proportional to the force per unit height per unit base bending moment are renormalized such that

$$\int_0^H \frac{\textit{force / unit height}}{\textit{base moment}}\, z\, dz = 1.0 \qquad \text{(K.2)}$$

The resulting effective load diagram can be used directly to determine the effective force per unit height at any height by simply multiplying the coordinate of the diagram at that height by the base bending moment associated with the forces in the direction of interest. These forces per unit height can then be used to determine:

- Floor-by-floor loads by integrating the force per unit height over the tributary height associated with each floor;
- Shear loads at any level by integrating the force per unit heights over the height above the particular level;
- Bending Moments at any level by integrating the force per unit height multiplied by the moment arm over the height above the particular level
- Effective pressures at any level by dividing the force per unit height at that level by the building width at that level.

K.2 Combined Load Cases

The determination of combined load factors to be applied to the structure is based on the requirement that the specified loads have to be sufficient to generate the resulting load effects due to wind. Since the peak loads and responses for each principal direction (x, y and torsion about the z-axis are determined independently in the prediction process, the peak loads are unlikely to occur simultaneously. The simultaneous application of the predicted peak loads in all three principal directions is clearly conservative.

Specific load effects can be evaluated using the wind tunnel data if influence coefficients are supplied. However, it would be prohibitively expensive for the engineers to produce a range of influence coefficients for numerous structural members. Instead, relative influence coefficients are used to reflect the contribution of the loads in the three principal axes.

$$E(\alpha) = \gamma_x M_x(\alpha) + \gamma_y M_y(\alpha) + \gamma_t M_t(\alpha) \qquad \text{(K.3)}$$

where E is the load effect, α is the wind direction, γ are the relative influence coefficients. A simplifying assumption is made that the distributed loads are represented by their respective base moments, M.

The relative influence coefficients can range from the case of any one dominating direction to the case of all three directions contributing approximately equally. In the design of a structural member having dominating influence in one load direction only, the inherent structural influence would govern that design as long as load cases with 100% of peak load to be applied in the dominating direction is included.

The development of the load cases is therefore in the form of

$$E \leq c_x \gamma_x \hat{M}_x + c_y \gamma_y \hat{M}_y + c_t \gamma_t \hat{M}_t \qquad \text{(K.4)}$$

where c are the load factors for various load cases and $\hat{E}$ is the predicted load effect.

The load combination factors, c, are selected by matching the target load effects determined from the predictions of the load effects using information from equation K.3. It is assumed that the largest load effects occur when the loads in one of the three principal load directions is at its peak; i.e. 100% of the predicted load. At the same time, nominal load levels occur in the other two principal directions. The number of load cases is kept to a minimum by eliminating redundant load cases based on load effects.

All load effects are evaluated for combinations of loads acting in the positive and negative directions. With the predicted peak moments and corresponding distributed loads are based on the larger of the positive and negative predicted values, the differences in the predicted values in the positive and negative directions are taken into account in the specifications of the load combination factors for the corresponding load directions. The nominal number of load cases covering all combinations of positive and negative x, y and torsion loads is 24.

APPENDIX L

THE PEDESTRIAN LEVEL WIND ENVIRONMENT

L.1 Introduction

The essence of the approach adopted by the Boundary Layer Wind Tunnel Laboratory is the combination of model measurements with statistics of the full-scale wind climate to provide predictions of the expected wind environment at pedestrian level. This combination of the wind speed measurements with the full-scale wind climate statistics is considered the most meaningful way to interpret the overall nature of the resulting pedestrian level wind climate. For example, a wind direction found to produce strong pedestrian level winds in the wind tunnel is more significant if that wind direction occurs frequently in full scale. The predictions, then, reflect the degree of coincidence of wind directions producing high wind speeds at pedestrian level (as determined from the model study) with the likelihood of such full-scale wind directions occurring.

Pedestrian comfort depends largely on the magnitude of the ground level wind speed regardless of the local wind direction. As a result, quantitative evaluation of the pedestrian level wind environment at the Laboratory is normally restricted to measurements of the magnitude of ground level wind speeds unless information on local wind direction is of special interest. Measurements are made of coefficients of wind speed (pedestrian level wind speed as a fraction of an upper level reference speed) for a full range of wind directions at various locations near the site, and in some cases, at a location well away from the development to provide a form of calibration with existing experience.

These wind speed coefficients are subsequently combined with the design probability distribution of gradient wind speed and direction for the area to provide predictions of the full-scale pedestrian level wind environment.

L.2 Test Procedure

Wind speed measurements are made using one of two types of sensor: linearized single-ended cylindrical hot-film sensors or pressure sensors (described in references L-1 and L-2). Both types of sensors are omni-directional and measure both the mean and the fluctuating components of the wind speed parallel to the ground.

The experimental program comprises measurement of maximum, mean and rms (root-mean-square) wind speed at all locations for a full range of wind direction varied in steps of 10°. The sampling time in all cases is chosen to provide stable estimates of the mean and rms wind speeds and corresponds approximately to 1 hour in full scale. The measured pedestrian level wind speeds are subsequently expressed as speed coefficients or speed ratios by normalizing the measured data by the mean wind speed at an upper level height away from the influence of the building. All measurements are carried out using the automated computer-controlled data acquisition system available at the Laboratory.

L.3 Statistical Predictions of Pedestrian Level Winds

Wind tunnel measurements of pedestrian level mean and gust wind speeds at the various locations are combined with the probability distribution of gradient wind speed and direction to provide predictions of full-scale pedestrian level wind speeds. Such predictions essentially use the following technique: An arbitrary speed of interest is set for a particular surface position (say 4 m/s). By using the measured speed ratios, the gradient wind speed required to produce this surface speed can be calculated for each upper level direction. The corresponding probability of this upper level wind speed occurring can be determined from the probability distribution of gradient wind speed and direction. Integrating over all

possible upper level wind directions provides the total probability of exceeding the original surface wind speed (4 m/s). This can be repeated for any surface wind speed and, conversely, the surface wind speed corresponding to any probability level or recurrence period can be calculated. As a result two types of predictions are available:

1. Predictions of mean and peak or "gust" wind speeds exceeded during different percentages of the time at the various measuring locations. For comparison, similar speeds are predicted for typical suburban and typical open country locations;
2. Predictions of mean wind speeds exceeded during particular events or "storms" associated with various frequencies of occurrence. The duration of such "storms" can also be estimated and is typically in the range of several hours.

Both types of predictions can be evaluated on an annual or a seasonal basis.

L.4 Acceptance and Safety Criteria for Pedestrian Level Wind Conditions

The criteria used to judge the acceptability and safety of the pedestrian level wind climate are shown in Table L.1. They were developed by the BLWTL together with building officials in London England in conjunction with a study there (L-3). They are based broadly on the Beaufort scale, shown in Table L.2, and on previous criteria that were originally developed by Davenport (L-4, L-5, L-6). These criteria allow for the reduction of the comfort and/or tolerance level of people engaged in more leisurely activities. The comfort criteria for each indicated activity level gives the mean wind speed exceeded 5% of the time above which wind conditions may become objectionable to individuals engaged in that activity. These criteria do not allow for differences in air temperature, solar radiation, clothing, sex, age, physical fitness, and the acclimatization of individuals exposed to particular wind environments. The safety criteria give the mean wind speed exceeded once per year above which wind conditions may become unsafe. Somewhat higher wind speeds can be tolerated in areas that are not used during severe weather.

References

(L-1) Irwin, H.P.A.H., "A Simple Omnidirectional Sensor for Wind Tunnel Studies of Pedestrian Level Winds", National Research Council, NAE Rep. LTR-LA-242, 1980.

(L-2) Irwin, H.P.A.H., "A Simple Omnidirectional Sensor for Wind-Tunnel Studies of Pedestrian Level Winds", Journal of Wind Engineering and Industrial Aerodynamics, Vol. 7 (1981), pp. 219-239.

(L-3) Kapoor, V., Page, C., Stepfanowicz, P., Livesey, F., Isyumov, N., “Pedestrian Level Wind Studies to Aid in the Planning of a Major Development”, Structures Congress Abstracts, American Society of Civil Engineers, 1990.

(L-4) Davenport, A.G., "An Approach to Human Comfort Criteria for Environmental Wind Conditions", Colloquium on Building Climatology, Stockholm, September 1972.

(L-5) Isyumov, N and Davenport, A.G. "The Ground Level Wind Environment in Built-Up Areas", Proceedings of 4th International Conference on Wind Effects on Buildings and Structures, London, England, September 1975, Cambridge University Press, 1977.

(L-6) Isyumov, N., "Studies of the Pedestrian Level Wind Environment at the Boundary Layer Wind Tunnel Laboratory of The University of Western Ontario", Journal of Industrial Aerodynamics, Vol. 3 (1978), pp. 187-200.

TABLE L.1 CRITERIA FOR PEDESTRIAN COMFORT AND SAFETY

CRITERIA	DESCRIPTION	MEAN WIND SPEED EXCEEDED 5% OF THE TIME
Comfort level 1	Fast Walking	10 m/s
Comfort level 2	Leisurely Walking	8 m/s
Comfort level 3	Standing, Sitting – short exposure	6 m/s
Comfort level 4	Standing, Sitting – short exposure	4 m/s

CRITERIA	DESCRIPTION	MEAN WIND SPEED EXCEEDED ONCE PER YEAR
Safety level 1	Fair-Weather Areas	20 m/s
Safety level 2	All-Weather Areas	15 m/s

Note: Fair-weather areas refer to areas that are not used in severe weather, such as park benches, lookout points, etc. All weather areas are areas that need to be used in all weather conditions, such as building entrances, sidewalks, etc.

TABLE L.2 EXTRACTS FROM THE BEAUFORT SCALE

FORCE	DESCRIPTION	WIND SPEEDS* (m/s)		SPECIFICATIONS
		MEAN	LIMITS	
2	Light Breeze	2.5 (2)	1.6 - 3.3 (1.3 - 2.6)	Wind felt on faces; leaves rustle
3	Gentle breeze	4.4 (3.5)	3.4 - 5.4 (2.7 - 4.3)	Leaves and small twigs in constant motion; wind extends light flag
4	Moderate breeze	6.7 5.4	5.5 - 7.9 (4.4 - 6.3)	Raises dust and loose paper; small branches are moved
5	Fresh breeze	9.4 7.5	8.0 - 10.7 (6.4 - 8.6)	Small trees in leaf begin to sway
6	Strong breeze	12.3 9.8	10.8 - 13.8 (8.7 - 11.0)	Large branches in motion; whistling heard in telephone wires; umbrellas used with difficulty
7	Moderate gale	15.5 12.4	13.9 - 17.1 (11.1 - 13.7)	Whole trees in motion; inconvenience felt when walking against wind
8	Gale	19 15.2	17.2 - 20.7 (13.8 - 16.6)	Breaks twigs off trees; generally impedes progress

* Wind speed at reference height of 10 m; nearer the ground, at 1.8 m, say, the speeds may be about 80% of the speeds indicated (figures shown in brackets above)

APPENDIX M

DYNAMIC WIND FORCES ON LONG SPAN BRIDGES USING EQUIVALENT STATIC LOADS

M.1 Introduction

The conventional treatment of wind loading on long span bridges has tended to consider the static design wind loading used in normal strength design and the aerodynamic stability as two separate and distinct aspects. The procedure described in this appendix takes a more unified approach. It depends on the measurement of the dynamic response of section models to grid turbulence rather than smooth flow. The response is corrected for discrepancies in the intensity and spectrum of turbulence, the damping, and the joint acceptance function for the mode shape. A small correction is also added for the deficiency in low frequency excitation from grid turbulence. The design loads are found from the estimates of dynamic motion in the lowest symmetric and asymmetric modes as well as the mean load. This approach is an outgrowth of earlier studies in turbulent flow on the Murray MacKay Bridge (M-1), the Bronx-Whitestone Bridge (M-2), and Sunshine Skyway Bridge (M-3).

M.2 The Description of Design Loads

The persistent movements of any long span bridge (M-4, M-5) in strong wind are organized through its various mode shapes - horizontal, vertical, and torsional. They cover a range of frequencies but take place mostly at or near the individual modes and have a random character due to the continual shifts in phase and amplitude.

To summarize the variety of load actions which the dynamic movements will produce in a severe wind storm, a wind load description for design has been proposed as in Figure M.1. In this *x, z* and denote the horizontal (downwind), vertical (upward) and torsional (nose-up) components; (see Figure M.2); W , W_1 and W_2 are the mean, symmetric and anti-symmetric components per unit length of deck; $a(\eta), a_1(\eta)$ and $a_2(\eta)$ are the mean and modal load distribution functions; γ_1 and γ_2 are statistical load combination factors and take on values of ± 1.0 if only one modal term is included; ± 0.8 for two terms; ± 0.7 for three terms and ± 0.6 for four or more terms.

The description of the mean time average wind load components produced by the mean wind is straightforward. They are defined through the force coefficients $C_x(\alpha), C_z(\alpha)$ and $C_\theta(\alpha)$ which may be measured for a range of angles of attack α, the deck width B, and the mean reference velocity pressure at deck height H, $q_H = 1/2\ \rho U_H^2$. The three mean forces per unit length are then:

$$\overline{W}_x = q_H\ B\ C_x(0);\ \ \overline{W}_z = q_H\ B\ C_z(0);\ \ \overline{W}_\theta = q_H\ B\ C_\theta(0) \qquad \text{(M.1)}$$

Two points should be made. First the coefficients in turbulent flow may differ from those in smooth flow. Second, normally only horizontal mean winds need to be considered. Only in steep mountainous valleys is there likely to be any appreciable inclination to the mean flow.

M.3 Evaluation of the Modal Load W_1 and W_2

Although the response of a suspension bridge has been represented by coupled vertical and torsional equations of motion (M-6, M-7), in fact the aerodynamic coupling terms are usually negligible, and the aerodynamic stiffness terms are usually small in comparison to the stiffness of the bridge itself. This leaves the aerodynamic damping as the most significant aerodynamic force induced by motion. If this is

negative and numerically greater than the structural damping, large motion will result. The response of each uncoupled mode of vibration to the turbulent wind can be studied separately and superimposed at the end; usually, only the lowest modes are significant.

We can represent the peak modal load amplitude by the following:

$$W = g\sqrt{\sigma_{W_b}^2 + \sigma_{W_r}^2} \tag{M.2}$$

where g is a statistical peak factor, $\sigma_{W_b}^2$ is the mean square background excitation acting quasi-statically, and $\sigma_{W_r}^2$ is the mean square excitation at or near the resonant frequency.

The two components of the excitation can be identified in the typical power spectrum shown in Figure M.3. The background excitation covers a broad frequency band below the natural frequency; the resonant excitation is concentrated in a peak at the natural frequency, the height of which is controlled by the damping. The two components can be estimated from the following expressions:

$$\sigma_{W_{b_{x,z,\theta}}}^2 = \int_0^\infty f^*\ S_{F_{x,z,\theta}}\left(f^*\right)\cdot\left|J_{x,z,\theta}\left(f^*\right)\right|^2 \cdot d\left(ln\ f^*\right) \tag{M.3}$$

$$\sigma_{W_{r_{x,z,\theta}}}^2 = \frac{\pi\ /\ 4}{\xi_s + \xi_a\left(f_0^*\right)}\cdot f_0^*\ S_{F_{x,z,\theta}}\left(f_0^*\right)\cdot\left|J_{x,z,\theta}\left(f_0^*\right)\right|^2 \tag{M.4}$$

In the above, the subscripts x, z, θ imply the equations are written for each variable in turn; f^* and f_0^* are the reduced frequencies $f\ B\ /\ U_H$ and $f_0\ B\ /\ U_H$; ξ_s and $\xi_a\left(f^*\right)$ are the structural damping and aerodynamic damping at frequency f^*; $f^*\ S_{F_{x,z,\theta}}\left(f^*\right)$ is the power spectral density of the externally induced x, z, θ components on a cross-section of the bridge deck at the reduced frequency f^*; $\left|J_{x,z,\theta}\left(f^*\right)\right|^2$ is the "joint acceptance function", relating the generalized modal force component with the mode shape and the force components at frequency f^* at cross-sections of the bridge and involves the spanwise correlation of the forces.

The external forces on a bridge cross-section arise from either the direct action of turbulence in the wind or through the action of flow fluctuations in the wake. The latter are commonly described as vortex shedding. We can write:

$$f^*\ S_F\left(f^*\right) = \left[f^*\ S_F\left(f^*\right)\right]_{turb} + \left[f^*\ S_F\left(f^*\right)\right]_{wake} \tag{M.5}$$

The turbulent term can be written

$$\left(f^*\ S_F\left(f^*\right)\right)_{turb} = \left(q_H\ B\right)^2 \cdot \left(C_{x,z,\theta}^2\left|A\left(f^*\right)\right|^2\right)\cdot\left(f^*\ S_{u.v.w}\left(f^*\right)\right) \tag{M.6}$$

where $f^*\ S_{u.v.w}\left(f^*\right)$ = the power spectra of the turbulent velocity fluctuations u, v and w;

$A\left(f^*\right)$ = "aerodynamic admittance" which translates the turbulent fluctuations into forces on a cross-section;

$C_{x,z,\theta}$ = a reference aerodynamic coefficient.

The contributions of the turbulence to the expressions for $\sigma^2_{W_b}$ and $\sigma^2_{W_r}$ can be written as follows. To simplify the notation we will consider the lift (z) force and only include the vertical (w) component of turbulence, which normally will dominate.

$$\sigma^2_{W_{b_z}} = \left(q_H\ B\ C_z^{'}\right)^2 \left(\frac{\sigma_w}{U_H}\right)^2 \int_0^{\infty} \frac{f^*\ S_w\left(f^*\right)}{\sigma_w^2} \left|A_z\left(f^*\right)\right|^2 \left|J_z\left(f^*\right)\right|^2\ d\ ln\ f^* \tag{M.7}$$

$$\sigma^2_{W_{r_z}} = \left(q_H\ B\ C_z^{'}\right)\left(\frac{\sigma_w}{U_H}\right)^2 \frac{f_0^*\ S_w\left(f_0^*\right)}{\sigma_w^2} \left|A_z\left(f_0^*\right)\right|^2 \left|J_z\left(f_0^*\right)\right|^2 \frac{\pi\ /\ 4}{\xi_s + \xi_a\left(f_0^*\right)} \tag{M.8}$$

The coefficient $C_z^{'}$ denotes $\left(\partial C_z\ /\ \partial\alpha\right)$. Similar expressions for the torsion can be written with θ replacing z and introducing an additional factor B^2. For the drag direction $2C_x$ replaces $C_z^{'}$ and u replaces w.

If the left hand terms are normalized by the $\left(q_H\ B\ C_z^{'}\right)^2$ term, the response is a function primarily of the reduced frequency f^* and the intensity of turbulence $\left(\sigma_w\ /\ U_H\right)$, two homologous quantities which link the full-scale bridge behaviour with any dynamically scaled model. Otherwise, the turbulence controlled response is bound up in the functional form of the turbulence spectrum, S_w, the aerodynamic admittance, A_z, the joint acceptance function, J_z, and the aerodynamic damping ξ_a.

The aerodynamic admittance reflects the efficiency of the bridge deck as a lift generator, as well as the correlation of the flow in the vicinity of the deck. The theoretical and observed form of this function is shown in Figure M.7. The joint acceptance function can be written

$$\left|J\left(f^*\right)\right|^2 = \int_0^L \int_0^L R_{F_1F_2}\left(\eta_1, \eta_2; f^*\right) \mu\left(\eta_1\right) \mu\left(\eta_2\right) d\eta_1\ d\eta_2 \tag{M.9}$$

where $\mu(\eta)$ = mode shape with unit mean square amplitude; and

$$R_{F_1F_2}\left(\eta_1, \eta_2; f^*\right) = exp\left(-c\ f^*\ \frac{L}{B}\ \frac{\left|\eta_1 - \eta_2\right|}{L}\right) \tag{M.10}$$

in which c is a constant which defines the effective width of the correlation. A similar expression can be written for the spanwise cross-correlation of the velocity component, in which case $c \approx 8$ is representative. It is reasonable to assume the same value holds for the forces F_1 and F_2 on the basis of the "strip assumption".

Equations M.7 and M.8 apply to both the full scale bridge and a model in a turbulent wind tunnel flow. Ideally the latter should be an exact scaling of the former. This ideal, however, is difficult to satisfy in the wind tunnel and some compromises may have to be made. There are significant advantages to using an elongated section model in a turbulent flow generated behind a coarse grid. Although the turbulence scale and intensity cannot be made to exactly correspond to full scale, the values can be made sufficiently close.

To adapt the results of the dynamic section model testing to full scale, corrections need to be applied as follows: (a) Corrections of the low frequency quasi-static, "background" response, $\sigma^2_{W_b}$, largely omitted from the section model due to the deficit in the vertical velocity spectrum generated by the grid. This can be estimated with reasonable accuracy from equation M.7 using either theoretical or experimental data as

outlined below. (b) Correction of the terms in the resonant response $\sigma^2_{W_r}$ for the discrepancies in the turbulence intensity, vertical velocity spectrum, joint acceptance function and damping. No correction is needed in the aerodynamic admittance. The following formula encompasses these corrections:

$$\left(\sigma^2_{W_r}\right)_{full\ scale} = \left(\sigma^2_{W_r}\right)_{model}\ \phi_{\sigma_w}\ \phi_{S_w}\ \phi_J\ \phi_\xi \tag{M.11}$$

where the terms $\phi_{\sigma_w}, \phi_{S_w}, \phi_J$ and ϕ_ξ reflect corrections to the terms in the response due to the discrepancies between the section model and the full scale. These correction factors are found from the ratios of the quantities involved for model and full-scale. Through the appropriate selection of turbulence characteristics in the section model test and the model length, these corrections are relatively small. This last fact should lead to satisfactory reliability.

M.4 Experimental Determination of Design Load Components

The wind tunnel testing of the section models of the two Sunshine Skyway Bridge alternates provided an opportunity to apply the proposed method. The proposed structure, over Tampa Bay in Tampa Florida is a cable-stayed design with a 366m main span. The concrete alternate used a precast, segmental box girder 29.03m wide and 4.27m deep. Two single strut pylons carry a system of radiating stays located on the longitudinal axis of the bridge (Figure M.4).

The 1 in 80 scale model of the bridge section is 7 ft. (2m) in length corresponding to a 170m section of the full scale structure. The model was tested with spring mounting giving the correct frequency ratio in lift and torque and 0.5% damping. Measurements of mean and peak dynamic motion are plotted in Figure M.5, and show marked differences between smooth and turbulent flow. With smooth flow there is evidence of some coupling between static lift and torque (i.e. the twisting of the deck due to torque modifies the lift). Although not essential to the method, aerodynamic damping and admittance functions were also measured in the experiments.

The large mesh size and bar spacing of the turbulence grid was selected to give a close representation of the natural wind. The measured vertical turbulence intensity behind this grid is found to be 0.05 compared to the expected full scale value of 0.06 over open water. The grid turbulence spectrum and the target full scale spectrum have similar form, although the full scale has slightly more energy than does the grid turbulence at lower frequency.

M.5 Determination of Design Wind Loads

Following equation M.8, the wind load from the background turbulence excitation is found through the integration with reduced frequency of the product of the vertical wind spectrum (Figure M.6), Aerodynamic Admittance Function (Figure M.7) (assuming the Sears function), and the Joint Acceptance Function for the particular mode (Figure M.8). The form of these functions is such that the bulk of the energy is in the range of reduced frequency f^* between 0.01 and 0.1 and any uncertainty of the functional values at these low frequencies generally introduces little error. Added to this is the resonant component following equation M.8. The resonant modal response, measured in terms of deflection has been converted to an equivalent static load through the modal stiffness:

$$\sigma_{W_{r_z}} = m\left(2\pi\, f_0\right)^2\ \sigma_z;\ \sigma_{W_{r_\theta}} = I_0\left(2\pi\, f_0\right)^2\ \sigma_\theta \tag{M.12}$$

The correction terms are determined from the ratios of the quantities involved between full scale and model scale. The correction factor for the turbulence intensity, ϕ_{σ_w} is a constant equal to $(0.06 / 0.05)^2 = 1.44$ (i.e. this is the ratio of target full scale to model values). Similarly, the correction factor for the vertical velocity spectrum ϕ_{S_w} is shown in Figure M.6, the joint acceptance function, ϕ_J, in Figure M.8, and the damping, ϕ_ξ, in Figure M.9. The addition of the background and resonant components as in equation M.2, results in the loading shown in Figures M.10a and b. The final wind

speed scaling will depend upon the final design frequencies of the structure. Thus the example wind loads have been determined for a nominal wind speed at deck height based on the estimates of vertical and torsional frequencies noted in the figures.

Verification of this procedure, using 1:350 scale aeroelastic models of both the steel and concrete bridges tested in a turbulent boundary layer, showed excellent agreement.

M.6 Conclusions

A method has been presented whereby wind tunnel section model test results can be incorporated directly into a load format suitable for the definition of the design wind loads of long span structures. The procedure has been verified experimentally with the satisfactory prediction of the response of two full bridge aeroelastic models to boundary layer shear flow.

References

(M-1) Davenport, A.G., Isyumov, N., Fader, D.J. and Bowen, C.F.P., "A Study of Wind Action on a Suspension Bridge During Erection and Completion", University of Western Ontario, Faculty of Engineering Science, Research Report BLWT-3-1969, London, Ontario, Canada, May 1969 and March 1970.

(M-2) Davenport, A.G., Isyumov, N., Rothman, H. and Tanaka, H., "Wind Induced Response of Suspension Bridges, Wind Tunnel Model and Full Scale Observations", Proc. 5th Int. Conf. Wind Engineering, Ft. Collins, Colorado, 1979, pp. 807-824.

(M-3) Davenport, A.G. and King, J.P.C., "The Incorporation of Dynamic Wind Loads into the Design Specifications For Long Span Bridges", ASCE Fall Convention, New Orleans, La., 1982.

(M-4) Tanaka, H. and Davenport, A.G., "Wind Induced Response of Golden Gate Bridge", University of Western Ontario, Faculty of Engineering Science Research Report, BLWT-1-1982, Paper accepted for publication by JSD, ASCE, June 1982.

(M-5) Melbourne, W.H., "Model and Full Scale Response to Wind Action of the Cable Stayed Box Girder West Gate Bridge", Practical Experience With Flow Induced Vibrations, Symposium Karlsruhe, Germany, 1979, pp. 625-652.

(M-6) Ukeguchi, N., Sakata, H. and Nishitani, H., "An Investigation of Aeroelastic Instability of Suspension Bridges", Proc. International Symposium on Suspension Bridges, Lisbon, 1966, pp. 273-284.

(M-7) Scanlan, R.H., "An Examination of Aerodynamic Response Theories and Model Testing Relative to Suspension Bridges", Proc. Wind Effects on Buildings and Structures, Tokyo, 1971, pp. 941-951.

$$W_x(\eta) = \bar{W}_x\,\bar{\alpha}(\eta) \pm \gamma\,\tilde{W}_{1_x}\,\alpha_1(\eta) \pm \gamma\,\tilde{W}_{2_x}\,\alpha_2(\eta)$$

$$W_z(\eta) = \bar{W}_z\,\bar{\alpha}(\eta) \pm \gamma\,\tilde{W}_{1_z}\,\alpha_1(\eta) \pm \gamma\,\tilde{W}_{2_z}\,\alpha_2(\eta)$$

$$W_\theta(\theta) = \bar{W}_\theta\,\bar{\alpha}(\eta) \pm \gamma\,\tilde{W}_{1_\theta}\,\alpha_1(\eta) \pm \gamma\,\tilde{W}_{2_\theta}\,\alpha_2(\eta)$$

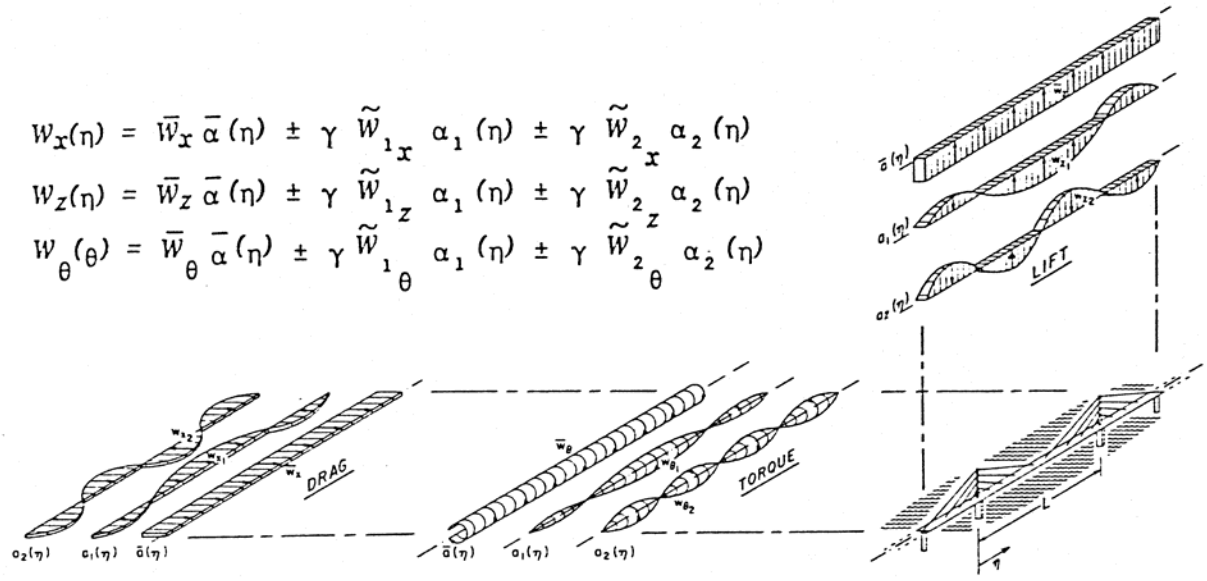

FIGURE M.1 DISTRIBUTED WIND LOAD COMPONENTS

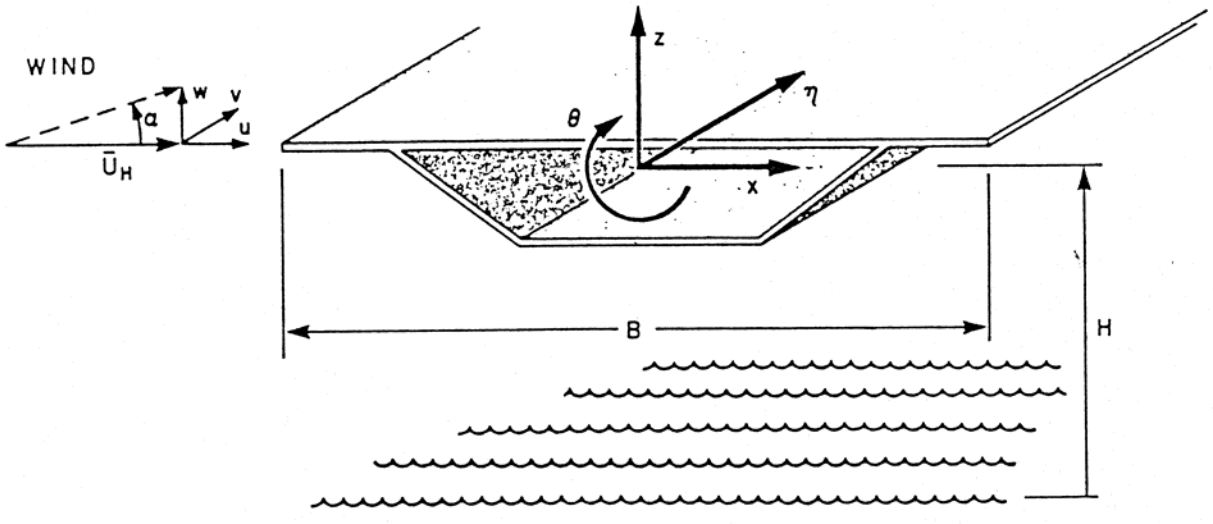

FIGURE M.2 NOTATION

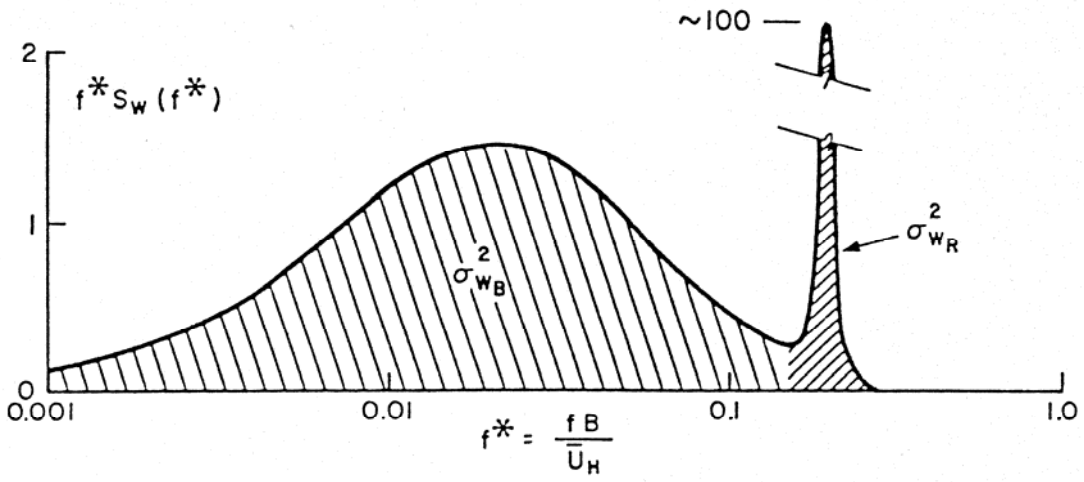

FIGURE M.3 SPECTRUM OF MODAL LOAD AMPLITUDE

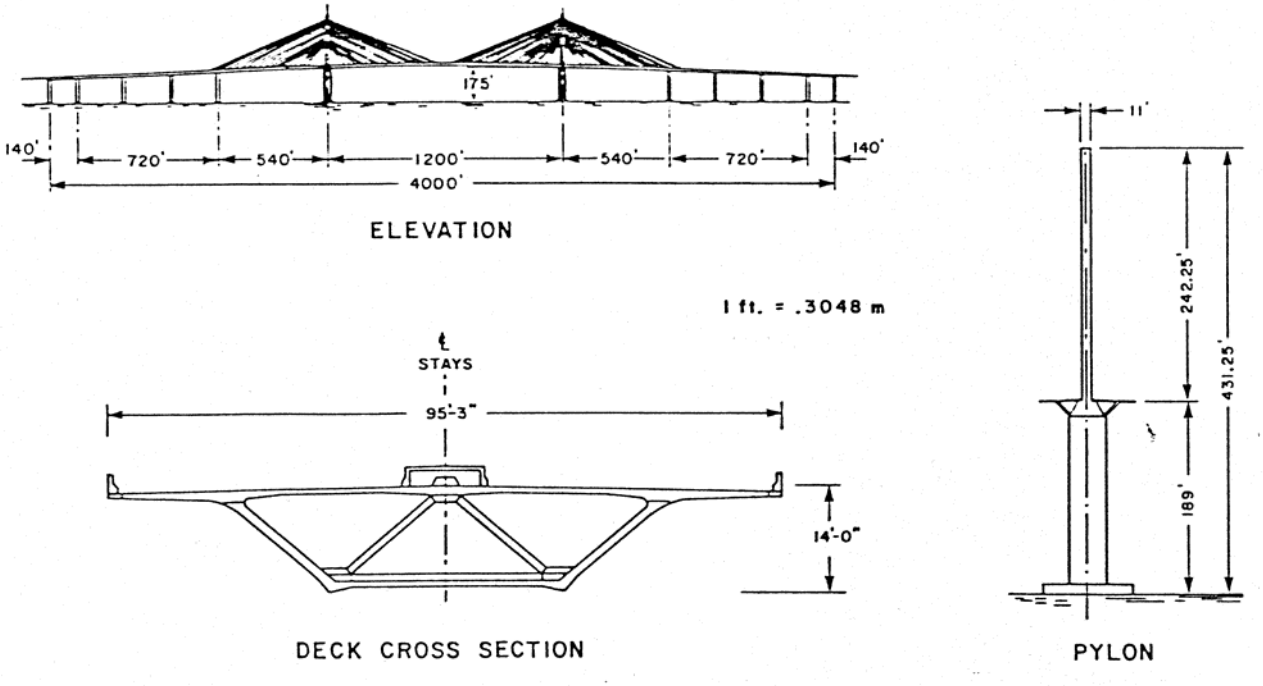

FIGURE M.4 SUNSHINE SKYWAY BRIDGE

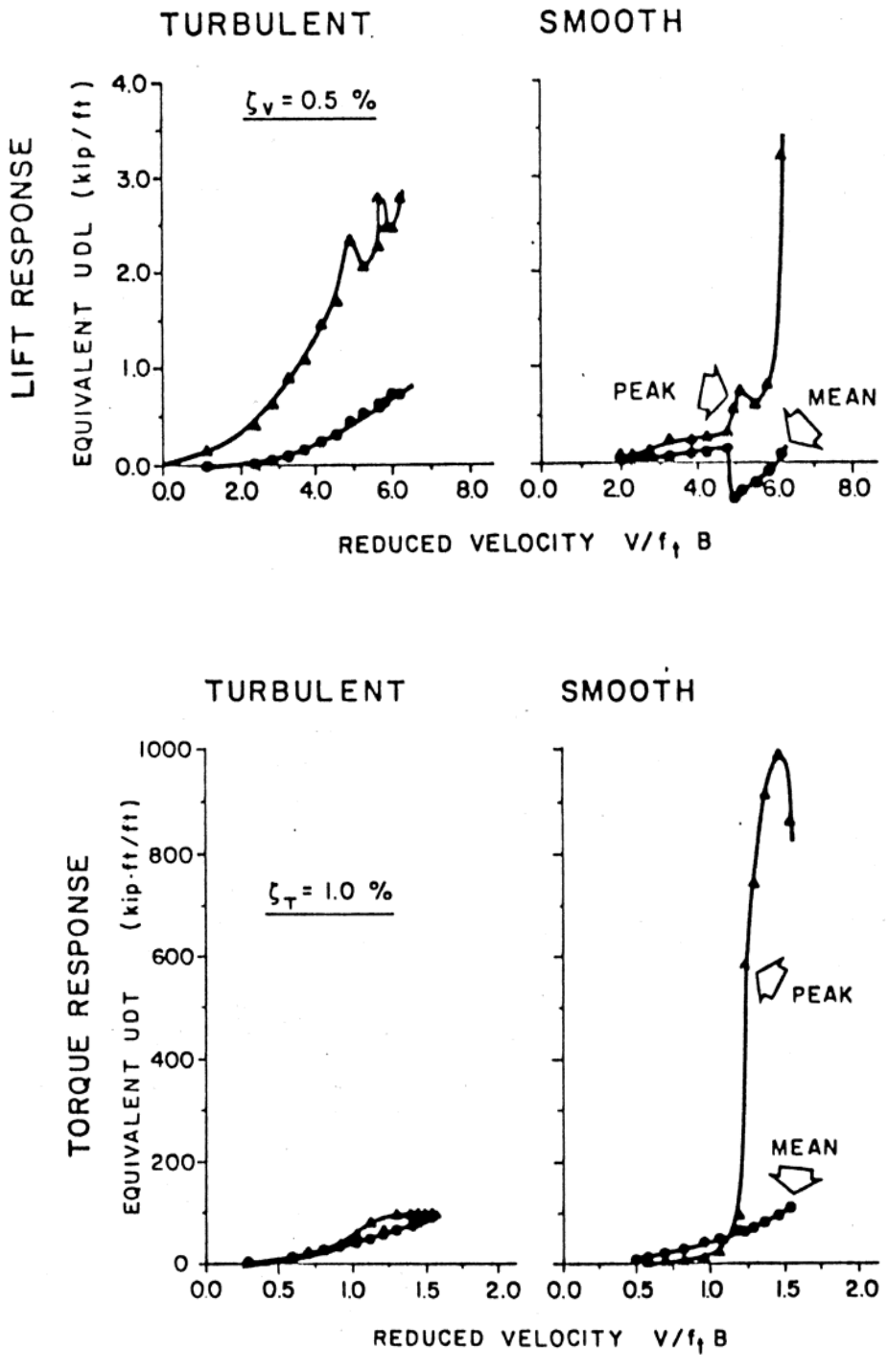

FIGURE M.5 SECTION MODEL RESPONSE (UNCORRECTED)

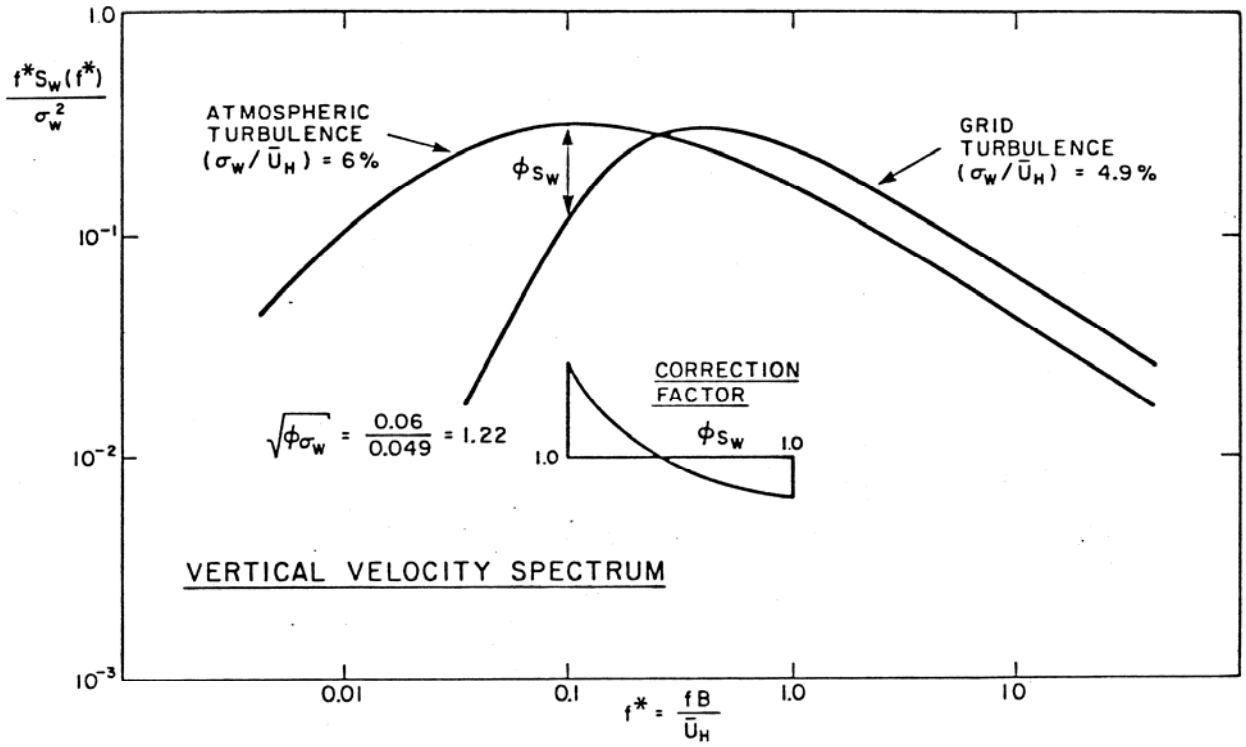

FIGURE M.6 VERTICAL VELOCITY SPECTRUM

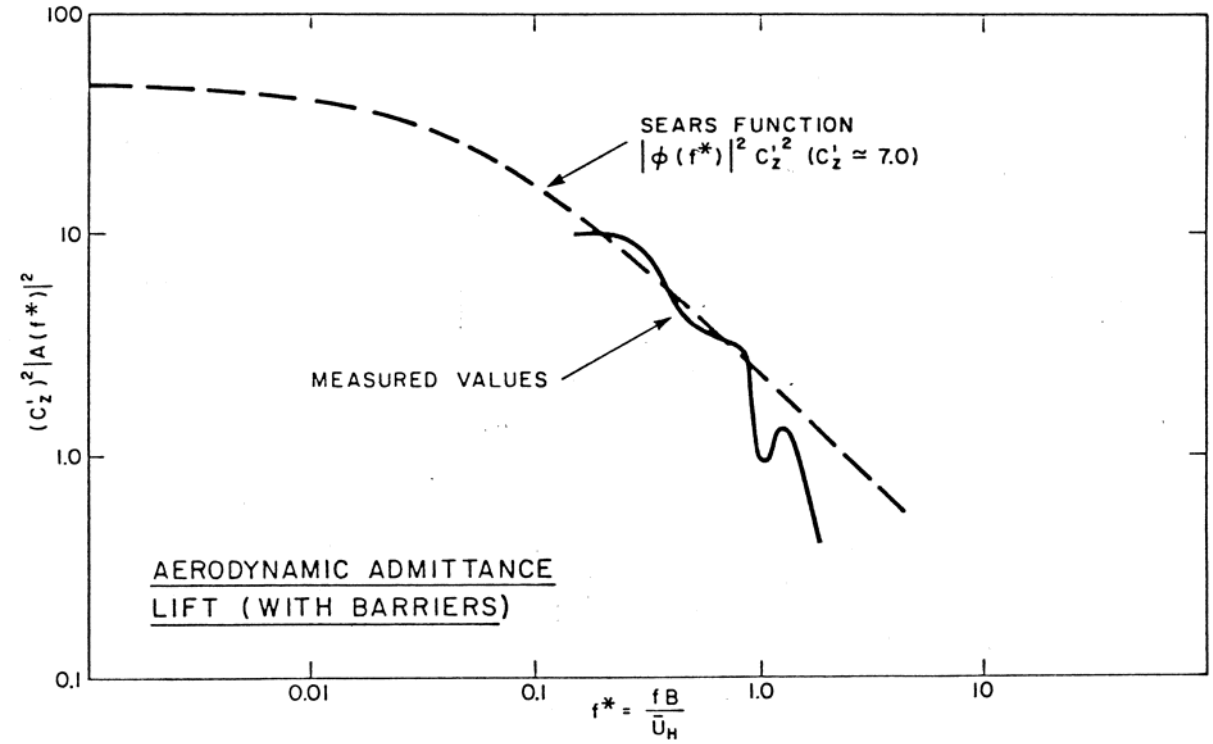

FIGURE M.7 AERODYNAMIC ADMITTANCE RESPONSE (UNCORRECTED)

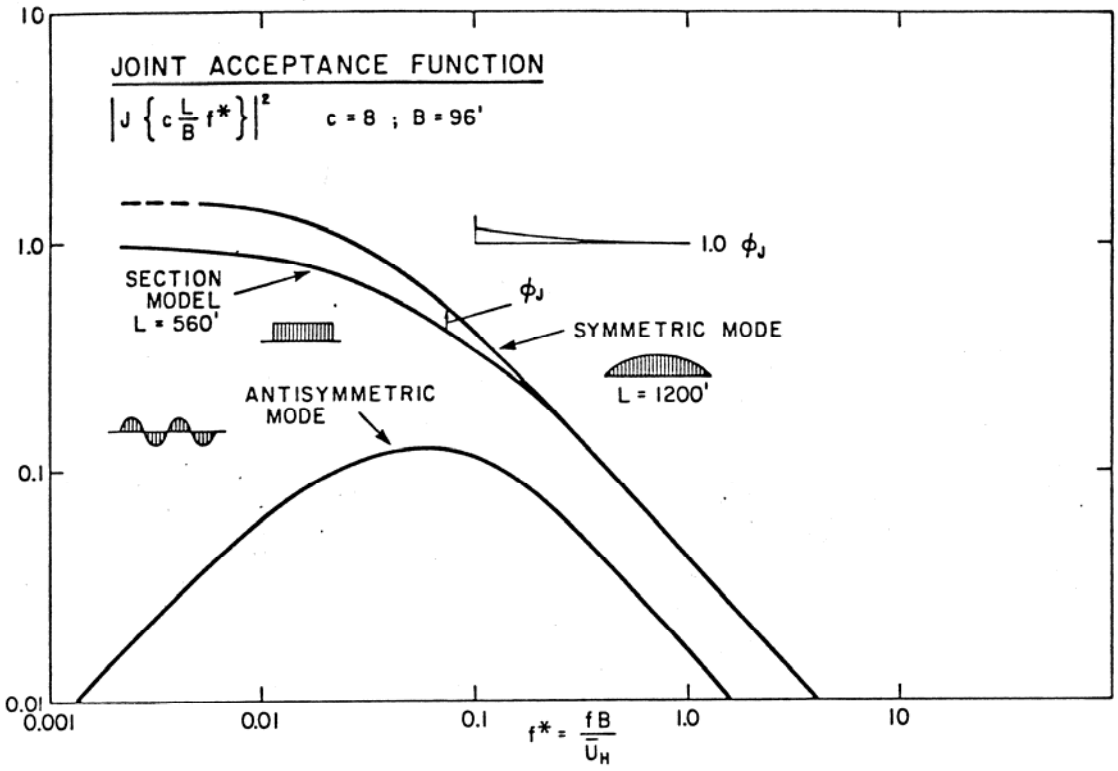

FIGURE M.8 JOINT ACCEPTANCE FUNCTION

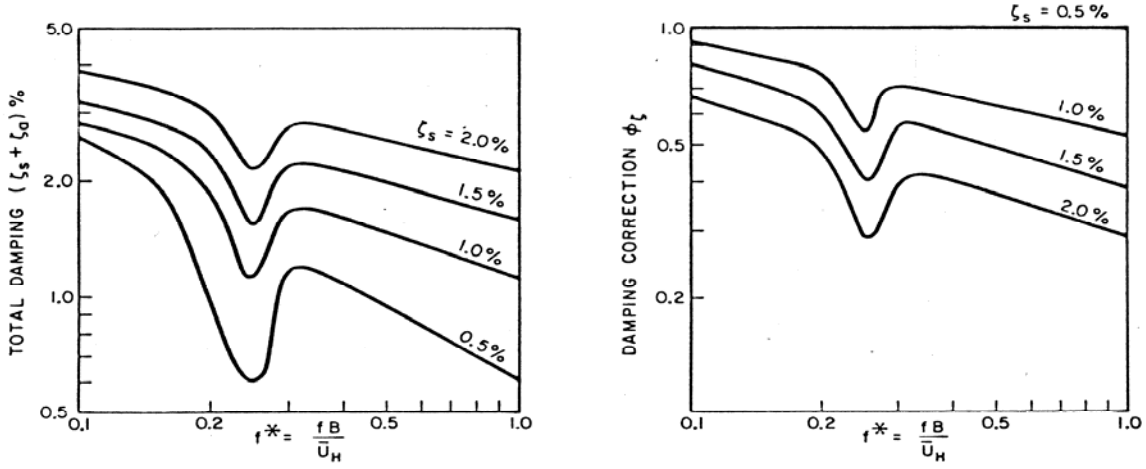

FIGURE M.9 DAMPING FUNCTIONS

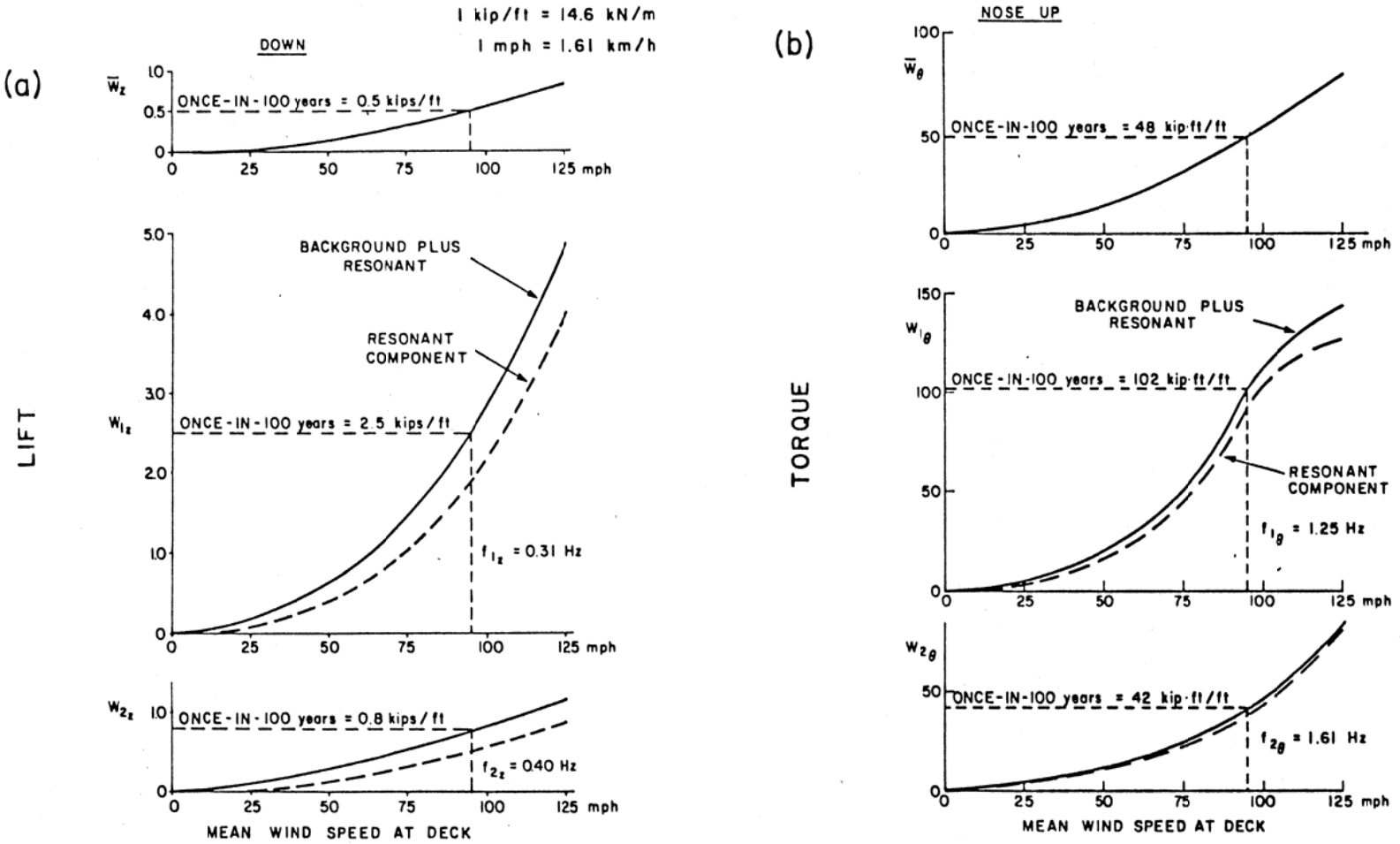

FIGURE M.10 WIND LOAD COMPONENTS ON COMPLETED BRIDGE

Alan G. Davenport Wind Engineering Group

Update History

September 17, 2002 - Updated effective loads appendix.
September 17, 2002 - Improved wording in section G.5 of the balance appendix (and carried the improved wording to section J.3 of the pressure loads appendix).
March 2006 – general update of all chapters, add description of effective load distributions and load combination factors. Improve consistency of notations.